Uncertainty in structural dynamic models.

Fonseca, Jose Manuel Rios

Uncertainty in Structural Dynamic Models

José Manuel Rios Fonseca

Submitted to the University of Wales in fulfilment of the requirements for the Degree of Doctor of Philosophy

University of Wales Swansea

2005

Summary

Modelling of uncertainty increases trust in analysis tools by providing predictions with confidence levels, produces more robust designs, and reduces design cycle time/cost by reducing the amount of experimental verification and validation that is required. However, uncertainty-based methods are more complex and computationally expensive than their deterministic counterparts, the characterisation of uncertainties is a non-trivial task, and the industry feels comfortable with the traditional design methods.

In this work the three most popular uncertainty propagation methods (Monte Carlo simulation, perturbation, and fuzzy) are extensively benchmarked in structural dynamics applications. The main focus of the benchmark is accuracy, simplicity, and scalability. Some general guidelines for choosing the adequate uncertainty propagation method for an application are given.

Since direct measurement is often prohibitively costly or even impossible, a novel method to characterise uncertainty sources from indirect measurements is presented. This method can accurately estimate the probability distribution of uncertain parameters by maximising the likelihood of the measurements. The likelihood is estimated using efficient variations of the Monte Carlo simulation and perturbation methods, which shift the computational burden to the outside of the optimisation loop, achieving a substantial time-saving without compromising accuracy. The approach was verified experimentally in several applications with promising results.

A novel probabilistic procedure for robust design is proposed. It is based on reweighting of the Monte Carlo samples to avoid the numerical inefficiencies of resampling for every candidate design. Although not globally convergent, the proposed method is able to quickly estimate with high accuracy the optimum design. The method is applied to a numerical example, and the obtained designs are verified with regular Monte Carlo.

The main focus of this work was on structural dynamics, but care was taken to make the approach general enough to allow other kinds of structural and non-structural analyses.

DECLARATION

This work has not previously been accepted in substance for any degree and is not being concurrently submitted in candidature for any degree.

Signed _____

Date 20th January 2006

STATEMENT 1

This thesis is the result of my own investigations, except where otherwise stated. Other sources are acknowledged by explicit references. A bibliography is appended.

Signed _____

Date 20th January 2006

STATEMENT 2

I hereby give my consent for my thesis, if accepted, to be available for photocopying and for interlibrary loan, and for the title and summary to be made available to outside organisations.

Signed _____

Date 20th January 2006

Contents

List of Figures

List of Tables

List of Symbols

$\mathrm{Cov}(\cdot)$	covariance
d	diameter
D	generic probability distribution
$\mathrm{E}(\cdot)$	expected value
$f(\cdot)$	probability density
$\mathbf{f}(\cdot)$	system function
$\mathbf{g}(\cdot)$	constraints function
h	height
$\mathbf{H}$	bandwidth matrix
$\mathbf{J}$	Jacobian matrix
$\mathbf{J}(\cdot)$	objectives function
K	stiffness
$\mathbf{K}$	stiffness matrix
l	length
$l(\cdot)$	log likelihood
L	correlation length
$L(\cdot)$	likelihood
m	number of response variables; mass
M	number of measurements
$\mathbf{M}$	mass matrix
n	number of parameters
N	number of samples
$\mathrm{N}(\cdot)$	normal probability distribution
$\mathrm{N}_n(\cdot)$	n-variable normal probability distribution

$\mathbf{p}$	system parameters vector
$P(\cdot)$	probability
r	radius
t	thickness
U	uniform probability distribution
$\mathrm{Var}(\cdot)$	variance
w	width; weight
x	uncertain parameter; position
x_i	i-th uncertain parameter
$\mathbf{x}$	uncertain parameters vector
$\mathbf{x}_i$	i-th sample of the parameter vector
y	response
y_i	i-th response variable
$\mathbf{y}$	response vector
$\mathbf{y}_i$	i-th sample of the response vector
α	confidence level
ϵ	relative error
$\kappa(\cdot)$	kernel probability density function
λ	eigenvalue
μ	mean
$\boldsymbol{\mu}$	mean vector
ω	frequency
ω_i	i-th natural frequency
ϕ	eigenvector
$\boldsymbol{\Sigma}$	covariance matrix
$\boldsymbol{\theta}_x$	parameters of the uncertain parameters distribution

Acknowledgements

I hereby acknowledge the financial support given by the Portuguese Foundation for Science and Technology through the scholarship SFRH/BD/7065/2001.

I thank the guidance from Professor Arthur W. Lees, my supervisor, and Professor Michael I. Friswell, my initial supervisor, who always supported me.

Finally, I thank my family, for impelling and encouraging me to undertake PhD studies.

Chapter 1

Introduction

The increase of computing power has shifted the modelling of structures to early design stages in order to cut development costs. However, it is increasingly apparent that the deterministic nature of the modelling methods employed for low frequency structural dynamics modelling have serious drawbacks. The variance in the noise and vibration response of structures, such as vehicles, is still a major concern and large resources are expended to identify and remove sources of variability.

Many engineers believe that any structure may be modelled to arbitrary accuracy merely by increasing the finite element mesh density. But this is not so. These refined meshes are able to model the geometry of the structure more accurately, but the modelling errors due to uncertainty can never be resolved in such a fashion.

The use of nondeterministic models allows the estimation of the uncertainty in the model predictions. These estimates can be given as standard deviations, confidence bounds, or even probability distributions. But the major advantage is in the feedback of these uncertainty estimates into the design decisions, via robust design techniques. These allow the designs to quickly reach the stage where they are insensitive to the uncertainty in the model.

Therefore the modelling of uncertainty is advantageous. It increases confidence in analysis tools by providing predictions with confidence levels. It produces more robust designs. And it reduces design cycle time and cost by reducing the amount of experimental verification and validation that is required.

However, there are barriers to the adoption of uncertainty-based design meth-

ods. The major barrier is that uncertainty-based design methods are more complex and computationally expensive than their deterministic counterparts. The computational overhead caused can be of several orders of magnitude higher. Another barrier is that the characterisation of uncertainties, which are necessary for accurate uncertainty modelling, is a non-trivial task. There is little existing knowledge for such characterisation. The uncertainty characterisation depends on the chosen structural configuration, materials, and manufacturing processes. Finally, the industry feels comfortable with the traditional design methods, which are supported by well-established tools.

1.1 Objective

The objective of this thesis is to determine ways to overcome the above mentioned barriers to the adoption of uncertainty-based methods for the particular application domain of structural dynamics. It aims to provide a set of methodologies to efficiently and accurately incorporate uncertainty into structural dynamic modelling and design. More specifically, how to adequately characterise the uncertainty in dynamic structures, how to accurately propagate that uncertainty through the dynamic models of structures, and how to efficiently and accurately design the structures so that their dynamical properties are robust to those uncertainties.

1.2 Outline

Chapter 2 gives the background terminology and methodology for uncertainty analysis within the scope of computational engineering. The main sources of uncertainties are identified and classified. The most popular uncertainty representations are described along with their benefits and disadvantages. The most common uncertainty propagation methods are also presented.

In chapter 3 the three most popular uncertainty propagation methods (the Monte Carlo simulation method, the perturbation method, and the fuzzy method) are extensively benchmarked in structural dynamics applications. The applications range from a simple cantilever beam to a curved shell model. The main focus of the bench-

mark is accuracy, simplicity, and scalability with respect to the model size and the number of uncertain parameters. Finally, some general guidelines for choosing the adequate uncertainty propagation method for an application are given.

Chapter 4 presents a novel method to identify uncertainty in parameters from measured experimental data; it can be used for uncertainty characterisation in domains where bespoke measurements are difficult. The method is based on the application of maximum likelihood estimation, where the likelihoods are estimated using efficient variations of the perturbation and Monte Carlo simulation methods. These variations shift most of the computational burden to the outside of the optimisation loop, achieving a substantial time-saving without compromising accuracy. The method is applied to numerical and experimental applications, and the results of the perturbation and Monte Carlo approaches are compared.

In chapter 5 a novel probabilistic method for the optimisation of robust design problems is presented. The method is based on the same variation of the Monte Carlo simulation approach presented in chapter 4. By shifting most of the computational burden to outside of the optimisation loop, optimum designs can be achieved efficiently and accurately. The method is applied to a numerical example, and the obtained designs are verified with regular Monte Carlo.

Chapter 6 presents the main conclusions of this work together with some directions for future work.

Chapter 2

Background terminology and methodology

2.1 Uncertainty classification

Uncertainty can stem from:

- *lack of knowledge*
- physical *randomness*
- *ambiguity* due to incompletely or improperly defined outcomes
- *vagueness* due to uncertainty in set membership (i.e., *fuzziness*) or boundaries (i.e., *roughness*)
- *conflicting* or *inaccurate* information

Uncertainty may be distinguished into *epistemic* and *aleatory uncertainty* [51]. *Epistemic uncertainty* is a measure of the lack of knowledge. It can be reduced by further research. It is also referred to as *reducible uncertainty. Aleatory uncertainty* is a measure of heterogeneity or diversity in a population. It can not be reduced by further research. It is also referred to as *irreducible uncertainty* or *variability.*

For a mathematical model it is possible to distinguish *parametric* and *model form uncertainty* [50]. *Parametric uncertainty* can be entirely specified as parameters in a

model. *Model form uncertainty* concerns structural changes within a model. While both forms commonly occur together in a realistic analysis, only the parametric form of uncertainty will be addressed in this work.

A general problem with parametric uncertainty can be formally described by the equation

$$\mathbf{y} = \mathbf{f}(\mathbf{x}) \tag{2.1}$$

where $\mathbf{x} = [x_1\, x_2\, \ldots\, x_n]^{\mathrm{T}}$ are uncertain parameters, and $\mathbf{y} = [y_1\, y_2\, \ldots\, y_m]^{\mathrm{T}}$ are the desired response quantities. Examples of parameters are structure geometry and material properties. Examples of response quantities are natural frequencies, frequency response functions, and time responses.

2.2 Uncertainty representation

Mathematical tools such as intervals, the probability theory, or fuzzy sets can be used to represent uncertainty. This section briefly describes such representations, highlighting the associated advantages and disadvantages.

2.2.1 Probability theory

Probability theory provides a sound basis for modelling uncertainty. Using probability distributions to quantify uncertainty allows the designer either to optimise the mean performance or to minimise the failure risk.

Frequencist interpretation The probability of an event is commonly defined as the ratio of the number of occurrences of that event over the total number occurrences, as the number of experiments approaches infinity. This is the frequencist probability interpretation, which is intuitive and widely accepted.

Probability theory is applied to the general problem in equation (2.1) by assuming the parameters $\mathbf{x}$ and response $\mathbf{y}$ are realisations of the random vectors X and

Y, respectively, which follow the probability distributions

$$\mathrm{X} \sim \mathrm{D_X} \tag{2.2}$$

$$\mathrm{Y} \sim \mathrm{D_Y} \tag{2.3}$$

where D_X and D_Y are the parameter and response multivariate probability distributions. The parameter and response joint probability density functions are denoted by $f_\mathrm{X}(\mathbf{x})$ and $f_\mathrm{Y}(\mathbf{y})$. Section 2.3 describes numerical methods to derive the response distribution from the parameter joint probability density function $f_\mathrm{X}(\mathbf{x})$.

Care must be taken in choosing the parameter and response distributions. Normal or multivariate normal distributions are often chosen, because of their well-known statistics properties, their easily estimated parameters, and their wide availability in software packages. While some physical phenomena has been shown to follow a normal distribution, many do not, making distributions with different properties (e.g., positiveness or asymmetry) a more sensible choice [2].

Bayesian interpretation The frequencist interpretation of probability is well-suited for *aleatory uncertainty*, but is less-so for for *epistemic uncertainty*. The problem arises when no experiment has been performed, or could ever be. In such situations frequency makes no sense: "What is the probability of life on Mars?", "What is the probability that a building can withstand a major earthquake?". To address this difficulty, the Bayesian interpretation of probability considers probability as a degree of belief, conditional upon some prior information. The probability p of an event can be seen as the willingness to bet $£p$ in exchange for a $£1$ if the event occurs. The name comes from Bayes' theorem, which is often used to update the probability of a given statement (prior probability) in the face of new evidence (conditional probability).

The Bayesian interpretation helps in manipulating *epistemic uncertainty*. Imagine that equation (2.1) refers to the dynamic response of a building. If we assign prior distributions of the construction material and soil properties then we can calculate posterior probabilities of the building collapsing to a given excitation. Also, we can dynamically test the building to update the prior probabilities and/or the collapse probability.

The Bayesian interpretation requires the specification of the prior probabilities. When those prior probabilities are unknown, the *principle of maximum entropy* can be used to choose the most uninformative of the prior distributions, e.g., assigning $1/2$ as the probability of a binary parameter, but this leads to a paradox such as the following [33].

> (...) A factory produces cubes with side-length between 0 and 1 foot; what is the probability that a randomly chosen cube has side-length between 0 and $1/2$ a foot? The tempting answer is $1/2$, as we imagine a process of production that is uniformly distributed over side-length. But the question could have been given an equivalent restatement: A factory produces cubes with face-area between 0 and 1 square-feet; what is the probability that a randomly chosen cube has face-area between 0 and $1/4$ square-feet? Now the tempting answer is $1/4$, as we imagine a process of production that is uniformly distributed over face-area. This is already disastrous, as we cannot allow the same event to have two different probabilities (especially if this interpretation is to be admissible!). But there is worse to come, for the problem could have been restated equivalently again: A factory produces cubes with volume between 0 and 1 cubic feet; what is the probability that a randomly chosen cube has volume between 0 and $1/8$ cubic-feet? Now the tempting answer is $1/8$, as we imagine a process of production that is uniformly distributed over volume. And so on for all of the infinitely many equivalent reformulations of the problem (in terms of the fourth, fifth, ... power of the length, and indeed in terms of every nonzero real-valued exponent of the length). What, then, is the probability of the event in question?
>
> The paradox arises because the principle of indifference can be used in incompatible ways. We have no evidence that favours the side-length lying in the interval $[0, 1/2]$ over its lying in $[1/2, 1]$, or vice versa, so the principle requires us to give probability $1/2$ to each. Unfortunately, we also have no evidence that favours the face-area lying in any of the four intervals $[0, 1/4]$, $[1/4, 1/2]$, $[1/2, 3/4]$, and $[3/4, 1]$ over any of the others, so we must give probability $1/4$ to each. The event "the side-length lies in $[0, 1/2]$", receives a different probability when merely redescribed. And so it goes, for all the other reformulations of the problem. We cannot meet any pair of these constraints simultaneously, let alone all of them.

Another problem with the Bayesian probability interpretation is that the probability itself cannot convey how much evidence is held. Consider the following three situations [78] where you have a box and:

1. you know that there are some white and some black balls in it;
2. you tried to draw some balls from it, and half the time you drew a black one and the other half a white one;
3. you know that there are exactly the same number of white and black balls in it.

If a Bayesian probability was assigned to the event "drawing a black ball" then a probability of 1/2 would be assigned in all these situations, spite the different amount of evidence in each.

2.2.2 Interval arithmetic

Uncertainty can be represented as intervals, whereby all parameters and response variables are bounded as

$$x_i \in [\underline{x}_i, \overline{x}_i],\ i = 1, 2, \ldots, n \tag{2.4}$$

$$y_j \in [\underline{y}_j, \overline{y}_j],\ j = 1, 2, \ldots, m \tag{2.5}$$

This representation is particularly useful to prevent the possibility of extreme events. For example, when proving the response lies within an admissible range.

Interval arithmetic, also called interval mathematics, interval analysis, and interval computation, defines the operations on intervals, such as

$$[\underline{a}, \overline{a}] + [\underline{b}, \overline{b}] = [\underline{a} + \underline{b}, \overline{a} + \overline{b}] \tag{2.6}$$

$$[\underline{a}, \overline{a}] - [\underline{b}, \overline{b}] = [\underline{a} - \overline{b}, \overline{a} - \underline{b}] \tag{2.7}$$

$$[\underline{a}, \overline{a}] \times [\underline{b}, \overline{b}] = [\min(\underline{a}\underline{b}, \underline{a}\overline{b}, \overline{a}\underline{b}, \overline{a}\overline{b},), \max(\underline{a}\underline{b}, \underline{a}\overline{b}, \overline{a}\underline{b}, \overline{a}\overline{b},)] \tag{2.8}$$

$$[\underline{a}, \overline{a}]/[\underline{b}, \overline{b}] = [\min(\underline{a}/\underline{b}, \underline{a}/\overline{b}, \overline{a}/\underline{b}, \overline{a}/\overline{b},), \max(\underline{a}/\underline{b}, \underline{a}/\overline{b}, \overline{a}/\underline{b}, \overline{a}/\overline{b},)] \tag{2.9}$$

Although interval arithmetic can be carried out for virtually any expression that can be evaluated using class arithmetic, a naive replacement of classical arithmetic by interval arithmetic will fail to produce adequately narrow bounds [36].

Interval arithmetic is *subdistributive* such that, if $\mathbf{x}$, $\mathbf{y}$, and $\mathbf{z}$, are intervals, then

$$\mathbf{x}(\mathbf{y}+\mathbf{z}) \subseteq \mathbf{xy}+\mathbf{xz} \tag{2.10}$$

so, although addition or multiplication of intervals is commutative and associative, the distributive laws do not hold [37]. For example, the following expressions

$$\mathbf{x}^2 - \mathbf{x}$$
$$\mathbf{x}(\mathbf{x}-1)$$

always produce equal results in classic arithmetic, yet when considered under the interval arithmetic they yield surprisingly different results. Taking, for example, $\mathbf{x}$ as the interval $[1,2]$, they yield

$$[1,2]^2 - [1,2] = [1,4] - [1,2] = [-1,3]$$
$$[1,2]([1,2]-1) = [1,2][0,1] = [0,2]$$

The reason behind this difference is that the dependency between operands is unaccounted for during intermediate computations. $\mathbf{x}^2$ and $\mathbf{x}$ are dependent quantities, but are considered as independent quantities in the subtraction, and the result is that the bounds are overestimated.

Furthermore, there is an additive identity $[0,0]$ and a multiplicative identity $[1,1]$, but additive and multiplicative inverses do not exist. For example

$$[1,2] - [1,2] = [-1,3]$$

This phenomena invariably reflects as an overestimation of the resulting interval width. And, if care is not taken, the interval width overestimation can grow to extremely large values (when compared to the mean), rendering the resulting intervals useless.

Therefore, most numerical algorithms need to be modified for interval arithmetic. With no alternative, the resulting interval for any function can be computed by resorting to a double-optimisation of that function. The response intervals for

equation (2.1) are then given by

$$[\underline{y}_j, \overline{y}_j] = [\min \mathbf{f}_j(\mathbf{x}), \max \mathbf{f}_j(\mathbf{x})] \text{ such that } x_i \in [\underline{x}_i, \overline{x}_i],\ i = 1, 2, \ldots, n \qquad (2.11)$$

for every j-th response variable.

Affine interval arithmetic provides a partial solution to the interval width overestimation problem, and has been proposed as an alternative for interval arithmetic for uncertainty modelling in finite element analysis [42].

2.2.3 Fuzzy sets

Fuzzy sets model uncertainties through vague definition rather than by chance. A conventional (crisp) set either contains an element, or not. However, fuzzy sets define a series of intermediary belonging states between these two statements.

The degree to which a real number x belongs to a fuzzy set is specified by the membership function $\mu(x)$. The membership function values range from zero to one. A membership value of one means that the given point is sure to belong to the fuzzy set. A membership value of zero means that the given point does not belong to the set. Fuzzy sets use membership functions as a replacement for probability density functions.

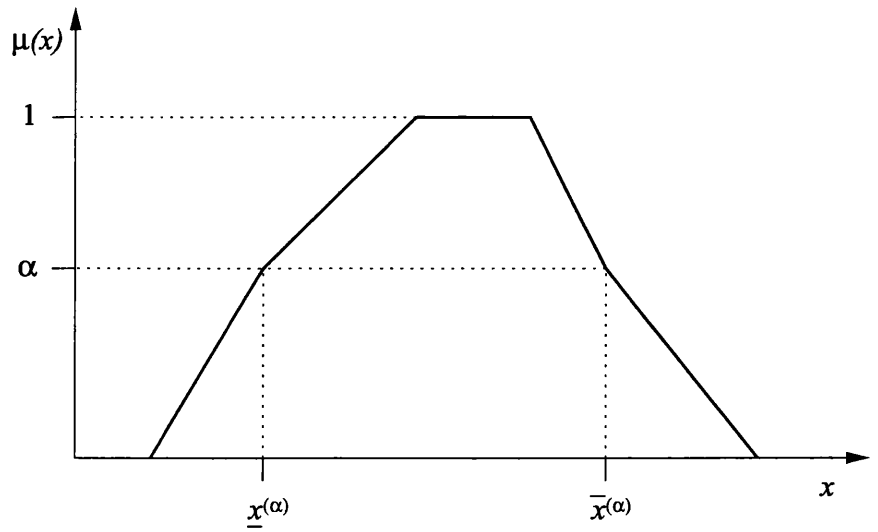

Figure 2.1: Interval representation of a fuzzy number

For numerical computation, a fuzzy number is approximated by a set of closed intervals corresponding to specific α-cuts of the membership function. This is illustrated by figure 2.1. However, this representation implies that membership functions must be convex; they cannot represent bi-modal variables.

Fuzzy arithmetic operations can be carried out by using interval arithmetic operations at each of the α-levels independently, so the membership functions have a simpler and computational more efficient algebra than the probability density functions. However fuzzy arithmetic also inherits all of the complications of interval arithmetic mentioned in section 2.2.2.

Construction of membership functions Membership functions may be constructed from expert knowledge. Alternatively, if probability density functions are known, the membership functions may be obtained by their normalisation [9] as

$$\mu(x) = \frac{1}{\max f(x)} f(x) \tag{2.12}$$

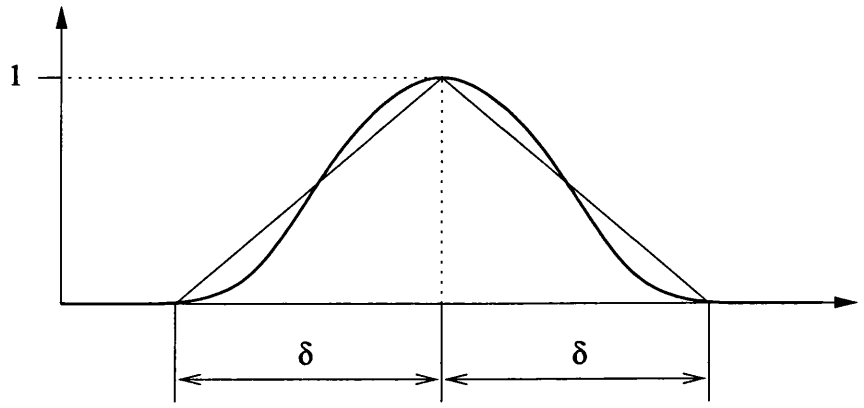

Figure 2.2: Approximating a Gaussian distribution by a triangular fuzzy number

It is common to approximate the Gaussian random variables by triangular fuzzy numbers, as seen in figure 2.2, where [31]

$$\delta = \sqrt{2\pi}\sigma \tag{2.13}$$

In the framework of possibility theory, fuzzy numbers can be used to define an

equivalence class of probability distributions compatible with the available data, specifying corresponding upper and lower cumulative density functions [64].

Imprecise probabilities

Imprecise probability theories overcome most of the limitations of probability theory when representing epistemic uncertainty by encoding both the amount of evidence *for* and *against* a hypotheses. In probability theory these two quantities are complementary. But in imprecise probability theory they do not necessarily add up to unity. The gap encodes the lack of evidence either way – the lack of knowledge.

Imprecise probabilities theories include many different models, such as probability intervals and Dempster-Shafer's belief functions.

The *Imprecise Probabilities Project* provides on its web site[1] a repository of information related to the imprecise probabilities theories.

2.2.4 Random fields

Uncertain properties, such as Young's modulus, mass density or plate thickness, vary in space. This variability can be described using random fields.

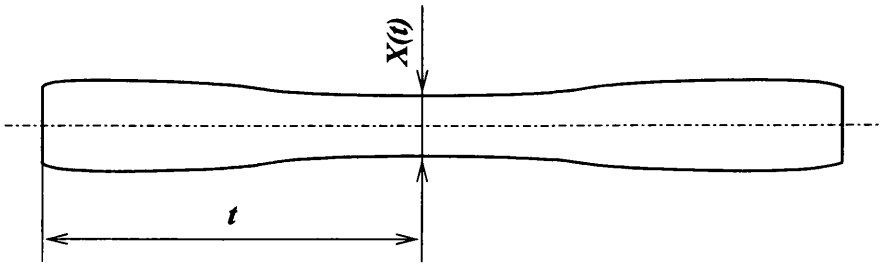

Figure 2.3: Random field example

A *random field* $X(\mathbf{t})$ is a collection of random variables at points with coordinates $\mathbf{t} = (t_1, \ldots, t_n)$ in a n-dimensional parameter space [75]. Figure 2.3 illustrates a beam's thickness as a random field.

In most engineering applications the random fields can be considered *homogeneous* and *isotropic*. For an *homogeneous* random field all of the joint probability

[1] `http://ippserv.rug.ac.be/`

distribution functions remain the same when the set of locations is *translated* in the parameter space. For an *isotropic* random field all of the joint probability distributions functions remain the same when the set of locations is *rotated* in parameter space. These two properties combined imply that the correlation ρ between the random field value at two locations $\mathbf{t}_1$ and $\mathbf{t}_2$ depends solely on the distance τ between these two points:

$$\rho(\mathbf{t}_1, \mathbf{t}_2) = \rho(\tau) \tag{2.14}$$

where $\tau = \|\mathbf{t}_2 - \mathbf{t}_1\|$.

Random field models

A simple random field model which observes the homogeneous and isotropic properties is the first order auto-regressive model, commonly abbreviated to AR(1).

First-order autoregressive model AR(1) The AR(1) model in space is given by

$$\left(\nabla^2 - \alpha^2\right) X(\mathbf{t}) = U(\mathbf{t}) \tag{2.15}$$

where $U(\mathbf{t})$ is an uncorrelated (white noise) random field and α is a parameter which specifies the scale of variation.

The quantity $L = 1/\alpha$ is usually referred to as the correlation length, and gives a measure of the roughness scale. Figure 2.4 shows instances of unidimensional AR(1) random fields with same zero mean and unit standard variation but different correlation lengths. Low correlation lengths yield rough curves while big correlation lengths yield smooth curves.

The coefficient of correlation of an AR(1) random field in an one-dimensional space by [75]

$$\rho(\tau) = (1 + \frac{\tau}{L})e^{-\frac{\tau}{L}} \tag{2.16}$$

and in a two-dimensional space is given by

$$\rho(\tau) = \frac{\tau}{L} K_0 \left(-\frac{\tau}{L}\right) \tag{2.17}$$

where L is the correlation length and K_0 is the modified Bessel function of the

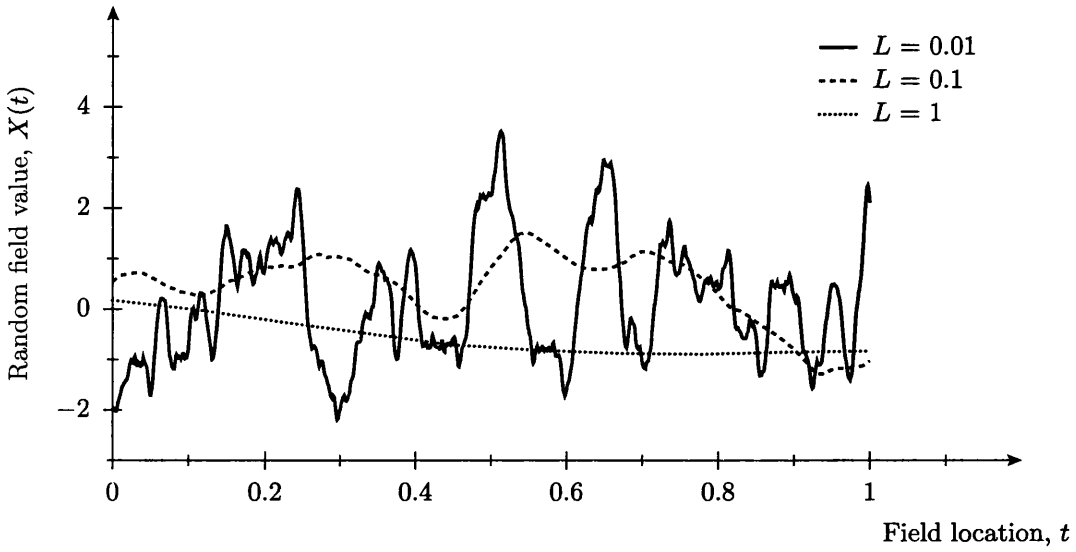

Figure 2.4: Samples of a single dimension AR(1) model with different values of α

second kind of order 0.

Random field discretisation

To incorporate a spatial random field in a finite element analysis the random field must be discretised to give a set of discrete random variables. Some methods developed for that purpose are described below.

Mid-point method In the mid-point method, which is the most straightforward random field discretisation method, the field value over an element is taken to be equal to the value at the mid-point of the element.

Local averaging method In the local averaging method the field value over an element is taken to be equal to the spatial average of the field over the element [76].

Weighted integral method In the weighted integral method the field is replaced by weighted integrals over its domain [69, 70, 13, 14, 46].

Orthogonal series expansion By making use of the Karhunen-Loève expansion of the covariance function the random field can be represented in terms of a finite set

of uncorrelated random variables [67].

Optimum linear estimation The optimum linear estimation method represents the random field as a linear function of nodal random variables using a set of shape functions and applying the principles of optimal linear estimation [41].

The mid-point method is the most simple to implement, and for that reason is often used. However it is not the most accurate. Li and Der Kiureghian [41], Schüeller [65] reviewed most of the random field discretisation methods.

2.2.5 Transformation of random variables into normal variables

Some probabilistic methods require that the uncertain parameters are specified as normal or multivariate normal distributions, because of their well-known statistical properties. Nevertheless, it is generally possible to transform a set of non normal variables into a set of independent normal variables.

Random variables may be transformed into uncorrelated Gaussian variables exactly using the Rosenblatt transformation, or approximately using the Nataf transformation [45, 80].

Rebba and Mahadevan [59] reviewed several of the normal transformation methods.

2.3 Uncertainty propagation

Incorporating uncertainty in a deterministic analysis by having its inputs as uncertain and quantifying the consequent uncertainty in the outputs is commonly referred as *uncertainty propagation.*

The response statistics, such as mean and variance, are usually sought

$$\mathrm{E}(\mathbf{y}) = \int f_{\mathrm{X}}(\mathbf{x}) \cdot \mathbf{f}(\mathbf{x})\, \mathrm{d}\mathbf{x} \tag{2.18}$$

$$\mathrm{Var}(\mathbf{y}) = \int f_{\mathrm{X}}(\mathbf{x}) \cdot \left(\mathbf{f}(\mathbf{x}) - \mathrm{E}(\mathbf{f}(\mathbf{x}))\right)^2 \mathrm{d}\mathbf{x} \tag{2.19}$$

The response joint probability density function

$$f_Y(\mathbf{y}) = f_X(\mathbf{x}) / \left| \frac{\partial \mathbf{f}}{\partial \mathbf{x}}(\mathbf{x}) \right| \tag{2.20}$$

may be sought so it can be integrated over a failure/safe subset of the parameter space and assess the structure failure/survival probability, respectively.

The analytical solution of these integrals is rarely available. The system function $\mathbf{f}$ usually includes highly complex simulations and analyses, such as the finite element method, and its evaluation is costly. Therefore, approximate methods for uncertainty propagation have been developed.

Most uncertainty propagation methods fall within three main categories: sampling methods, response surface approximation methods, and convex methods.

Sampling methods The sampling methods propagate uncertainty by performing sample evaluations of equation (2.1). The Monte Carlo simulation method and its variants are the prime example, and is described in section 2.3.1.

Response surface approximation methods Response surface approximation methods replace equation (2.1) by a simpler low-order approximation, from which response statistics are more easily derived. It includes the first and higher order perturbation methods, described in section 2.3.2.

Convex methods Convex methods produce bounds on the response from the input bounds. The interval and fuzzy methods are included in this category. The fuzzy method is described in section 2.3.3.

The choice of the uncertainty propagation method is largely dependent on the chosen uncertainty representation. Monte Carlo and perturbation methods are more akin to the probabilistic representation of uncertainty. Each of the convex methods is associated with the respective uncertainty representation.

2.3.1 Monte Carlo simulation method

The Monte Carlo simulation (MCS) method is named after the city in Monaco and its casinos. It is applied in many different fields of computational science, to problems with and without probabilistic content. It provides approximate solutions by performing statistical sampling experiments.

A large number N of samples of the uncertain parameters $\mathbf{x}_i$, for $i = 1, 2, \ldots, N$, is generated according to the parameters' probability distribution, and the respective response values $\mathbf{y}_i = \mathbf{f}(\mathbf{x}_i)$ are evaluated from equation (2.1). The response statistical properties, such as mean and variance, can be determined directly from the response samples.

A major advantage of the Monte Carlo simulation method is that accurate solutions can be obtained for problems whose deterministic solution is know. Since it is completely general the Monte Carlo simulation method is frequently used to calibrate and validate other methods. It is thereby the workhorse of the uncertainty propagation methods.

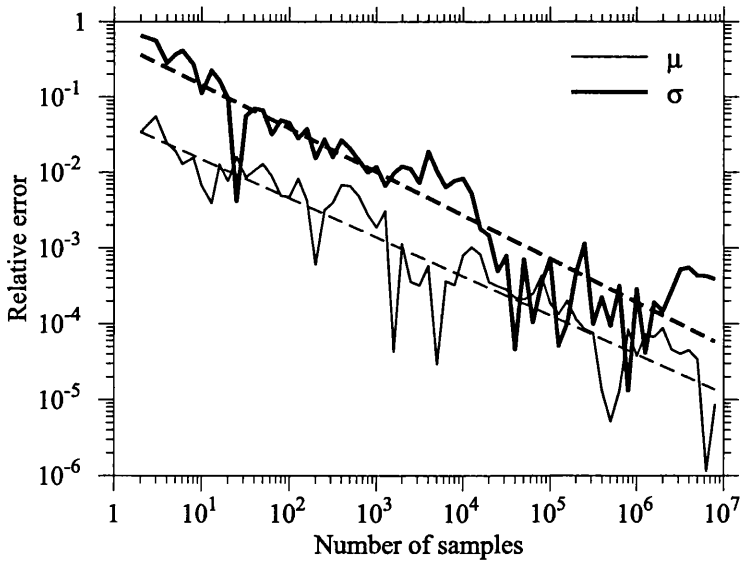

Figure 2.5: Convergence of the Monte Carlo method estimating the mean and standard deviation of a normal random variable $\mathrm{N}(\mu = 1, \sigma = 0.1)$.

The main disadvantage is that it is time consuming. Monte Carlo displays $1/\sqrt{N}$ convergence, i.e., it is necessary to perform one hundred times more experiments in

order to achieve another decimal place of accuracy in estimates. Figure 2.5 illustrates the Monte Carlo convergence by displaying the evolution of the mean and standard variance estimate errors of a normal random variable with the number of random samples taken for the estimate. Nevertheless, all other numerical methods that rely on N point evaluations in a n-dimensional space to produce an approximate solution have, in the absence of an exploitable special structure, an error that decreases as $N^{-1/n}$ at best. Therefore the Monte Carlo simulation method is frequently used for numerical integration in high dimensional and irregular domains [55].

Since each realisation is independent of all others, the Monte Carlo simulation method can be easily parallelised.

Sampling

The crucial step of the Monte Carlo method is the generation of samples that are compatible with the statistical information of the problem, such as spectral density, correlation, and density distributions.

Multivariate normal sampling When the uncertain parameters are multivariate Gaussian the Mahalanobis transformation can be used to transform the parameters into uncorrelated Gaussian variables.

A vector $\mathbf{X}$ of Gaussian (or normal) random variables is characterised by the vector of mean values $\boldsymbol{\mu}_X$ and the covariance matrix $\boldsymbol{\Sigma}_X$. A property of the covariance matrix is that it is *positive definite*, so there exists a linear transformation $\mathbf{Z} = \mathbf{C}\mathbf{X}$ that has a *diagonal* covariance matrix $\boldsymbol{\Sigma}_Z$ [75]. The new random variables of $\mathbf{Z}$ are uncorrelated and their variances are the eigenvalues of $\boldsymbol{\Sigma}_X$. The random vector $\mathbf{X}$ can be expressed as

$$\mathbf{X} = \boldsymbol{\mu}_X + \mathbf{C}^{-1}\boldsymbol{\Sigma}_Z^{1/2}\mathbf{Z} \tag{2.21}$$

where $\mathbf{Z}$ is a vector of uncorrelated normal variables with zero mean and unit variance.

Samples of $\mathbf{X}$ can be obtained by sampling $\mathbf{Z}$ and evaluating equation (2.21).

Latin hypercube sampling In the Monte Carlo simulation method, random sampling can be replaced by other adequate quasi-random or pseudo-random sampling sequences. A commonly used alternative is the Latin hypercube sampling (LHS).

In LHS the parameter space is partitioned in subspaces of equal probability, and samples are taken from each subspace ensuring that every parameter is covered evenly.

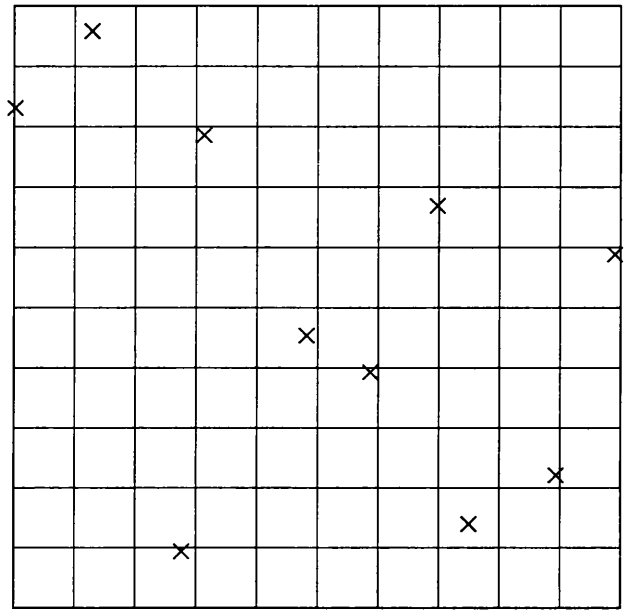

Figure 2.6: Latin hypercube sampling from a bidimensional parameter space

If sampling n samples of m independent parameters, the parameter space is divided into n subspaces for each parameter. Samples are taken randomly from each subspace such that for every parameter no sample is taken from the same subspace twice, as illustrated by figure 2.6 for a bidimensional parameter space.

The advantage of LHS over conventional random sampling is that if the response is dominated by a single parameter then it guarantees that the response is evaluated for all levels of that parameter. Conventional sampling does not guarantee that. If the response is dominated by more than a single parameter, the LHS provides no clear advantage over other sampling methods.

LHS can also be performed adaptively [63], whereby subspaces are again subdivided by an integer number, allowing further samples to be generated without

discarding the existing set.

Kernel Density Estimation

Response statistics such as mean, variance, and higher order moments can be directly calculated from the response samples. However, continuous probability density functions cannot be calculated directly from discrete response samples. Kernel density estimation allows the estimation of probability density functions from a discrete set of samples, so it can be used together with the Monte Carlo simulation method to estimate the response probability density function.

If $[\mathbf{x}_1\, \mathbf{x}_2\, \ldots\, \mathbf{x}_N]$ are the N parameter samples generated during the Monte Carlo simulation method and $[\mathbf{y}_1\, \mathbf{y}_2\, \ldots\, \mathbf{y}_N]$ are the respective response evaluations then the response probability density function can be estimated using the kernel density estimator [66, 34] as

$$\hat{f}(\mathbf{y}|\boldsymbol{\theta}_x) = \frac{1}{N}\sum_{i=1}^{N} \kappa_{\mathbf{H}}(\mathbf{y} - \mathbf{y}_i) \tag{2.22}$$

where $\kappa_{\mathbf{H}}$ is the kernel function with a $\mathbf{H}$ bandwidth matrix

$$\kappa_{\mathbf{H}}(\mathbf{y}) = |\mathbf{H}|^{-1}\kappa\left(\mathbf{H}^{-1}\mathbf{y}\right) \tag{2.23}$$

The multivariate normal is a common choice of kernel function, where

$$\kappa(\mathbf{y}) = (2\pi)^{-m/2} e^{-\mathbf{y}^{\mathrm{T}}\mathbf{y}/2} \tag{2.24}$$

A careful choice for the bandwidth matrix must be made for accurate estimates. Härdle et al. [34] suggested the following rule-of-thumb

$$\mathbf{H} = N^{-1/(m+4)}\boldsymbol{\Sigma}_y^{1/2} \tag{2.25}$$

where $\boldsymbol{\Sigma}_y$ is the covariance matrix of the response samples, but if the number of parameters n is smaller than the response dimensionality m then the response components are necessarily dependent, and better results are achieved using

$$\mathbf{H} = N^{-1/(d+4)}\boldsymbol{\Sigma}_y^{1/2} \tag{2.26}$$

where $d = \min(n, m)$ is the effective number of degrees of freedom in the response.

2.3.2 Perturbation method

The perturbation method is equivalent to a low-order Taylor expansion, and has been widely used for its tractability and computational time-saving [65]. It expresses the structural matrices and response in terms of a low-order polynomial function with respect to the parameters centred at the mean values, i.e., it makes an approximation of the response surface.

It is assumed that the uncertain parameters follow a multivariate normal distribution

$$\mathrm{X} \sim \mathrm{N}_n \left(\boldsymbol{\mu}_x, \boldsymbol{\Sigma}_x \right) \tag{2.27}$$

This incurs no loss in generality as random variables can be transformed into Gaussian variables, as mentioned in section 2.2.5.

For the perturbation method equation (2.1) is first expanded as

$$\begin{aligned} \mathbf{y} &= \mathbf{f}(\boldsymbol{\mu}_x) \\ &+ \sum_{i=1}^{n} \frac{\partial \mathbf{f}}{\partial x_i}(\boldsymbol{\mu}_x) \cdot (x_i - \mu_{x_i}) \\ &+ \frac{1}{2} \sum_{i=1}^{n} \sum_{j=1}^{n} \frac{\partial^2 \mathbf{f}}{\partial x_i \partial x_j}(\boldsymbol{\mu}_x) \cdot (x_i - \mu_{x_i}) \cdot (x_j - \mu_{x_j}) \\ &+ \cdots \end{aligned} \tag{2.28}$$

around the mean point $\boldsymbol{\mu}_x$. Taking only the first order terms, equation (2.28) can be rewritten as

$$\mathbf{y} \approx \mathbf{f}(\boldsymbol{\mu}_x) + \mathbf{J} \cdot (\mathbf{x} - \boldsymbol{\mu}_x) \tag{2.29}$$

where $\mathbf{J}$ is the Jacobian of $\mathbf{f}$, evaluated at the point $\boldsymbol{\mu}_x$. From equations (2.27) and (2.29),

$$\mathrm{Y} \sim \mathrm{N}_m \left(\boldsymbol{\mu}_y, \boldsymbol{\Sigma}_y \right) \tag{2.30}$$

where

$$\boldsymbol{\mu}_y = \mathbf{f}(\boldsymbol{\mu}_x) \tag{2.31}$$

$$\boldsymbol{\Sigma}_y = \mathbf{J}\boldsymbol{\Sigma}_x\mathbf{J}^{\mathrm{T}} \tag{2.32}$$

The response joint probability density function is then given by

$$f_{\mathrm{Y}}(\mathbf{y}) = (2\pi)^{-m/2}|\boldsymbol{\Sigma}_y|^{-1/2}e^{-(\mathbf{y}-\boldsymbol{\mu}_y)^{\mathrm{T}}\boldsymbol{\Sigma}_y^{-1}(\mathbf{y}-\boldsymbol{\mu}_y)/2} \tag{2.33}$$

Natural frequency derivatives Introducing the following notation

$$\Phi^0 = \Phi(\mu_{x_1}, \mu_{x_2}, \ldots, \mu_{x_n}) \tag{2.34}$$

$$\Phi_i^I = \frac{\partial \Phi}{\partial x_i}(\mu_{x_1}, \mu_{x_2}, \ldots, \mu_{x_n}) \tag{2.35}$$

$$\Phi_{ij}^{II} = \frac{\partial^2 \Phi}{\partial x_i \partial x_j}(\mu_{x_1}, \mu_{x_2}, \ldots, \mu_{x_n}) \tag{2.36}$$

for any variable Φ which depends on the parameters $x_1, x_2, \ldots, x_n$, then the stiffness and mass matrices are expanded as

$$\mathbf{K} = \mathbf{K}^0 + \sum_{i=1}^{n} \mathbf{K}_i^I \epsilon_i + \frac{1}{2}\sum_{i=1}^{n}\sum_{j=1}^{n} \mathbf{K}_{ij}^{II} \epsilon_i \epsilon_j + \cdots \tag{2.37}$$

$$\mathbf{M} = \mathbf{M}^0 + \sum_{i=1}^{n} \mathbf{M}_i^I \epsilon_i + \frac{1}{2}\sum_{i=1}^{n}\sum_{j=1}^{n} \mathbf{M}_{ij}^{II} \epsilon_i \epsilon_j + \cdots \tag{2.38}$$

where $\epsilon_i = x_i - \mu_{x_i}$. In the same manner, for the eigenvalue problem

$$(\mathbf{K} - \lambda\mathbf{M})\boldsymbol{\phi} = 0 \tag{2.39}$$

the resulting eigenvalues λ and eigenvectors $\boldsymbol{\phi}$ are expanded as

$$\lambda = \lambda^0 + \sum_{i=1}^{n} \lambda_i^I \epsilon_i + \frac{1}{2}\sum_{i=1}^{n}\sum_{j=1}^{n} \lambda_{ij}^{II} \epsilon_i \epsilon_j + \cdots \tag{2.40}$$

$$\boldsymbol{\phi} = \boldsymbol{\phi}^0 + \sum_{i=1}^{n} \boldsymbol{\phi}_i^I \epsilon_i + \frac{1}{2}\sum_{i=1}^{n}\sum_{j=1}^{n} \boldsymbol{\phi}_{ij}^{II} \epsilon_i \epsilon_j + \cdots \tag{2.41}$$

The mean and variances of the eigenvalues are

$$\mathrm{E}[\lambda] = \lambda^0 + \frac{1}{2}\sum_{i=1}^{n}\sum_{j=1}^{n}\lambda_{ij}^{II}\mathrm{Cov}[x_i, x_j] + \cdots \tag{2.42}$$

$$\mathrm{Var}[\lambda] = \sum_{i=1}^{n}\sum_{j=1}^{n}\lambda_i^I\lambda_j^I\mathrm{Cov}[x_i, x_j] + \cdots \tag{2.43}$$

It can be shown that λ^I is given by [22, 61, 48]

$$\lambda_i^I = \frac{\boldsymbol{\phi}^{0T}\left(\mathbf{K}_i^I - \lambda^0\mathbf{M}_i^I\right)\boldsymbol{\phi}^0}{\boldsymbol{\phi}^{0T}\mathbf{M}\boldsymbol{\phi}^0} \tag{2.44}$$

where λ^0 and $\boldsymbol{\phi}^0$ are obtained by the mean eigenvalue problem

$$(\mathbf{K}^0 - \lambda^0\mathbf{M}^0)\boldsymbol{\phi}^0 = 0 \tag{2.45}$$

The natural frequencies can be expanded as

$$\begin{aligned}\omega &= \sqrt{\lambda} \\ &= \mu_\lambda^{\frac{1}{2}} + \frac{1}{2}\mu_\lambda^{-\frac{1}{2}}(\lambda - \mu_\lambda) - \frac{1}{8}\mu_\lambda^{-\frac{3}{2}}(\lambda - \mu_\lambda)^2 + \cdots\end{aligned} \tag{2.46}$$

Considering up to the first order term, the mean and standard deviation of the natural frequencies can be obtained from equations (2.42) and (2.43) as

$$\mu_\omega = \sqrt{\mu_\lambda} \tag{2.47}$$

$$\sigma_\omega = \frac{1}{2\sqrt{\mu_\lambda}}\sigma_\lambda \tag{2.48}$$

A detailed study of the distribution of eigenvalues was carried out by Adhikari and Langley [1]. Fox and Kapoor [22], Rudisill and Chu [61] developed efficient numerical methods to calculate the eigenvector derivatives. Qu [57] described methods to calculate frequency response functions derivatives using the modal superposition.

Limitations The perturbation method requires that the random variables involved in the analysis do not deviate much from their expected values. If the coefficient of

variation is insufficiently small then the solution cannot ever be improved by using a finer mesh [16].

Of greater importance than the magnitude of variability of the original random variables is how appropriate the response surface is. The response quantity should be chosen in such a way that these quantities are mostly linear with respect to the random variables, e.g., natural frequencies instead of a response in the time domain [65].

If the number of random variables is large, such as in problems involving random fields, or if a high-order expansion is used, then the calculation effort becomes prohibitive.

2.3.3 Fuzzy method

A common fuzzy finite element approach is to replace the crisp stiffness and mass matrices by fuzzy-valued matrices, and then solve the interval eigenvalue problem at each α-level.

Due to the lack of certain properties of fuzzy numbers almost all classical numerical techniques cannot be directly extended to fuzzy arithmetic. A method used to determine the upper and lower bounds of the eigenvalues was proposed by Qiu et al. [56]. The i-th eigenvalue lower bound $\underline{\lambda}_i$ and upper bound $\overline{\lambda}_i$ for each α-level satisfy

$$\underline{\mathbf{K}}\underline{\boldsymbol{\phi}}_i = \underline{\lambda}_i \overline{\mathbf{M}}\underline{\boldsymbol{\phi}}_i \tag{2.49}$$

$$\overline{\mathbf{K}}\overline{\boldsymbol{\phi}}_i = \overline{\lambda}_i \underline{\mathbf{M}}\overline{\boldsymbol{\phi}}_i \tag{2.50}$$

where $\underline{\mathbf{K}}$ and $\overline{\mathbf{K}}$ are the lower and upper bound of the stiffness matrix and $\underline{\mathbf{M}}$ and $\overline{\mathbf{M}}$ are the lower and upper bound of the mass matrix, for each α-level.

A major computational difficulty with fuzzy arithmetic is the problem of overestimating the interval widths of the response quantities when the problem involves multiple occurrences of the same variable. To avoid this problem a combinatorial analysis of the upper and lower bounds of the parameters can be used, but involves 2^n times the crisp computational effort. Chen and Rao [4] proposed a methodology using Taguchi's philosophy to choose the parameters for which the optimal settings

should be found. Lallement *et al.* [40] developed a reanalysis technique to solve the uncertain eigenvalue problem and reduce the computational effort.

2.3.4 Meta modelling

A meta-model is not an uncertainty propagation method *per se*, but it can be used together with the sampling and convex uncertainty propagation methods to reduce the calculation time.

Most models have a smooth response surface, whereby neighbouring points in the parameter space map to neighbouring points in the response space. A meta-model takes advantage of this redundancy.

A meta-model is a fast-running surrogate of the model's response surface. It captures the input/output relationship over the domain of interest at a fraction of the computational time. Common meta-models are polynomials and artificial neural-networks.

Equation (2.1) is replaced by

$$\mathbf{y} = h(\mathbf{x}) + \epsilon \tag{2.51}$$

where $h(\mathbf{x})$ is the surrogate for $f(\mathbf{x})$, and ϵ is the error residual (or noise level).

The problem of constructing $h(\mathbf{x})$ from evaluations of $f(\mathbf{x})$ can be seen as a design of experiments problem. However, there are differences between the design of physical and computer experiments. Replicate observations of computer experiments will produce the same response, but physical experiments do not. This calls for different techniques, which are discussed by Sacks et al. [62].

Once an appropriate meta-model is constructed, the meta-model evaluations are cheap. So, together with a meta-model, the Monte Carlo method becomes more attractive, allowing more samples to be evaluated in a fraction of the time.

Chapter 3

Comparison of the uncertainty propagation methods

3.1 Introduction

The uncertainty propagation methods thrived in the risk modelling and structural reliability communities, but the different requirements and aims of structural dynamics applications pose other challenges. The purpose of this chapter is to study the application of the major uncertainty propagation methods to the specific field of structural dynamics, and to provide guidelines to aid the determination of which method is appropriate for a given kind of application, and which is not.

The scope of this work is actually narrower. The focus is not a single system with random excitation or unknown properties, such as the building response to an earthquake, but instead on repeated systems with intrinsic variability. For example, the frequency response of a number of car body-in-white produced in series. So care is required not only in preventing the occurrence of extreme events, but also in attaining good mean behaviour.

While there are some comparisons of uncertainty propagation methods available in the literature, few concern structural dynamics applications, and the depth of existing comparisons is mostly superficial. In the *IASSAR report on Computational Stochastic Mechanics* [65] the potential and limitations of the Monte Carlo simulation method and the perturbation method for stochastic mechanics were assessed,

but no comparison is made *per se*. de Lima and Ebecken [9] compared the Monte Carlo simulation, perturbation, and fuzzy uncertainty propagation methods on the displacement of simple structures under static loading where the Young's modulus was a random field. They found that, when the coefficient of variation of the random properties is less than 20%, the perturbation approach rendered the required precision in most applications, and also that the fuzzy method rendered good results, despite the use of triangular membership functions.

The three most common uncertainty propagation methods will be compared: the Monte Carlo simulation method, the perturbation method and the fuzzy method. The main application features that will be taken into account in the comparison are the number of parameters, the level of parameter variability, and the structure complexity. The two main benchmarks are accuracy and efficiency, and how these change for a wide range of applications, i.e., applicability and scalability, respectively. The methods will be applied to vibration applications of increasing complexity: a cantilever beam with uncertain thickness, a beam with an uncertain clamping stiffnesses, a beam with an uncertain thickness and a compressor blade with an uncertain thickness. The set of applications tries to capture particularly difficult situations for each method, and to cover a reasonable range of complexity. The chosen response quantities are modal frequencies and FRFs.

Note that the equivalence between possibilistic and probabilistic uncertainty representations is not a consensual matter. On the one hand, there is more than one way to convey probabilistic information in a fuzzy set (some of which were mentioned in section 2.2.3). On the other hand, some assert that no attempt of a probabilistic interpretation from fuzzy sets should be made at all, arguing these are two totally dissimilar concepts. This disagreement must be taken in consideration while interpreting the results presented in this chapter comparing fuzzy to the remaining methods.

3.2 Applications

3.2.1 Cantilever beam with point mass at uncertain position

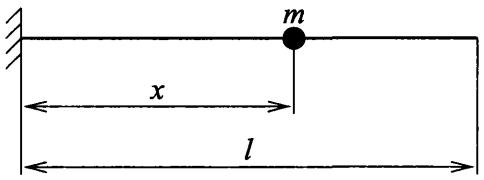

Figure 3.1: Application 1 – cantilever beam with point mass at uncertain position

The first application is a cantilever beam with a point mass at an uncertain position, as illustrated by figure 3.1. This is the most simple application presented here, having just a single parameter.

Table 3.1: Beam geometry

Dimension			
length	l	=	1000 mm
width	b	=	20 mm
height	h	=	2 mm

Table 3.2: Steel properties

Property			
Young modulus	E	=	210 GPa
Poisson coefficient	ν	=	0.3
density	ρ	=	7800 kg/m^3

The beam has a rectangular cross-section with dimensions specified in table 3.1, and it is made of steel with properties given in table 3.2.

The mass has a value of $m = 0.1\,\text{kg}$ and its position, x, follows a normal distribution with mean $\mu_x = 750\,\text{mm}$, and coefficient of variation (COV) $\sigma_x/\mu_x = 5\%$.

The beam is discretised into 20 elements, except where stated otherwise.

3.2.2 Cantilever beam with uncertain joint

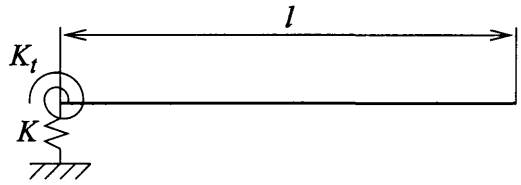

Figure 3.2: Application 2 – cantilever beam with an uncertain joint

The second application is a more realistic application which attempts to mimic an uncertain joint. It is similar to the beam described in section 3.2.1, with the exception that no mass is attached and the clamping stiffnesses are uncertain, as illustrated in figure 3.2.

The two uncertain parameters are the spring stiffness K and the torsional spring stiffness K_t. They follow a normal distribution with means $\mu_K = 200\,\mathrm{N/m}$ and $\mu_{K_t} = 10 \times 10^3\,\mathrm{N/rad}$ respectively, and a COV of 5% for both parameters.

3.2.3 Cantilever beam with uncertain thickness

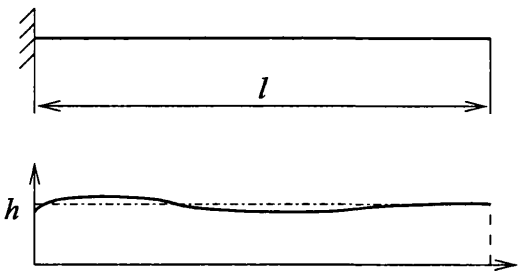

Figure 3.3: Application 3 – cantilever beam with uncertain thickness

The third application introduces the use of a random field. The beam described in section 3.2.1 is used, but with a uncertain thickness h, as illustrated in figure 3.3.

The thickness is modelled as a first-order auto-regressive random field with mean $\mu_h = 2\,\mathrm{mm}$, COV $\sigma_h/\mu_h = 5\%$ and correlation length $L = 100\,\mathrm{mm}$. The random field was discretised by the mid-point method, therefore resulting in a number of random parameters equal to the number of elements.

3.2.4 Compressor blade

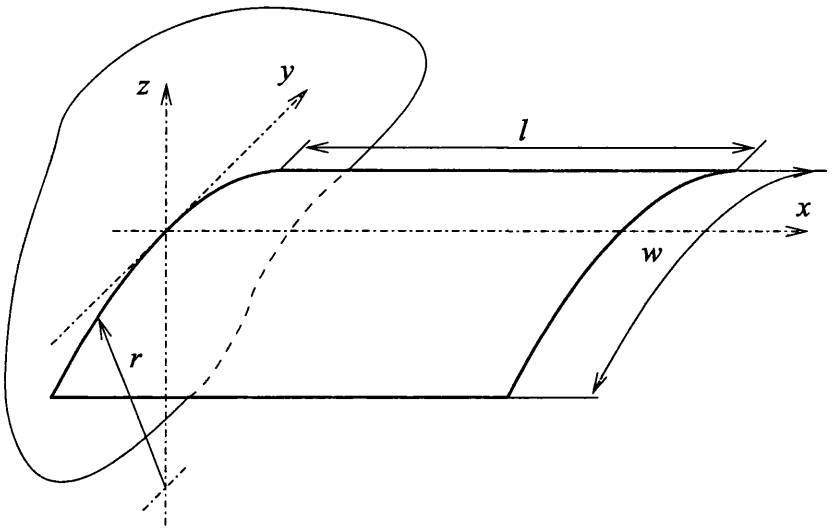

Figure 3.4: Application 4 – compressor blade with uncertain thickness

The last and most complex application is a compressor blade with uncertain thickness, as illustrated in figure 3.4.

Table 3.3: Blade geometry

Dimension				
length	l	=	304.8 mm	(12 in)
curvature radius	r	=	609.6 mm	(12 in)
curved width	w	=	304.8 mm	(24 in)
thickness	t	=	3.0 mm	(.12 in)

The blade nominal dimensions are given in table 3.3 and the blade is made of the same steel specified in table 3.2.

The thickness is modelled as a first-order auto-regressive random field with mean $\mu_t = 3.0\,\text{mm}(.12\,\text{in})$, COV $\sigma_t/\mu_t = 5\%$, and correlation length $L = 30.5\,\text{mm}(1.2\,\text{in})$.

The blade was modelled with a $4 \times 4 = 16$ element rectangular mesh, unless stated otherwise.

3.3 Methodology

Monte Carlo simulation method For the Monte Carlo simulation method, 10000 samples were used, unless stated otherwise. Compared to the other methods, the Monte Carlo results represent an accurate approximation of the true values.

Modes were tracked across the samples using the modal assurance criterion (MAC) to detect crossings in the natural frequencies.

The response probability density functions were estimated using kernel density estimation, as described in section 2.3.1.

Perturbation method The standard first-order perturbation approach was used. The derivatives of the stiffness and mass matrices were computed numerically by perturbing each parameter by a very small amount and reevaluating the affected element stiffness and mass matrices.

The eigenvalue, eigenvector, and FRF derivatives were calculated according to the procedures referred to in section 2.3.2.

Fuzzy method For the fuzzy method the normalised probability density function was taken as the membership function for the parameters, and vice-versa for the response. The number of α-cuts used is 4.

The response membership functions are evaluated in three passes. First, the response partial derivatives are computed for the crisp value of the parameters. Second, the response is evaluated for the combination of parameter bounds which maximise/minimise the response for each α-cut, assuming the response is monotonic within those intervals. Third, using the points of the intervals contained in each other (no further response evaluation), the response membership function intervals are adjusted [grown] in face of any detected nonmonotonicity. This procedure tries to capture the most information from a conservative number of response evaluations. It produces true bounds if the response is monotonic or inner bounds otherwise.

Appendix A gives more details about the implementation of these methodologies and applications.

3.4 Results

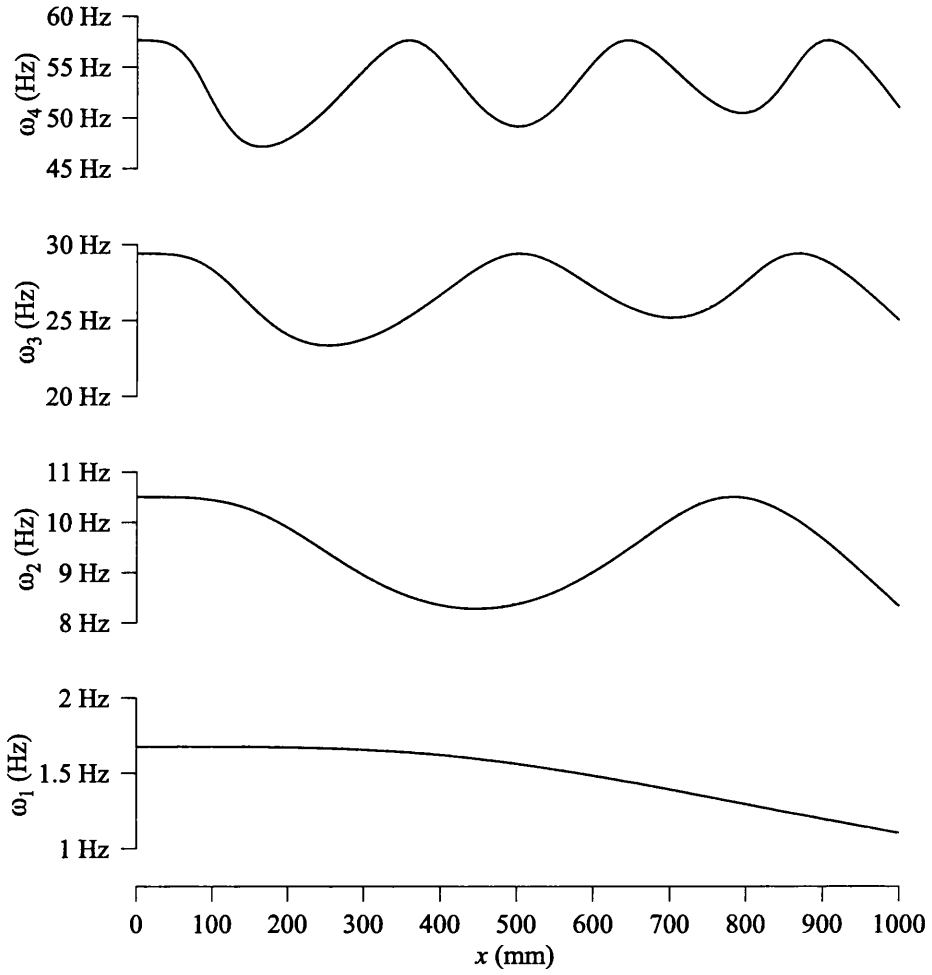

Figure 3.5: Application 1 – response curve of the first four natural frequencies of the cantilever beam vs. the point mass position.

Application 1 Having a single parameter the response surface for application 1 is reduced to a curve, allowing easy visualisation. Figure 3.5 shows the first four natural frequencies with respect to the uncertain parameter value (the point mass position). The most outstanding feature of this response is the increasing nonlinearity for the higher modes. This means that for the perturbation method the estimates of the standard deviations of the natural frequencies are worse for higher natural frequencies, as shown in figure 3.6. As expected this adversity can be either aggra-

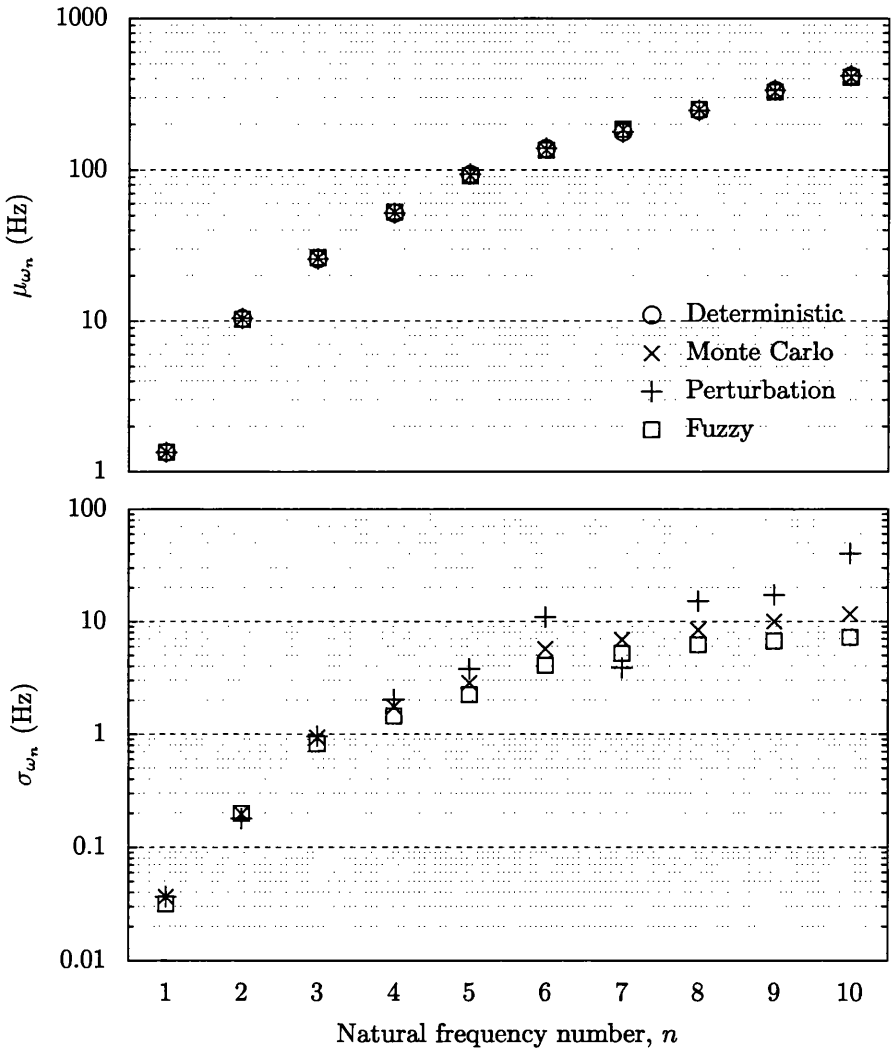

Figure 3.6: Application 1 – the mean and standard deviation of the natural frequencies estimated by several uncertainty propagation methods.

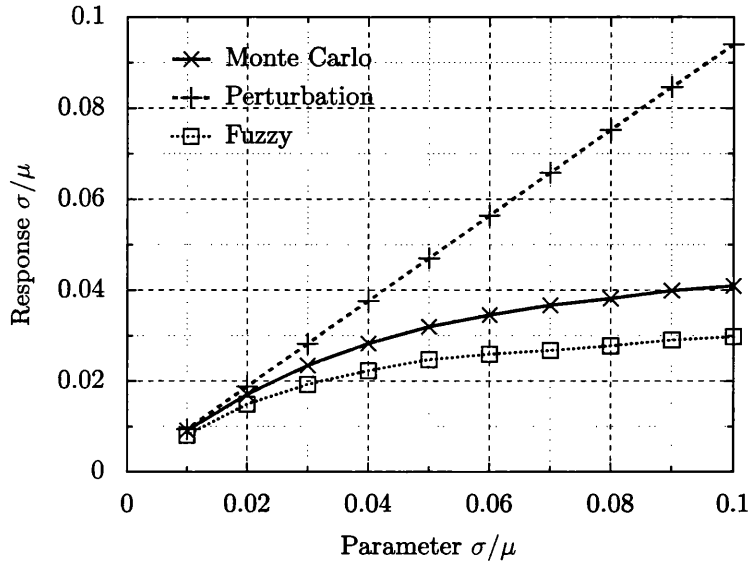

Figure 3.7: Application 1 – response COVs estimated by several uncertainty propagation methods with respect to the mass position COV. The ordinates axis is the average COV for the first ten natural frequencies.

vated or softened by increasing or decreasing the parameter variability, respectively. Figure 3.7 shows how the response COV estimated by each uncertainty propagation method varies with the parameter COV. The perturbation method, owing to the first-order approximation of the response curve, shows a perfectly linear relationship between the parameter COV and the response COV, which rapidly departs from the true values (given by the Monte Carlo method).

The fuzzy method estimates in figures 3.6 and 3.7 are substantially better (i.e., closer to the Monte Carlo estimates) than those obtained by the perturbation method. This is expected as the fuzzy method can capture the nonlinear parameter/response relationship, since the α-cut interval bounds of the response membership function are taken directly from response evaluations. On other hand, the natural frequency response for this application is nonmonotonic for modes higher than the first (recall figure 3.5), which breaks the assumption made for the fuzzy method. Indeed the fuzzy method, as implemented here, is unable to determine the true membership bounds, as suggested by the probability density function of the second natural frequency in figure 3.8.2. Nevertheless, the response variability – given by the area enclosed by the membership function – is quite close to the area

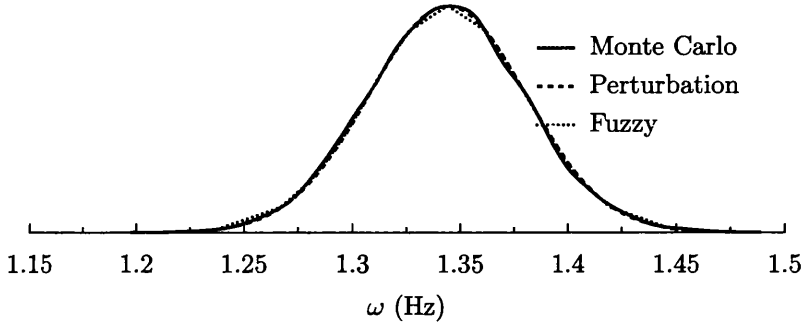

3.8.1: First natural frequency

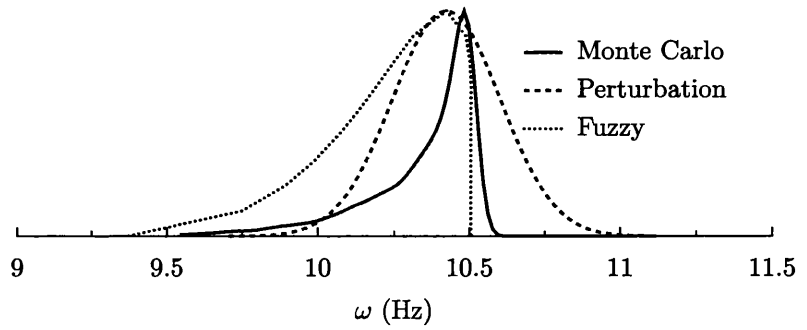

3.8.2: Second natural frequency

Figure 3.8: Application 1 – normalised probability density functions of the first two natural frequencies estimated by several uncertainty propagation methods.

obtained by the Monte Carlo simulation method, and hence relatively good overall results are obtained with the fuzzy method. However, the probability estimates in the tail would be poor, and a global optimisation procedure would have to be employed for each α-cut in order to find the true interval boundaries. Performing a global optimisation procedure, or employing any other fuzzy method variant which avoids the response monotonicity assumption, requires a excessive number of system response evaluations, as will be shown later.

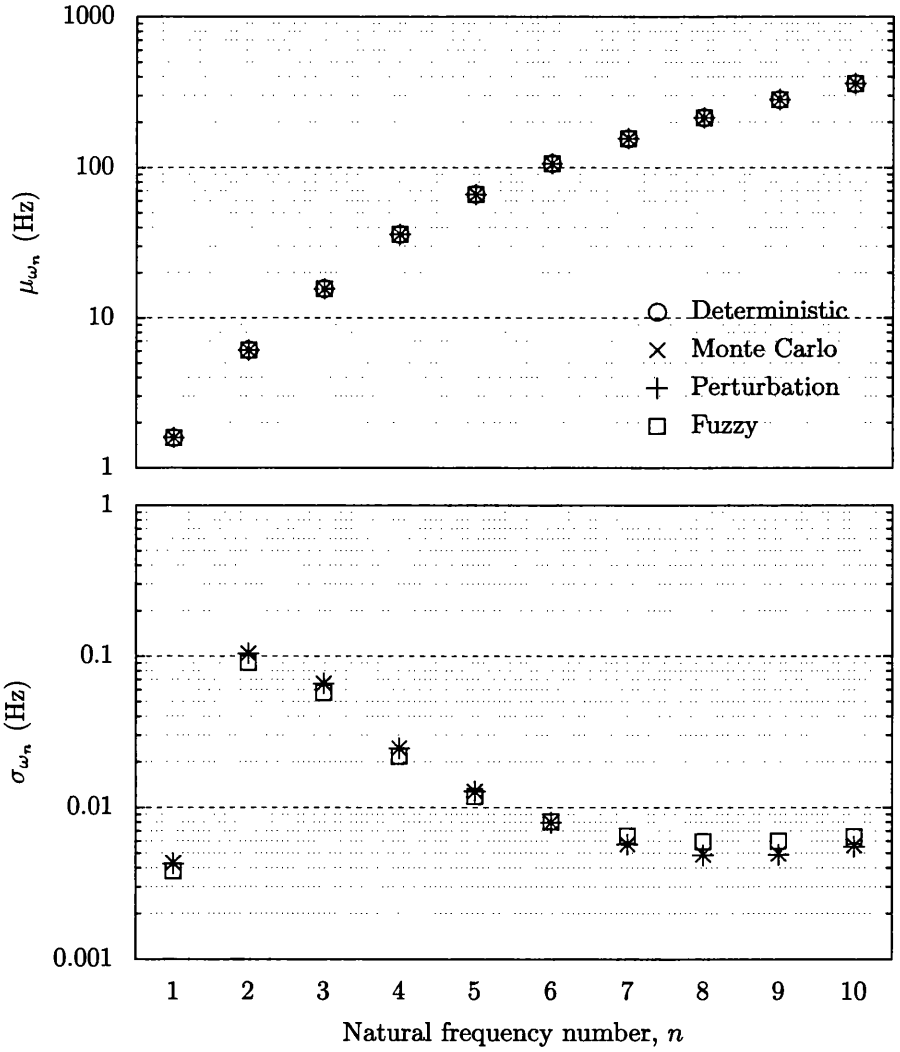

Figure 3.9: Application 2 – the mean and standard deviation of the natural frequencies estimated by several uncertainty propagation methods.

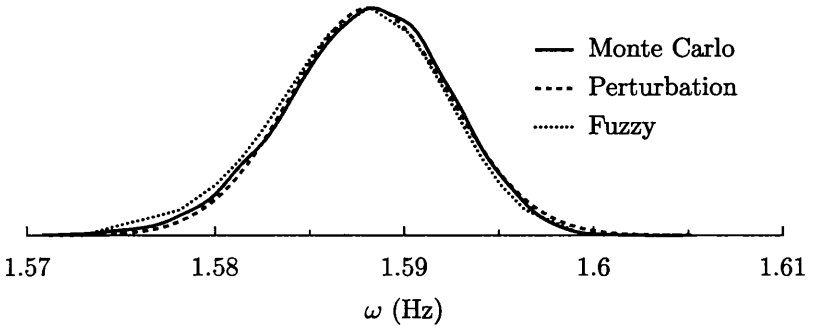

3.10.1: First natural frequency

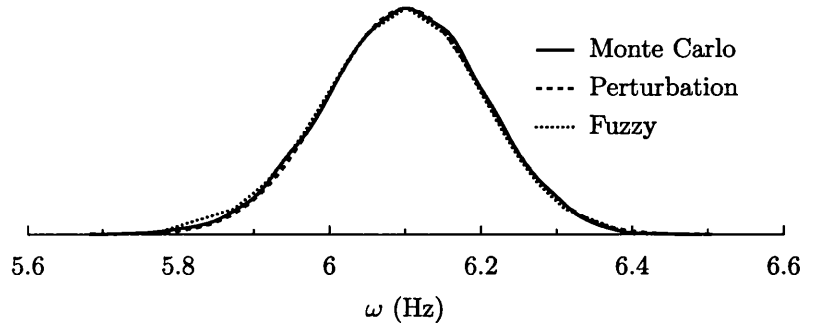

3.10.2: Second natural frequency

Figure 3.10: Application 2 – normalised probability density functions of the first two natural frequencies estimated by several uncertainty propagation methods.

Application 2 In application 2, the second natural frequency has the largest variation and the first natural frequency has the smallest, as shown in figure 3.9. But their probability density functions have the same slightly asymmetric bell shape (only with different mean and variance), as shown in figure 3.10.

As seen in figure 3.11, the perturbation method is valid over a wider range of parameter COV for this application than in the previous application (figure 3.7). The range is almost 25% against just 2% for application 1, which shows that the parameter COV is not the only limiting factor for employing the perturbation method – the response surface nonlinearity, and hence the application itself, is also a determining factor.

Application 3 The mean and standard deviation of the natural frequencies for application 3 obtained by the Monte Carlo and perturbation methods are quite similar, as shown in figure 3.12, but the standard deviations obtained with the fuzzy

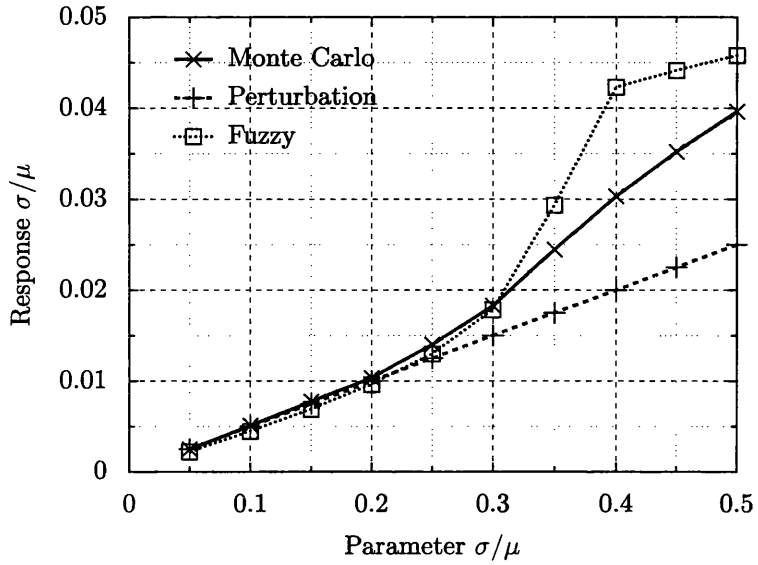

Figure 3.11: Application 2 – response COVs estimated by several uncertainty propagation methods with respect to the clamping stiffnesses COV. The ordinates axis is the average COV for the first ten natural frequencies.

method are slightly overestimated. This can be seen in more detail by comparing the estimated probability density functions in figure 3.13. This overestimation in standard deviation is most likely because the fuzzy method does not model the correlation between parameters. Parameters are seen as independent intervals for each α-cut, and the response interval upper/lower bounds for each α-cut are computed by choosing the parameter bound combination which maximises/minimises the response, regardless of how likely that combination is. For example, when choosing interval bound combinations of two positively correlated parameters, the fuzzy method makes no distinction between choosing the upper (or lower) bounds for both parameters (more likely) and choosing the diametrical bounds for each parameter (less likely). Often different parameters concern unrelated physical phenomena, and therefore are independent and uncorrelated. But a common situation where correlated parameters appear, and in a significant number, is as the result of discretising random fields – as with this application. This causes, for each α-cut, the choice of parameters combinations which are less possible than the possibility level specified by α, and, therefore, the estimation of wider response membership functions.

To compare the behaviour of the methods for large variations, figure 3.14 shows

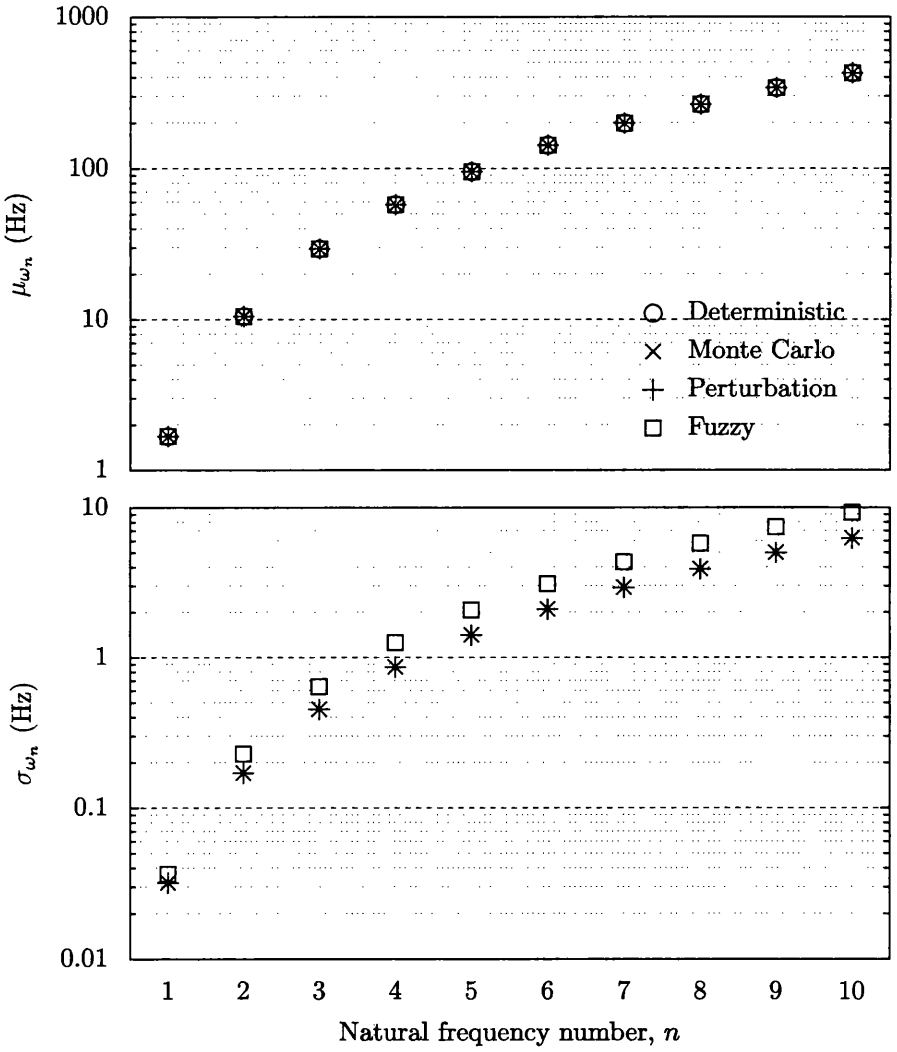

Figure 3.12: Application 3 – the mean and standard deviation of the natural frequencies estimated by several uncertainty propagation methods.

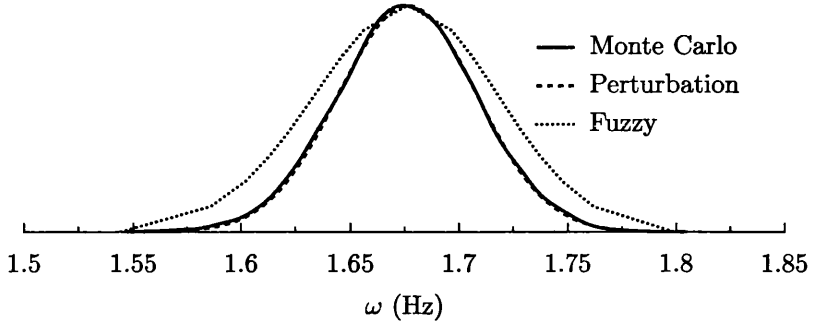

3.13.1: First natural frequency

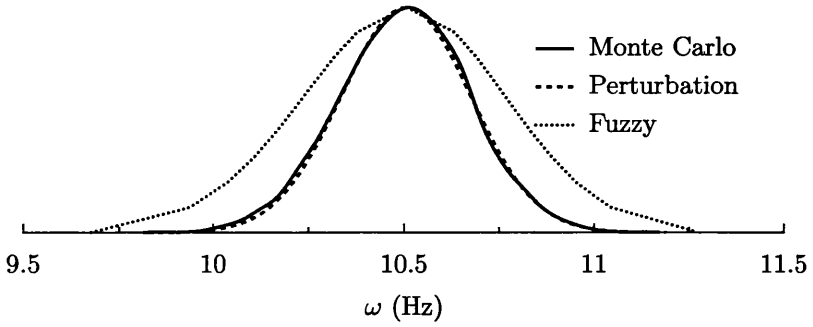

3.13.2: Second natural frequency

Figure 3.13: Application 3 – normalised probability density functions of the first two natural frequencies estimated by several uncertainty propagation methods.

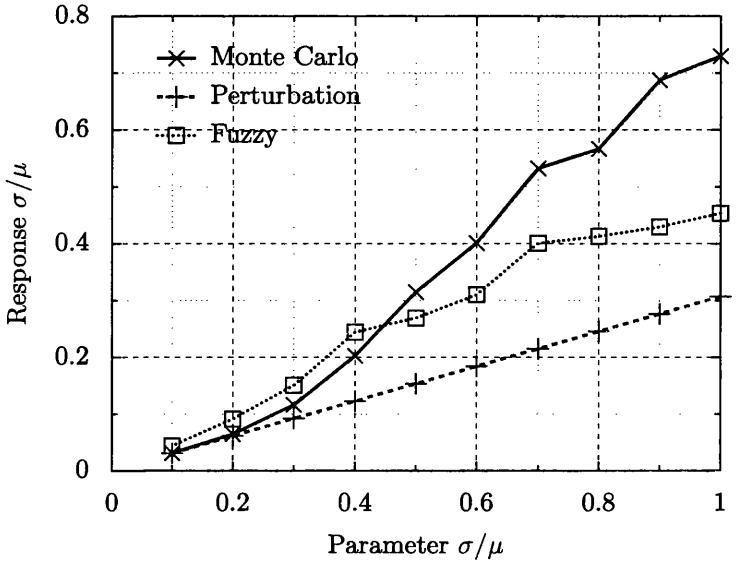

Figure 3.14: Application 3 – response COV with respect to the Young's modulus COV. The response COV used here was taken as the average COV of the first ten natural frequencies.

how the response COV varies with respect to the parameter COV. As expected, the perturbation methods shows again a perfectly linear relationship between the parameter COV and response COV, but that estimate is far from reality, as evidenced by the Monte Carlo curve. The fuzzy method can capture some of the nonlinear parameter/response relationship since the α-cut intervals are computed from the system response evaluation, but it is still far from accurate.

Application 4 The fuzzy variability overestimation is aggravated with the two dimensional random field in application 4, as shown in figures 3.15 and 3.16. The perturbation method gives goods results for a parameter COV up to 25%, as shown in figure 3.17.

FRFs Figure 3.18 shows the estimated FRFs of application 3 using several propagation methods. The FRF mean and $\pm 3\sigma$ envelope predicted by the Monte Carlo and perturbation methods are reasonably close. The peaks are where more differences can be found. In some peaks the mean FRF predicted by the Monte Carlo method looks flattened when compared to the deterministic FRF, but the perturba-

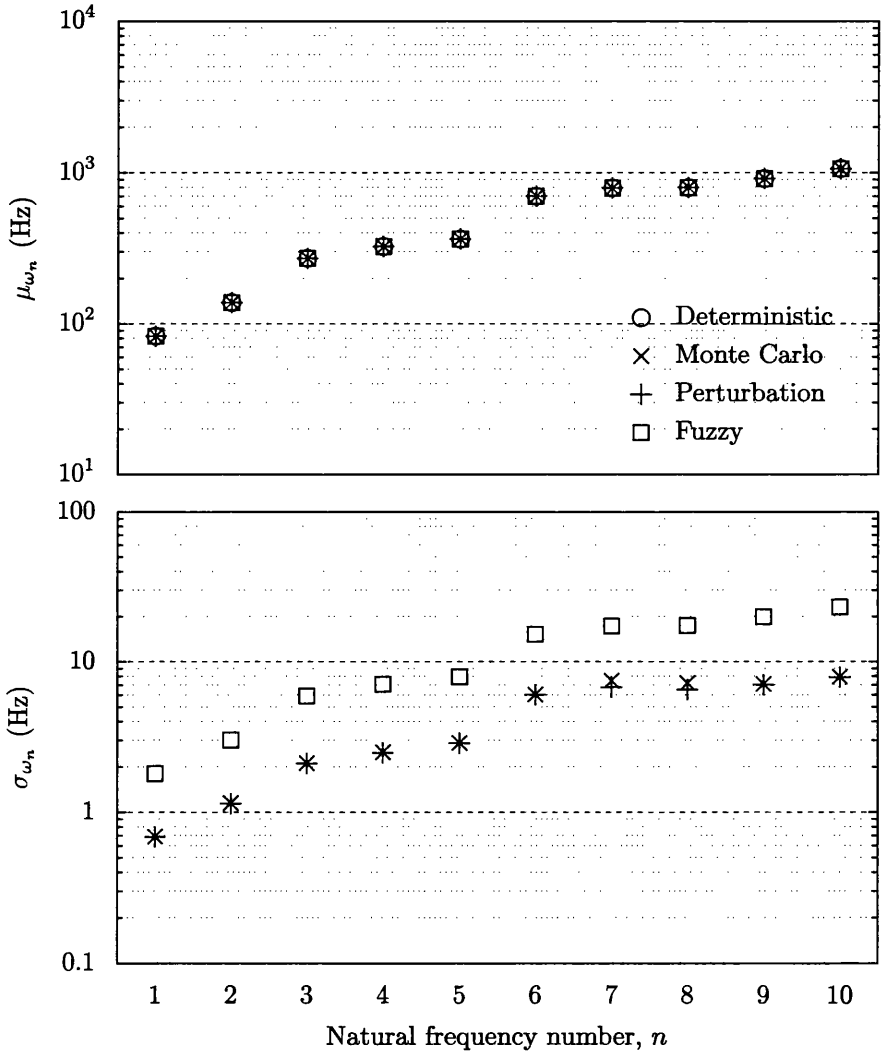

Figure 3.15: Application 4 – the mean and standard deviation of the compressor blade natural frequencies using several methods.

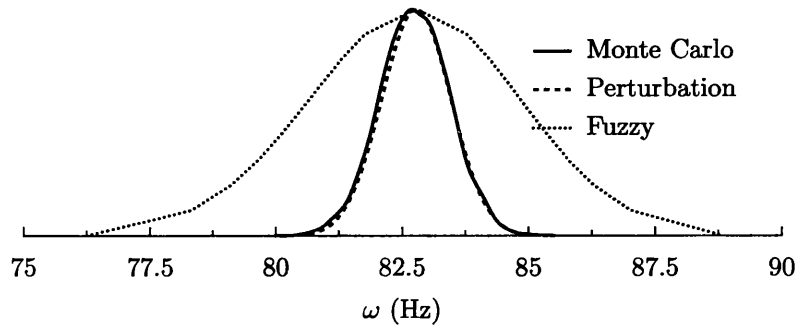

3.16.1: First natural frequency

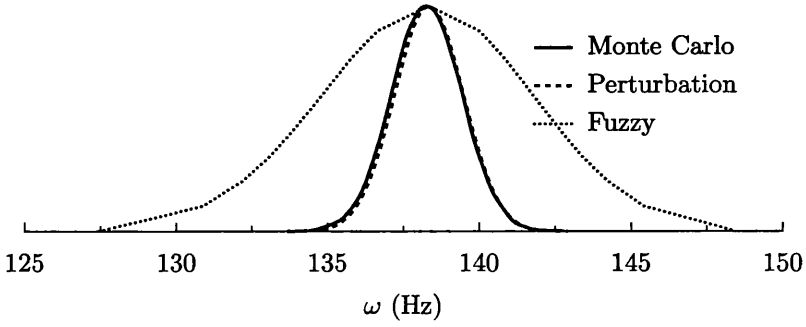

3.16.2: Second natural frequency

Figure 3.16: Application 4 – normalised probability density functions of the natural frequencies of the compressor blade obtained by several methods.

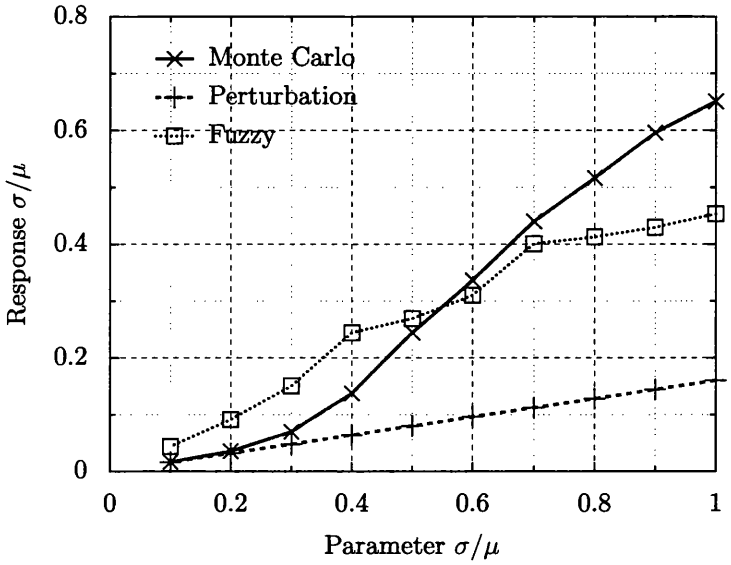

Figure 3.17: Application 4 – response coefficient of variance (COV) with respect to the thickness COV. The ordinates axis is the average of the first ten natural frequencies COV.

tion method fails to observe that. The reason is that no damping was used, yielding an infinite FRF peak at the natural frequencies and therefore a highly nonlinear response surface around them. The mean FRF obtained by the perturbation method is always equal to the deterministic FRF for the mean value of the parameters. Nevertheless the $\mu + 3\sigma$ envelope is quite close, even around the peaks.

No FRFs were obtained with the fuzzy method because the method is unsuited for such high dimension response quantities and parameters. For a problem with n parameters and m response variables the use of the fuzzy method with k α-cuts in its most simple form (assuming a monotonic response surface) requires up to $1 + n + k \times 2 \times m$ response evaluations (if computing the derivatives numerically, followed by the parameter combinations which maximises/minimises the response for each α-cut), or k^n (if propagating the full set of bounding vertices in the parameter space). So, to compute an example with 20 parameters, 4 α-cuts, and a 261 point FRF (as the one shown) the fuzzy method would require 885 evaluations. The Monte Carlo method provides competitive results with a number of samples of the same order.

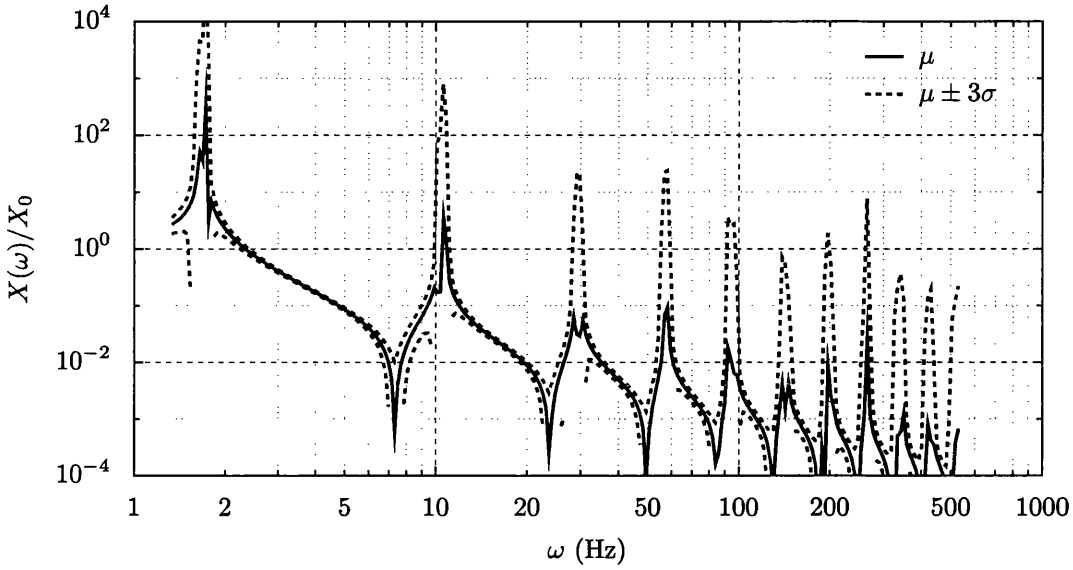

3.18.1: Monte Carlo

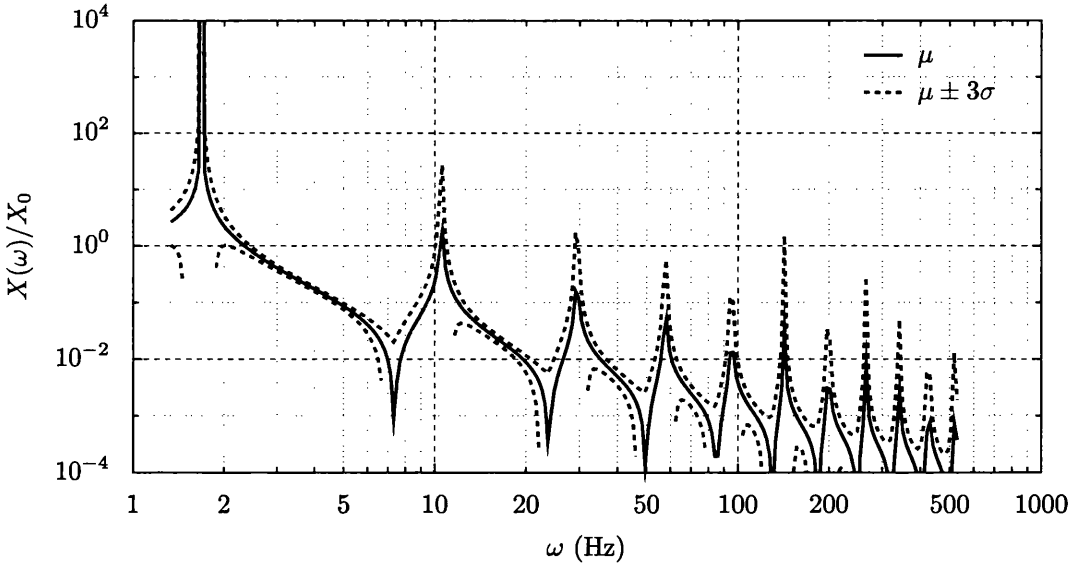

3.18.2: Perturbation

Figure 3.18: Application 3 – variability in the frequency response function. The response is calculated for the free end displacement resulting from an excitation at the same point.

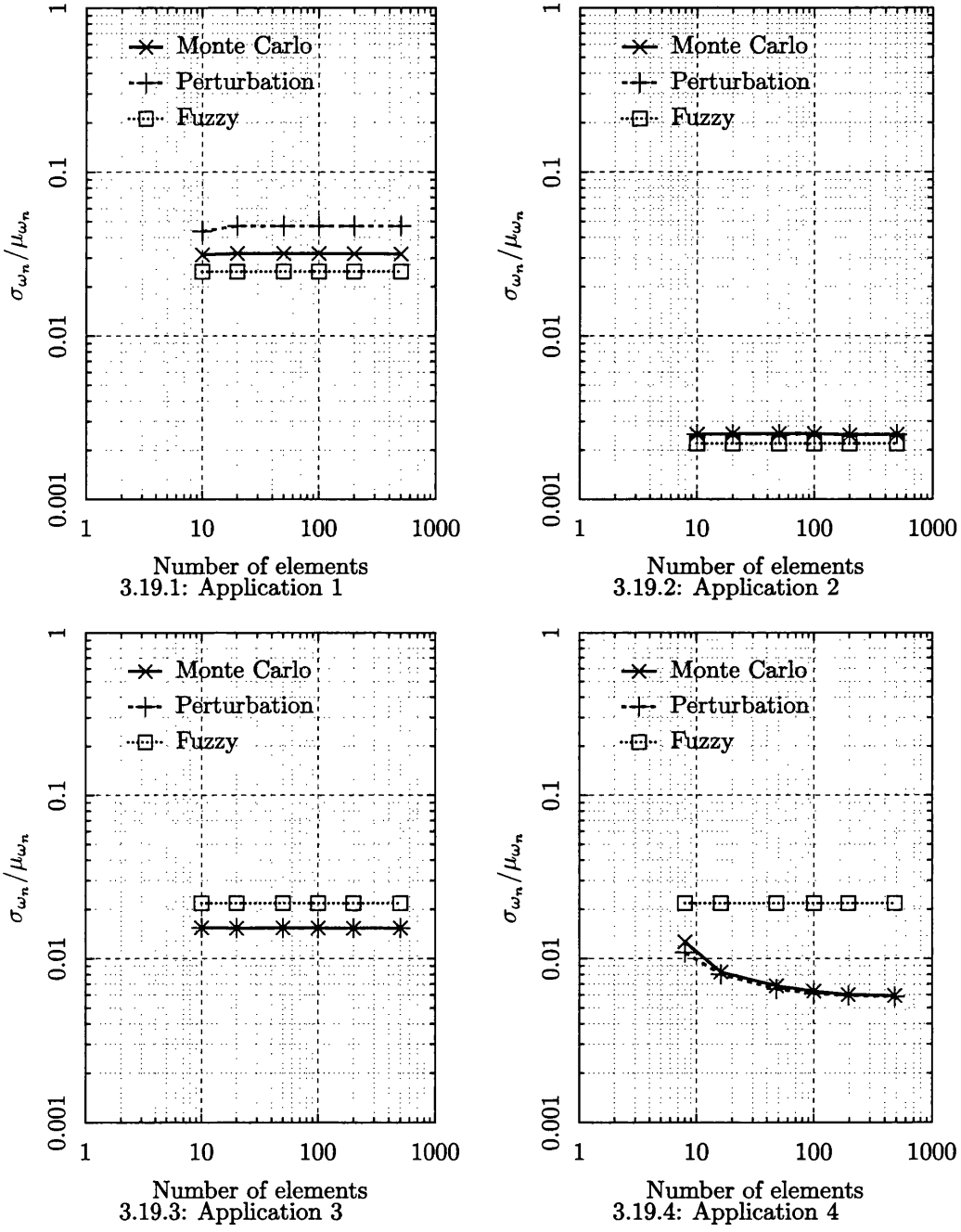

Figure 3.19: Applications 1-4 – convergence of the different methods as the number of mesh elements increases.

Convergence Figure 3.19 shows the influence of the mesh density on the methods' accuracy.

For applications 1 and 2 (with a small number of parameters), once a minimal accuracy is attained in the FE computations refining the mesh does not yield any noticeable improvement in the uncertainty estimation. Even for application 3 (with a two dimensional random field), there is no noticeable impact of the number of elements and parameters in the response variability prediction. This means, on the one hand, that the number of random parameters used in the random field discretisation are sufficient in the range studied. On the other hand, it corroborates the orthogonality between finer meshes and uncertainty quantification – increases in the former do not imply better accuracy in the latter.

For application 4 (with a two dimensional random field), the methods' accuracy is more dependant of the mesh size. It takes a mesh of around 100 elements to properly discretise the random-field, both for the Monte Carlo and perturbation methods. The fuzzy method is insensitive to the mesh size since it does not model the parameter correlation.

The slow convergence of the Monte Carlo method (which requires 100 times more samples to obtain a further digit of precision) can be seen in figure 3.20 for applications 1 and 4. Despite the difference in structural complexity, both applications show identical slopes of the error curves. The major difference in the error curves is in the initial error offset. This depends mostly on the response COV: higher response COVs lead to higher relative errors, and thereby require more samples to attain the same accuracy.

Scalability Figure 3.21 shows the influence of the mesh density on the computational time of the uncertainty propagation methods for all applications. The evolution of computational time for the cantilever beam with uncertain thickness (figure 3.21.3) is substantially different to the cantilever beam with a point mass at an uncertain position (figure 3.21.1). As the random parameters of the former application are those resulting from the random-field discretisation, the number of parameters is equal to the number of elements.

Since derivatives of stiffness and mass matrices with respect to each parameter must be computed for the perturbation method, an increase in the mesh size means

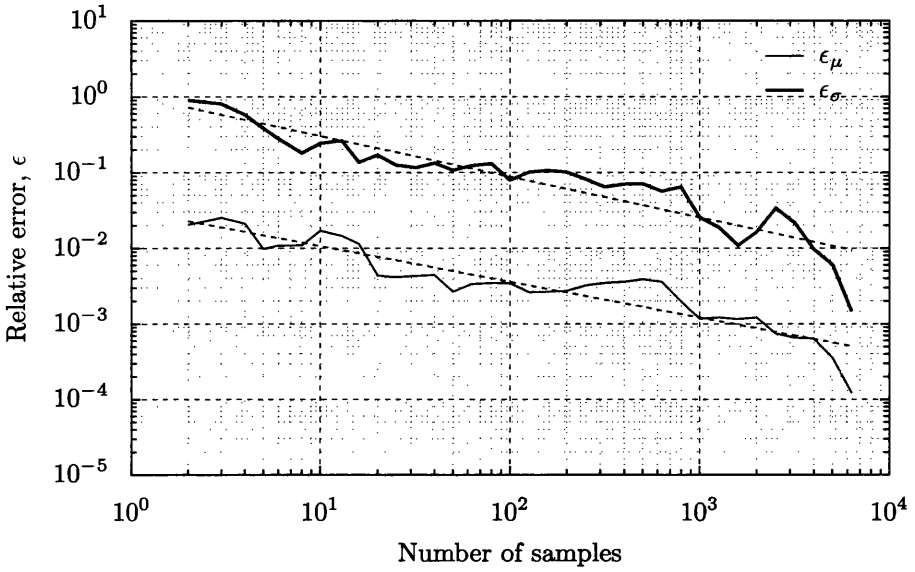

3.20.1: Application 1

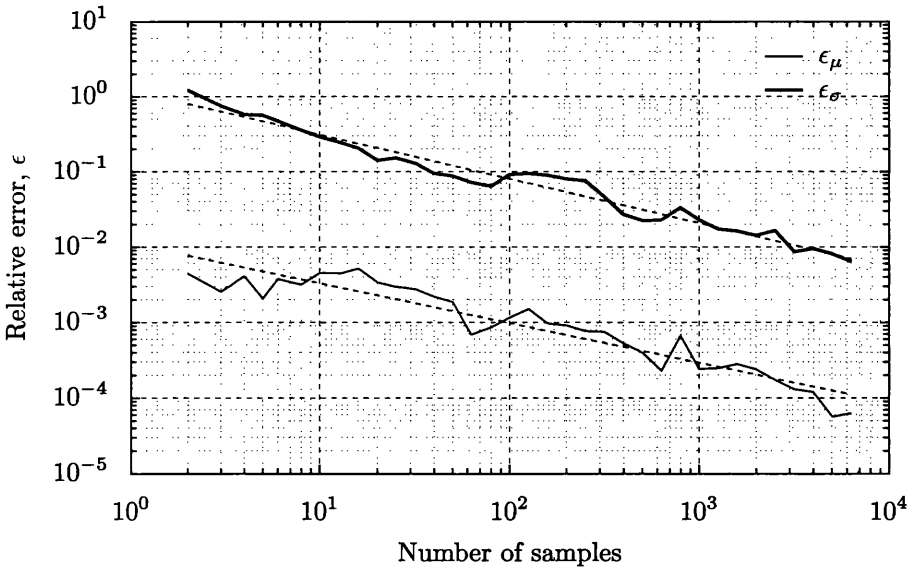

3.20.2: Application 4

Figure 3.20: Application 1 and 4 – convergence of the Monte Carlo method with the number of samples.

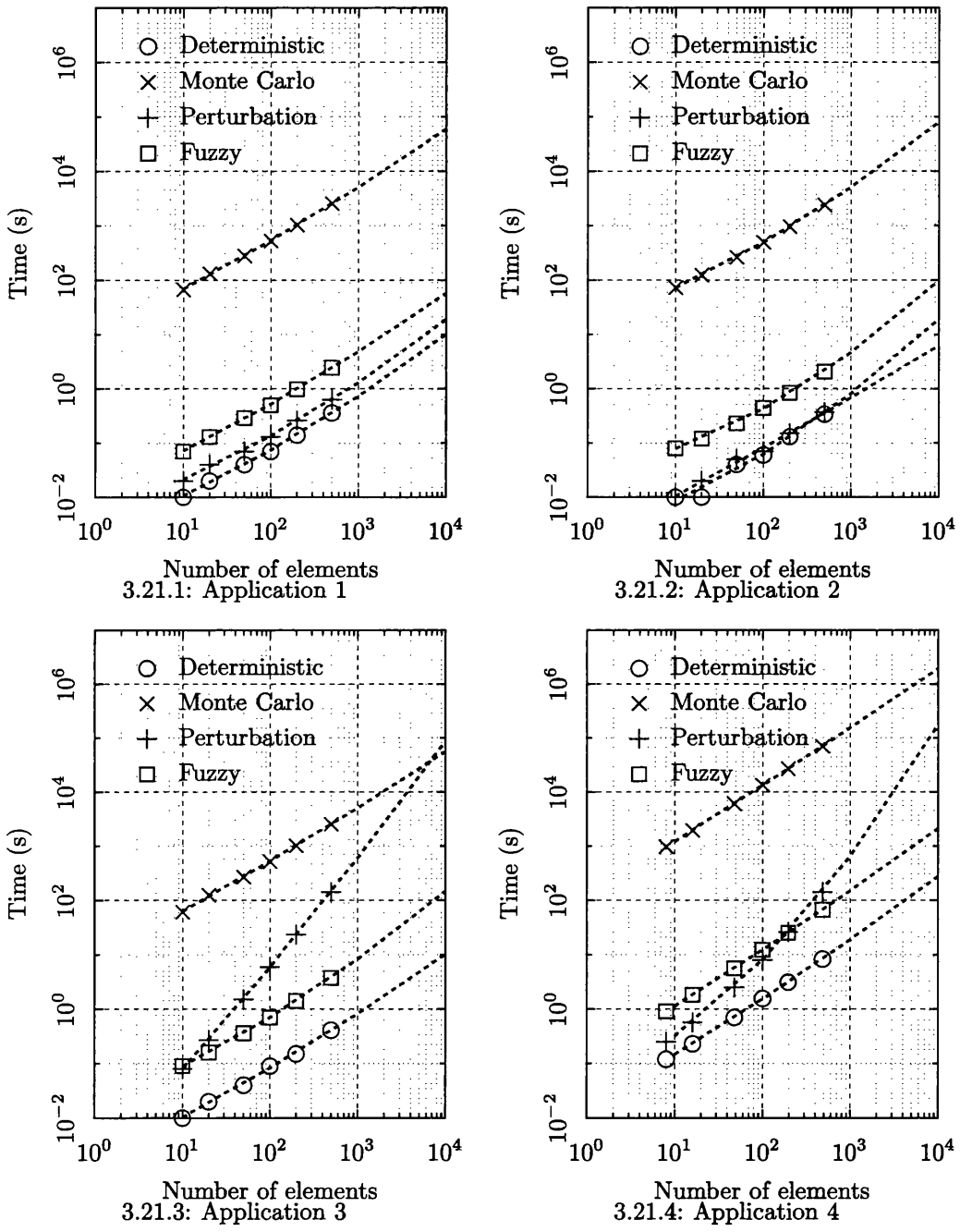

Figure 3.21: Applications 1-4 – computation time of several uncertainty propagation methods for several mesh densities.

not only an increase of the mass and matrices sizes, but also the number of derivatives to compute, and hence the steeper mesh-time curve.

The computation time of the methods shown in figure 3.21.4 follow the same evolution as application 3 (figure 3.21.3), particularly for the perturbation method. But since the computation time of a single response evaluation is so costly, the perturbation method is more appealing over a wider range of mesh size than before.

3.5 Summary

Structural dynamics applications generally require solving a eigen-value and -vector problem, which poses some mathematical difficulties to the uncertainty propagation methods. If there is a significant probability that two or more modes change their order then the mode shapes should be tracked using the MAC during the evaluation of Monte Carlo samples to accurately quantify their variation. The eigenvalue derivatives are undefined for multiple eigenvalues, and therefore the perturbation method cannot be used in those circumstances. The lack of an accurate interval eigenvalue algorithm forces the use of optimisation procedures instead of interval arithmetic for the computation of eigenvalue fuzzy membership functions. Natural frequencies, due to their smooth variation with respect to the parameters and their relatively low dimensionality, are well suited as response quantities for most uncertainty propagation methods. For undamped structures it is difficult to quantify uncertainty in the peaks of the FRFs around natural frequencies.

Except when dealing with an excessive number of parameters, the perturbation method usually produces the fastest results. Its accuracy varies greatly for each application: the existence of nonlinearities in the response surface or large parameter variations are problems. Moreover, the perturbation method lacks an easy way to estimate the error incurred – this would require either the computation of higher order derivatives or running the Monte Carlo simulation method separately – taking away much of its simplicity and speed. Therefore, unless past experience shows that it is applicable to a given application domain, the perturbation method should only be used as an initial estimate – final conclusions should be deferred until after running the Monte Carlo simulation method.

The fuzzy finite element method has proved to be less sensitive to the response

surface nonlinearities than the perturbation method. A drawback of the fuzzy finite element method is the required number of response evaluations. When the parameter and response dimensionality are large the number of required evaluations can easily exceed those required by the Monte Carlo method for equivalent accuracy. Other variants of the fuzzy finite element method which do not assume response monotonicity require an even more explosive number of evaluations [43]. The fuzzy membership functions do not model parameter inter-dependency, making the fuzzy finite element method inappropriate for applications with strongly correlated parameters, such as applications involving random fields. The issue of converting fuzzy membership functions to/from probability density functions is also a pertinent issue – not just for benchmarking purposes but also when incorporating the uncertainty analysis results back into the design process. Possibilities and probabilities are not completely interchangeable concepts. Probability density functions are a widely established and easily understood concept, but membership functions are not so. For robust design applications this is a minor limitation, since two different designs can be compared just by their membership functions, i.e., bypassing the conversion to probabilities. But whenever probabilities are effectively sought (e.g., for a reliability index of the structure) or as part of the design constraints (e.g., establishing a maximum probability of failure) it is impossible to avoid this issue. The fuzzy finite element method is an appealing choice for applications whose response nonlinearities prevent the employment of the perturbation method, and have a small number of independent parameters.

Although frequently seen as a *brute force* method, the universality of the Monte Carlo simulation method still makes it an invaluable tool for uncertainty quantification. The Monte Carlo method can easily be implemented in parallel, and together with meta-modelling (section 2.3.4) substantial time savings can be achieved. A drawback of the Monte Carlo simulation method is its difficulty in estimating the tails of probability distributions (since, by definition, samples are taken less often from the distribution tails) which makes it less attractive for estimating reliabilities, but this was not covered in this comparison. As it stands today, the Monte Carlo still is the workhorse of uncertainty analysis.

Figure 3.22 summarises the adequacy of the uncertainty propagation methods according to the application characteristics, namely, the parameter number and vari-

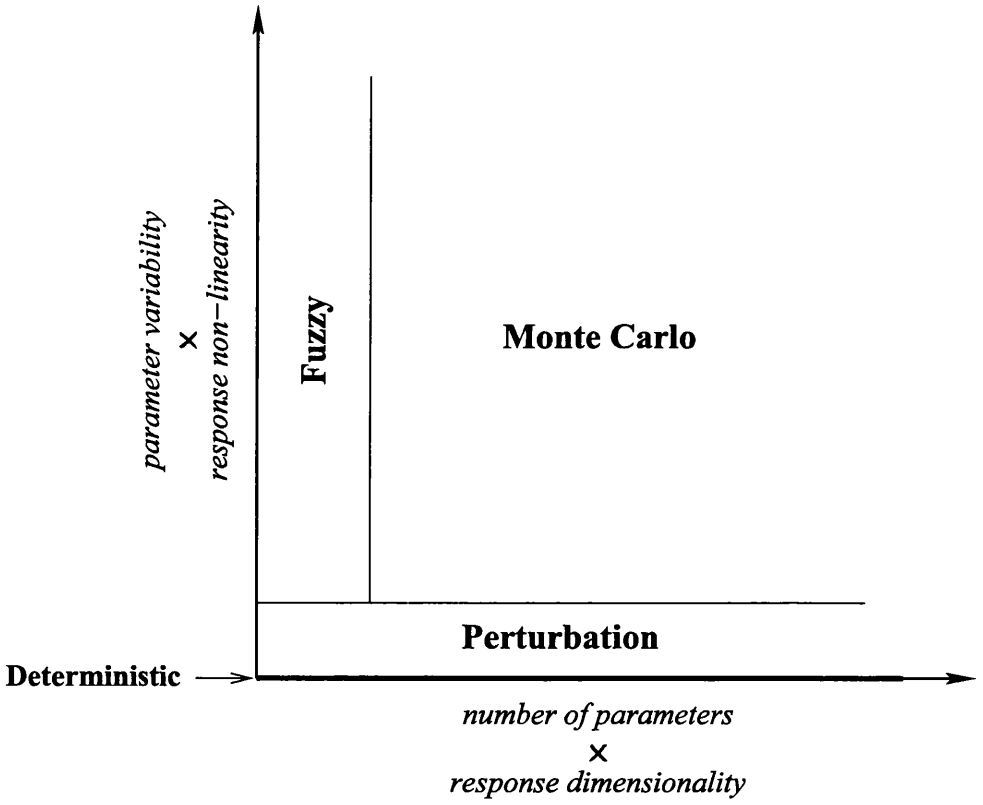

Figure 3.22: Choosing an adequate uncertainty propagation method

ability, and the response smoothness and dimensionality. The deterministic methods can only be used when the parameter variability is insignificant. The perturbation method should be chosen when the response is known to be approximately linear over the parameter variation range. When the response is nonlinear, the fuzzy method can be chosen if the dimensionality of both the parameter and response spaces is low. The Monte Carlo simulation method is the default choice when none of the previous conditions is met.

Chapter 4

Uncertainty identification

4.1 Introduction

Most often in probabilistic uncertainty problems, the parameter distributions are known while the response distributions is sought – the uncertainty forward propagation problem. But how is that knowledge created?

Parameter distribution knowledge can come from:

- direct parameter measurement
- expert knowledge
- design tolerances

Occasionally it may be possible to directly measure samples of the parameters, but often it is easier to measure another response quantity. For example, it is easier to measure the global natural frequencies or FRFs than to measure localised material properties such as densities, thicknesses or equivalent joint stiffnesses. The statistics of the parameters could be inferred from the measurements, and this knowledge could then be applied to new problems. The inverse problem of estimating the distribution of the parameters from that of the response measurements is called uncertainty identification, and is the subject of this chapter.

The deterministic version of this problem, where parameters are unknown but fixed, is addressed by model updating [24]. Statistical methods have been used in

model updating for many years. Usually the estimated variance of the measurements and parameters is used to weight the different terms in a least squares procedure [24, 7]. This is taken a stage further in the minimum variance estimation methods, where the parameters are estimated that have the minimum variance [6, 23]. It should also be emphasised that this work is not concerned with the choice of parameters to update or with regularisation. This has been the subject of significant research [24, 25], and most of the issues that are important in standard model updating will be equally important for uncertainty identification.

Quantification of epistemic uncertainty is addressed by Bayesian model updating [35, 54, 5] – a well-established procedure for refining parameter uncertainty using experimental data (for example to update the predicted reliability index of a single structure).

However, no such procedure is widely available for quantifying *irreducible* uncertainty. For example, to quantify the variability in a structure due to the uncertainties introduced by the manufacturing process. Attempting to fill the gap, an algorithm that characterises the parameter uncertainty by maximising the likelihood of the experimental data is developed. This algorithm is both reasonably efficient and accurate, and it relies upon the established uncertainty propagation methods.

Mares et al. [44], Mottershead et al. [47] developed a similar but different procedure, called the *stochastic model updating* method, where an experimental data cloud is converged upon by a simulated data cloud generated by the Monte Carlo method.

4.2 Maximum likelihood estimation

To solve the inverse uncertainty propagation problem one might be tempted to invert equation (2.1) as

$$\mathbf{x} = \mathbf{f}^{-1}(\mathbf{y}) \tag{4.1}$$

and then use the standard uncertainty propagation methods. The difficulty with this approach is determining $\mathbf{f}^{-1}$, since the inversion is usually ill-conditioned or even impossible. A better alternative is to employ the maximum likelihood estimation, which also allows the use of existing uncertainty propagation methods, but does not

require inverting $\mathbf{f}$.

For estimation purposes it is assumed that the parameters follow a certain probability distribution, X, belonging to a probability distribution family, such as

$$\mathrm{X} \sim \mathrm{D}(\boldsymbol{\theta}_x) \tag{4.2}$$

where $\boldsymbol{\theta}_x$ are the parameters of the family to be estimated. For example, for a multivariate normal distribution, the parameters would be the mean vector $\boldsymbol{\mu}_x$ and covariance matrix $\boldsymbol{\Sigma}_x$. For a given $\boldsymbol{\theta}_x$, the response probability density function $f(\mathbf{y}|\boldsymbol{\theta}_x)$ can be approximated by employing one of the well-known uncertainty propagation methods.

Let $\mathbf{Y}'$ be a set of M response measurements $[\mathbf{y}'_1\, \mathbf{y}'_2\, \ldots\, \mathbf{y}'_M]$. The measurements are assumed to be independent, therefore the measurement likelihood is

$$L(\boldsymbol{\theta}_x) = f(\mathbf{y}'_1, \mathbf{y}'_2, \ldots, \mathbf{y}'_M|\boldsymbol{\theta}_x) = \prod_{i=1}^{M} f(\mathbf{y}'_i|\boldsymbol{\theta}_x). \tag{4.3}$$

The log likelihood is more tractable and given by

$$l(\boldsymbol{\theta}_x) = \log L(\boldsymbol{\theta}_x) = \sum_{i=1}^{M} \log f(\mathbf{y}'_i|\boldsymbol{\theta}_x). \tag{4.4}$$

The maximum likelihood estimator $\hat{\boldsymbol{\theta}}_x$ is the value of $\boldsymbol{\theta}_x$ for which $l(\boldsymbol{\theta}_x)$ attains a maximum. A non-gradient based optimisation method such as the simplex method can be employed for the maximisation, allowing the use of standard uncertainty propagation methods without alteration.

The drawback of this approach is its iterative nature. The uncertainty propagation methods are by themselves computationally intensive, and to repeatedly execute these methods in an iterative optimisation loop would be prohibitive for most interesting applications. Ways to efficiently integrate the maximum likelihood estimation with the two most common propagation methods is the purpose of the following sections.

4.2.1 Perturbation approach

Figure 4.1 illustrates the straightforward application of the perturbation method for estimating the measurements likelihoods in a hypothetical single parameter, single response example. The x and y axes correspond to the parameter and response spaces, respectively, and $f(x)$ describes the relation between them. Testing different parameters distributions (different values of $\boldsymbol{\theta}_x$) implies reevaluating the system equation $f(x)$ and its first-order derivatives at the new parameters mean point.

Reevaluating $f(x)$ and its derivatives can be exceedingly time consuming for complex and high-dimensional models, where the most of the time is spent just on calculating these derivatives. Furthermore, there is little advantage doing so. As $\boldsymbol{\theta}_x$ converges to the maximum likelihood estimate, so will the parameters mean, thereby $f(x)$ and its derivatives will yield basically the same linear approximation, over and over. Therefore, reusing the same linearisation of $f(x)$ can result in a substantial time-saving, and with little impact in accuracy. Figure 4.2 illustrates this for the same hypothetical single parameter, single response example of figure 4.1.

It is assumed that the uncertain parameters follow a multivariate normal distribution

$$\mathrm{X} \sim \mathrm{N}_n \left(\boldsymbol{\mu}_x, \boldsymbol{\Sigma}_x \right) \tag{4.5}$$

where n is the number of variables, $\boldsymbol{\mu}_x$ is the mean vector and $\boldsymbol{\Sigma}_x$ is the covariance matrix. In theory this incurs no loss in generality since random variables may be transformed into uncorrelated Gaussian variables, as described in section 2.2.5.

All of the elements of $\boldsymbol{\mu}_x$ and $\boldsymbol{\Sigma}_x$ will be considered independent. However there are examples where this assumption is relaxed, such as random fields where there is a dependency structure. For example, when modelling a spatial AR(1) random field, $\boldsymbol{\mu}_x$ and $\boldsymbol{\Sigma}_x$ could be fully described by three scalars, namely the mean μ, variance σ, and correlation length L.

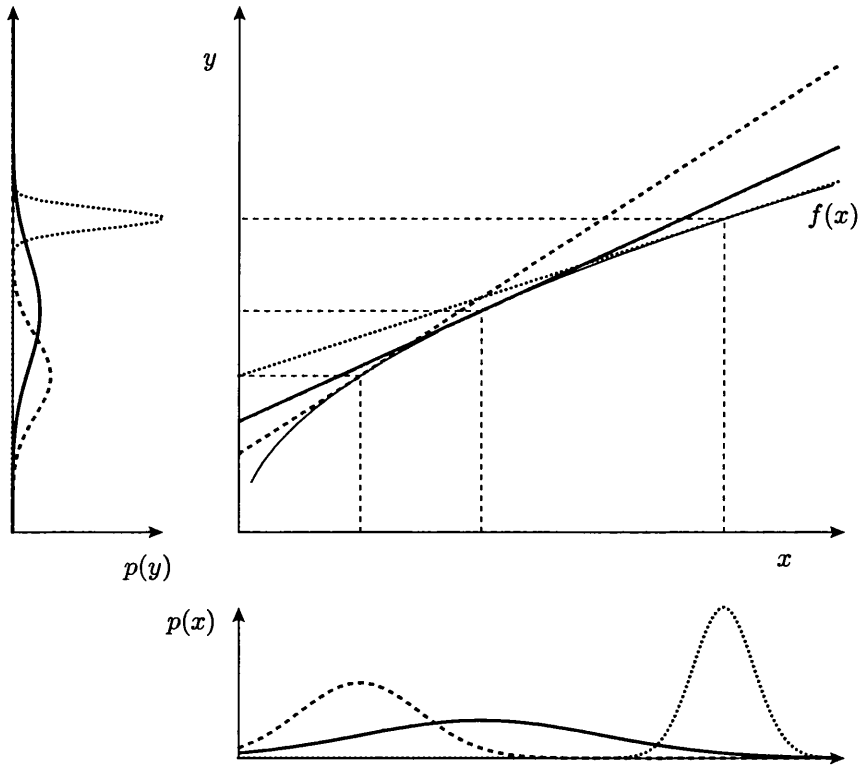

Figure 4.1: Straightforward application of the perturbation method – the different parameter distributions are shown by the continuous, dashed, and dotted curves; multiple linearisations of $f(x)$ are performed.

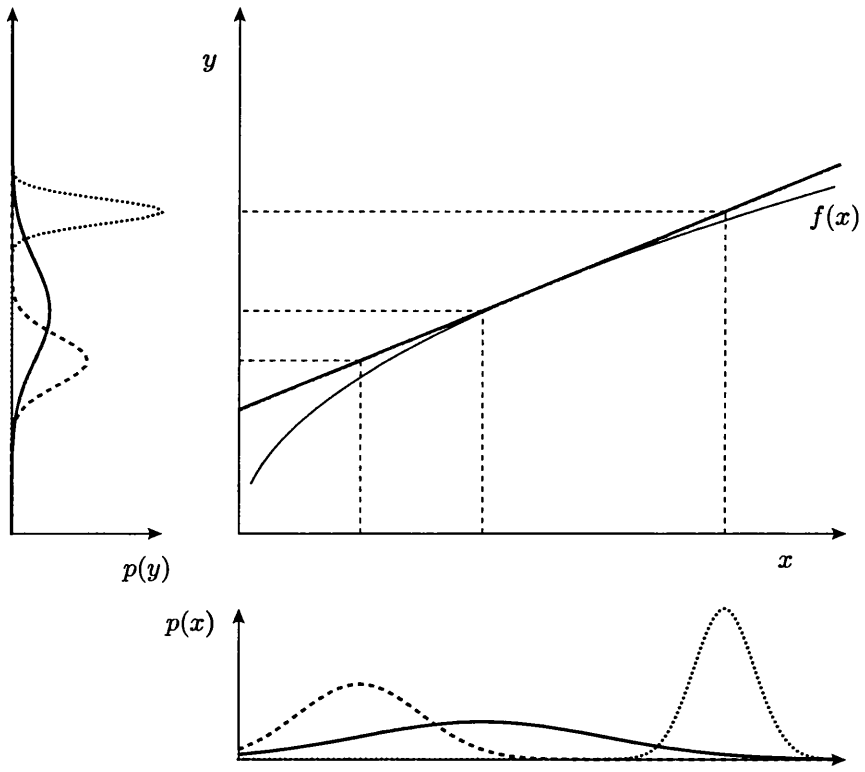

Figure 4.2: Optimised application of the perturbation method – the different parameter distributions are shown by the continuous, dashed, and dotted curves; a single linearisation of $f(x)$ is performed.

For the perturbation method equation (2.28) is rewritten as

$$\begin{aligned}\mathbf{y} &= \mathbf{f}(\mathbf{x}^0) \\ &+ \sum_{i=1}^{n} \frac{\partial \mathbf{f}}{\partial x_i}(\mathbf{x}^0) \cdot (x_i - x_i^0) \\ &+ \frac{1}{2} \sum_{i=1}^{n} \sum_{j=1}^{n} \frac{\partial^2 \mathbf{f}}{\partial x_i \partial x_j}(\mathbf{x}^0) \cdot (x_i - x_i^0) \cdot (x_j - x_j^0) \\ &+ \cdots\end{aligned} \tag{4.6}$$

around the point $\mathbf{x}^0 = [x_0^0 \, x_1^0 \, \ldots \, x_n^0]^{\mathrm{T}}$, which is assumed to be in the vicinity of $\boldsymbol{\mu}_x$. The importance of the choice of $\mathbf{x}^0$ will be considered in more detail later. Taking only the first order terms, equation (4.6) can be rewritten as

$$\mathbf{y} \approx \mathbf{f}^0 + \mathbf{J}^0 \left(\mathbf{x} - \mathbf{x}^0\right) \tag{4.7}$$

where $\mathbf{f}^0$ and $\mathbf{J}^0$ are the function and its Jacobian, respectively, evaluated at the point $\mathbf{x}^0$. From equations (4.5) and (4.7) the probability density distribution of $\mathbf{y}$ may be approximated by

$$\mathrm{Y} \sim \mathrm{N}_m(\boldsymbol{\mu}_y, \boldsymbol{\Sigma}_y) \tag{4.8}$$

where

$$\boldsymbol{\mu}_y = \mathbf{f}^0 + \mathbf{J}^0(\boldsymbol{\mu}_x - \mathbf{x}^0) \tag{4.9}$$

$$\boldsymbol{\Sigma}_y = \mathbf{J}^0 \boldsymbol{\Sigma}_x \mathbf{J}^{0\mathrm{T}} \tag{4.10}$$

and its probability density function by

$$\hat{f}(\mathbf{y}|\boldsymbol{\mu}_x, \boldsymbol{\Sigma}_x) = (2\pi)^{-m/2} |\boldsymbol{\Sigma}_y|^{-1/2} e^{-(\mathbf{y}-\boldsymbol{\mu}_y)^{\mathrm{T}} \boldsymbol{\Sigma}_y^{-1} (\mathbf{y}-\boldsymbol{\mu}_y)/2}. \tag{4.11}$$

Replacing $f(\mathbf{y}_i'|\boldsymbol{\theta}_x)$ in equation (4.4) by the approximation given in equation (4.11) yields

$$l(\boldsymbol{\mu}_x, \boldsymbol{\Sigma}_x) = -\frac{1}{2} \left(Mm \log 2\pi + M \log |\boldsymbol{\Sigma}_y| + \sum_{i=1}^{M} (\mathbf{y}_i' - \boldsymbol{\mu}_y)^{\mathrm{T}} \boldsymbol{\Sigma}_y^{-1} (\mathbf{y}_i' - \boldsymbol{\mu}_y) \right). \tag{4.12}$$

Ideally the linearisation point $\mathbf{x}^0$ would be equal to the mean value $\boldsymbol{\mu}_x$, but since the latter is unknown *a priori* a guess must be made for its initial value. Depending how far this initial guess is from the estimated $\hat{\boldsymbol{\mu}}_x$, it may be necessary to recalculate $\mathbf{f}^0$ and $\mathbf{J}^0$, to more accurately approximate the response surface near $\boldsymbol{\mu}_x$. It is unnecessary, however, to perform a recalculation at every evaluation of equation (4.12). For most applications, an approximate knowledge of the mean value is available, reducing the need for such recalculations.

4.2.2 Monte Carlo simulation approach

Figure 4.3 illustrates the straightforward application of the Monte Carlo simulation method for estimating the measurements likelihoods in a hypothetical single parameter, single response example. The x and y axes correspond to the parameter and response spaces, respectively, and $f(x)$ describes the relation between them. Here, testing different parameters distributions (different values of $\boldsymbol{\theta}_x$) implies resampling the parameters and reevaluating the system equation $f(x)$ for the new samples.

An alternative to resampling parameters is to reweight an otherwise constant set of samples, thereby avoiding repeated time-consuming reevaluations of $f(x)$. Figure 4.4 illustrates this for the same example of figure 4.3.

Let $\mathbf{X}''$ be a set of N samples of the parameters $[\mathbf{x}''_1\, \mathbf{x}''_2 \ldots \mathbf{x}''_N]$, and $\mathbf{Y}''$ the respective response set $[\mathbf{y}''_1\, \mathbf{y}''_2 \ldots \mathbf{y}''_N]$. If the uncertain parameters are sampled according to *their* probability density function $f(\mathbf{x})$ then the response probability density function can be estimated by kernel density estimation as in equation (2.22). If the parameters are sampled according to a *different* probability density function $g(\mathbf{x})$ then the probability density function of the response may be estimated by

$$\hat{f}(y|\boldsymbol{\theta}_x) = \frac{1}{N}\sum_{j=1}^{N} \frac{f(\mathbf{x}''_j|\boldsymbol{\theta}_x)}{g(\mathbf{x}''_j)} \kappa_{\mathbf{H}}(\mathbf{y} - \mathbf{y}''_j). \tag{4.13}$$

Figure 4.5 illustrates this.

The suitability of different probability density functions of the parameters may be tested using equation (4.13) without resampling $\mathbf{X}''$. If the function $g(\mathbf{x})$ is close to $f(\mathbf{x})$ then a smaller number of samples, N, would be required. However, the only requirements for $\mathbf{X}''$ are that $g(\mathbf{x}) \gg 0$ in the same region where $f(\mathbf{x}) \gg 0$

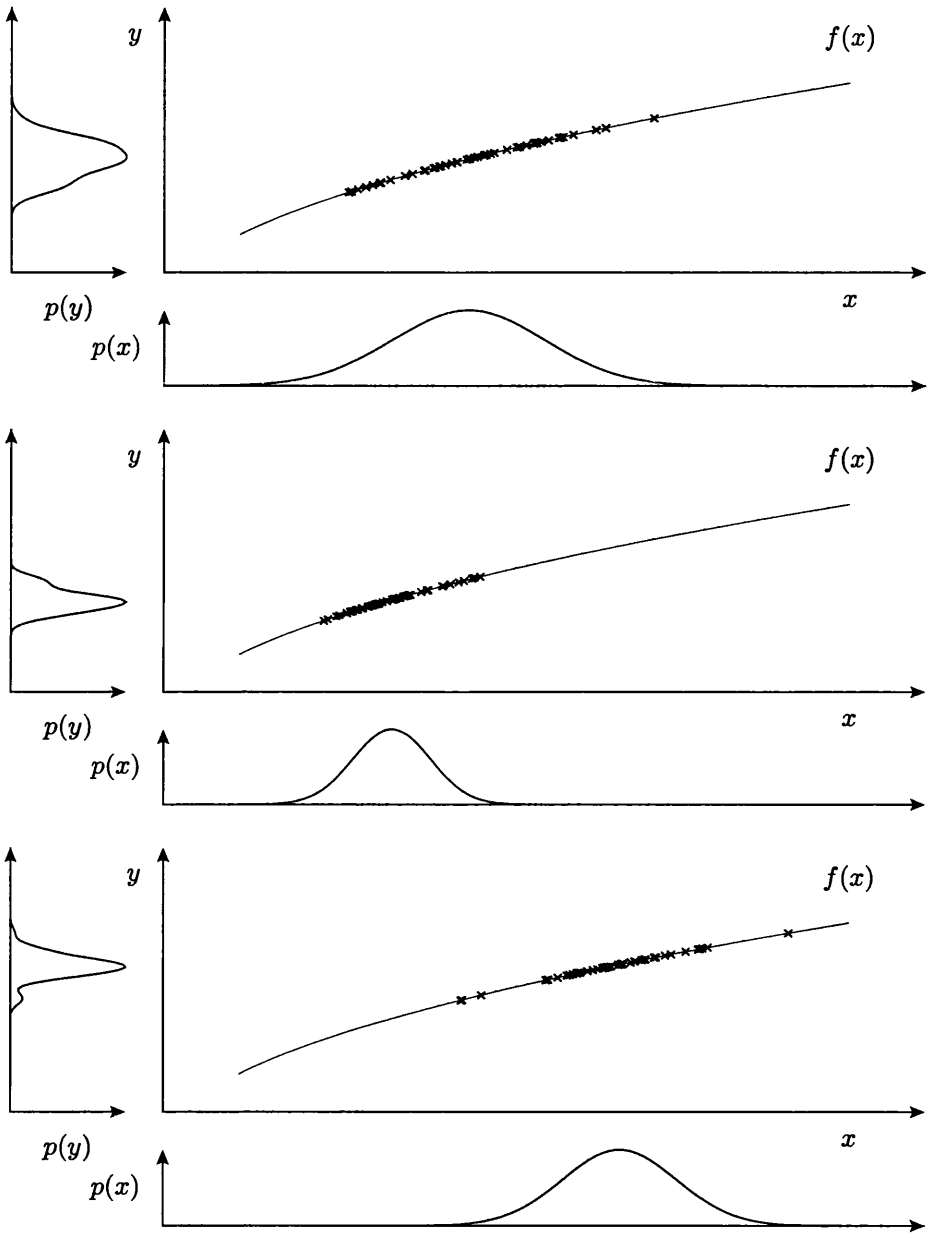

Figure 4.3: Straightforward application of the Monte Carlo simulation method – samples have different distributions according to the different parameter distributions.

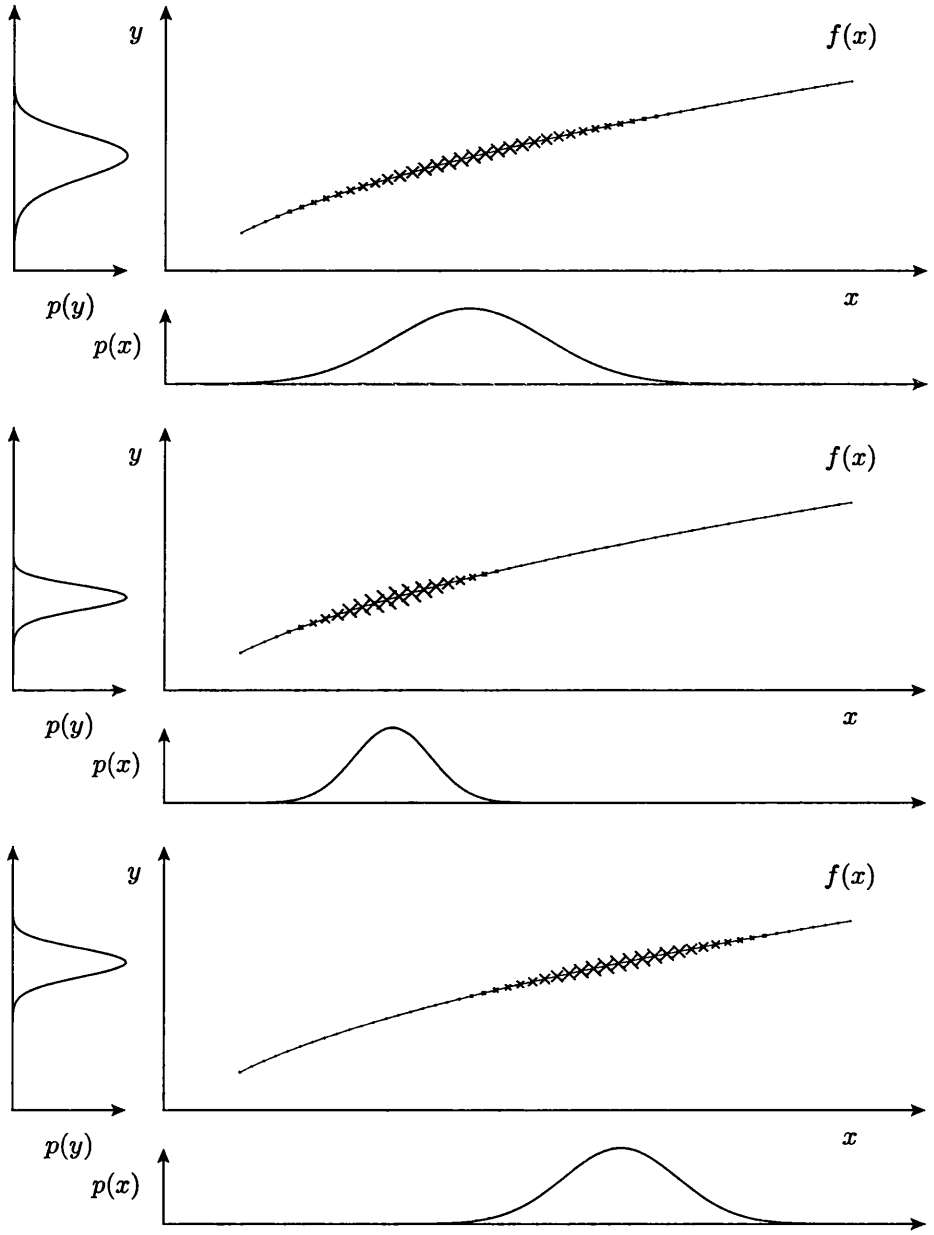

Figure 4.4: Optimised application of the Monte Carlo simulation method – samples have the same distribution, but different weights (here represented by the symbol size) according to the different parameter distributions.

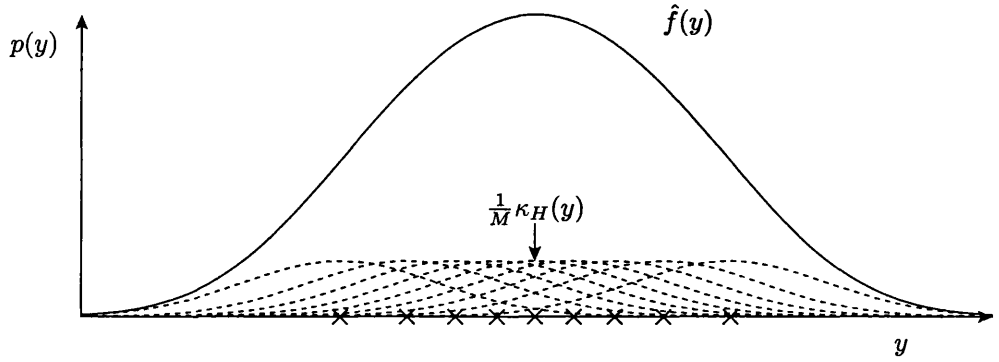

4.5.1: Conventional sampling

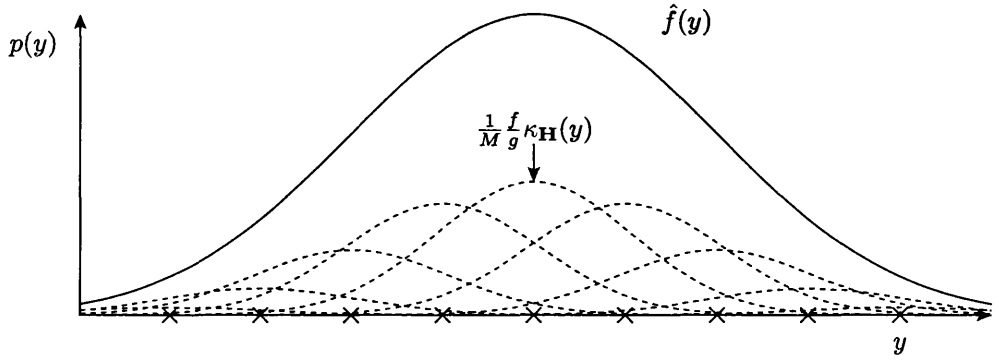

4.5.2: Non-conventional sampling

Figure 4.5: Estimating the response probability density function from the Monte Carlo simulation samples via kernel density estimation.

and that a sufficiently high number of samples N is generated. In practice uniform or Latin hypercube sampling of the parameters over the likely parameter subspace is sufficient. Further time-savings can be achieved by employing meta-models, as described in section 2.3.4.

Replacing $f(\mathbf{y}_i'|\boldsymbol{\theta}_x)$ in equation (4.4) by the approximation given in equation (4.13) yields

$$\begin{aligned} l(\boldsymbol{\theta}_x) = &-M \log N \\ &+ \sum_{i=1}^{M} \log \sum_{j=1}^{N} \exp\left[\log f(\mathbf{x}_j''|\boldsymbol{\theta}_x) - \log g(\mathbf{x}_j'') + \log \kappa_{\mathbf{H}}(\mathbf{y}_i' - \mathbf{y}_j'')\right] . \end{aligned} \tag{4.14}$$

Note that the only term in equation (4.14) that depends on $\boldsymbol{\theta}_x$ is the probability density function of the parameters, $f(\mathbf{x}_j''|\boldsymbol{\theta}_x)$. All of the other terms can be pre-calculated before entering the optimisation loop.

For the kernel density estimation a multivariate normal kernel was used, as per equations (2.24) to (2.25).

4.3 Applications

4.3.1 Cantilever beam – simulation

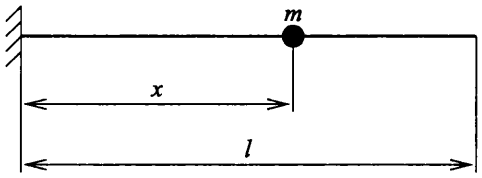

Figure 4.6: Application 1 – simulated cantilever beam with a discrete mass at an uncertain position.

The simulated example is a cantilever beam with a point mass at an uncertain position along the beam length, shown schematically in figure 4.6. The beam has length $l = 1\,\mathrm{m}$, a rectangular section of $100 \times 10\,\mathrm{mm}^2$ and is made of steel with Young's modulus $E = 210\,\mathrm{GPa}$ and density $\rho = 7800\,\mathrm{kg}\,/\,\mathrm{m}^3$. The discrete mass is

$m = 0.100\,\text{kg}$ and its position x follows a normal distribution $X \sim \text{N}(\mu = 0.75\,\text{m}, \sigma = 0.05\,\text{m})$.

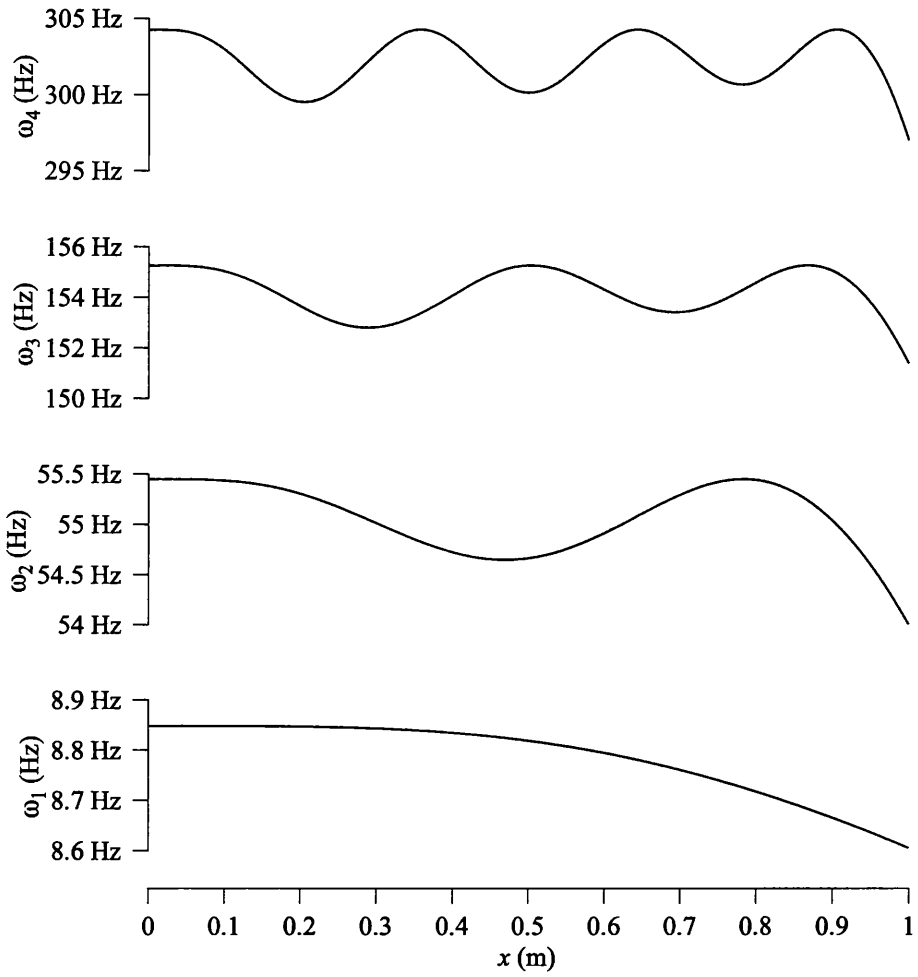

Figure 4.7: Application 1 – variation of the first four natural frequencies with the position of the lumped mass, x.

If the x variation is small enough, the natural frequencies vary almost linearly and the perturbation approach becomes attractive because of its computational efficiency. Figure 4.7 shows the variation of the natural frequencies with the position of the discrete mass and demonstrates that the perturbation approach is only suitable for the lower natural frequencies and for small position variations.

Figures 4.8 and 4.9 show the log-likelihood given by equation (4.4) for the simulated cantilever beam for the perturbation and Monte Carlo approaches. In both

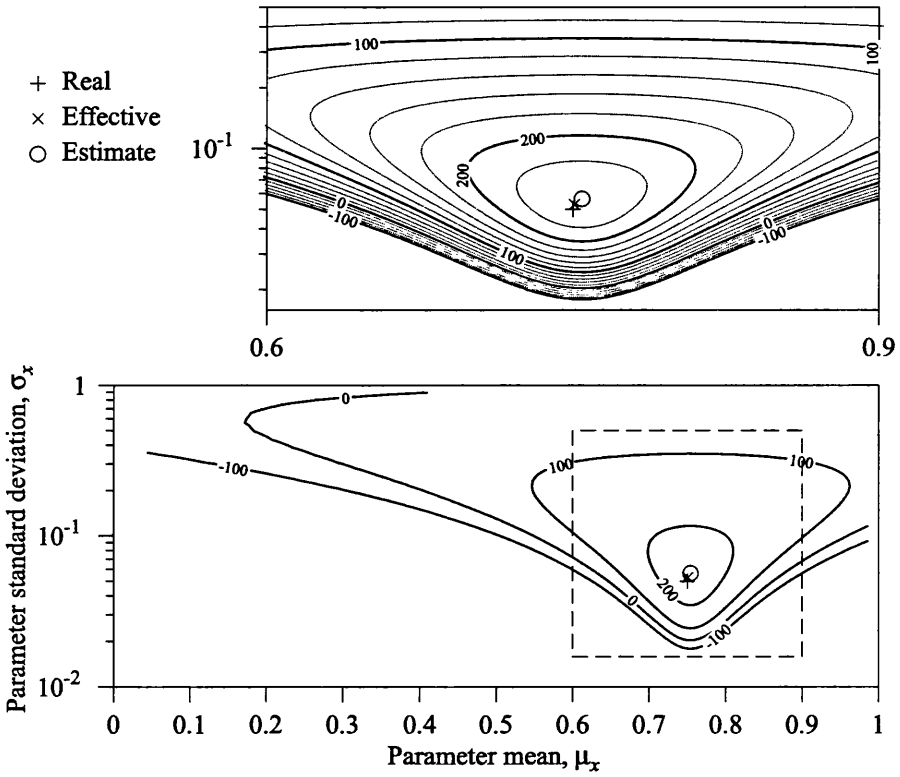

Figure 4.8: Application 1 – log-likelihood given by equation (4.12) for the perturbation method.

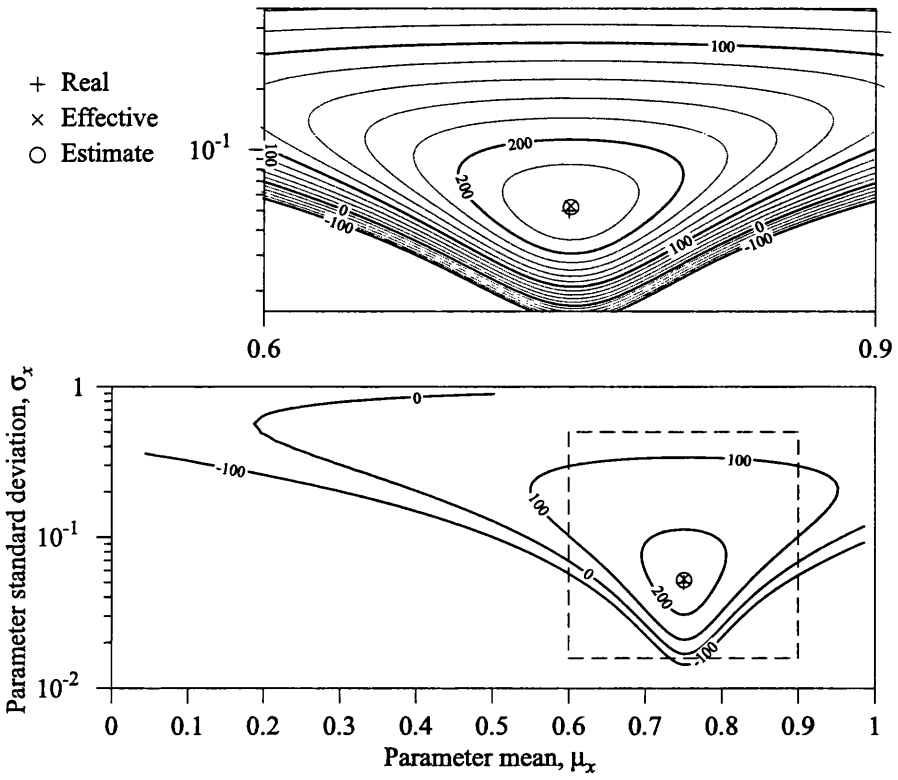

Figure 4.9: Application 1 – log-likelihood given by equation (4.14) for the Monte Carlo method.

approaches the function is steep for mean values away from the real mean and for low variance, but the function is flat for large variances. More importantly the log-likelihood only has one maximum, which is close to the real parameter values, and to which the estimation procedure will converge for any initial set of parameters.

For the analysis of the results two (relative) errors are defined. The *real* error is the error between the estimates and the *population* statistics

$$\epsilon_r = \frac{\hat{\mu}_x - \mu_x}{\mu_x} \quad \text{or} \quad \epsilon_r = \frac{\hat{\sigma}_x - \sigma_x}{\sigma_x} \tag{4.15}$$

The *effective* error is the error between the estimates and the *sample* statistics

$$\epsilon_e = \frac{\hat{\mu}_x - \bar{x}}{\bar{x}} \quad \text{or} \quad \epsilon_e = \frac{\hat{\sigma}_x - s_x}{s_x} \tag{4.16}$$

The effective error is often the most relevant error, since for a fixed set of M measurements the sample statistics are the best one can really ever hope to know.

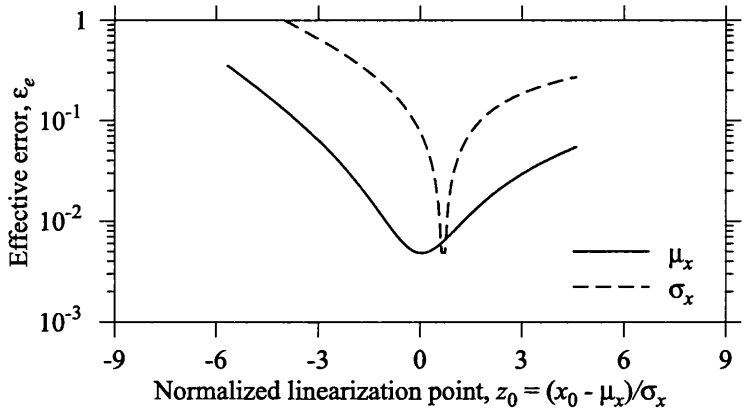

Figure 4.10: Application 1 – influence of the linearisation point on the effective estimation error.

As mentioned earlier, the best results for the perturbation approach are usually obtained when the linearisation is centred on the mean value of the parameters. However this point is unknown beforehand and a guess must be made. Figure 4.10 shows the effect that performing the linearisation away from the real mean has on the estimation error. Notice that the minimum error is not necessarily obtained at the real mean.

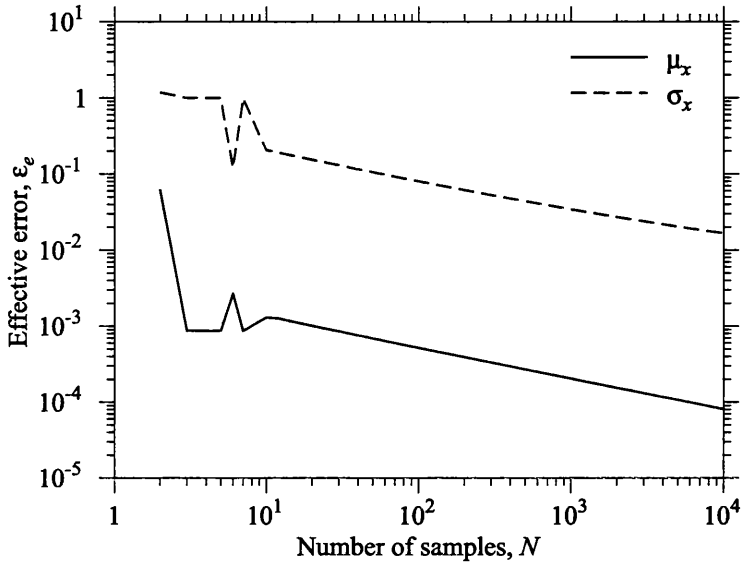

Figure 4.11: Application 1 – influence of the number of Monte Carlo samples on the effective estimation error.

The accuracy of the Monte Carlo approach depends on the number of samples, with an error estimate that decreases as $N^{1/2}$, as evidenced by figure 4.11 for this example.

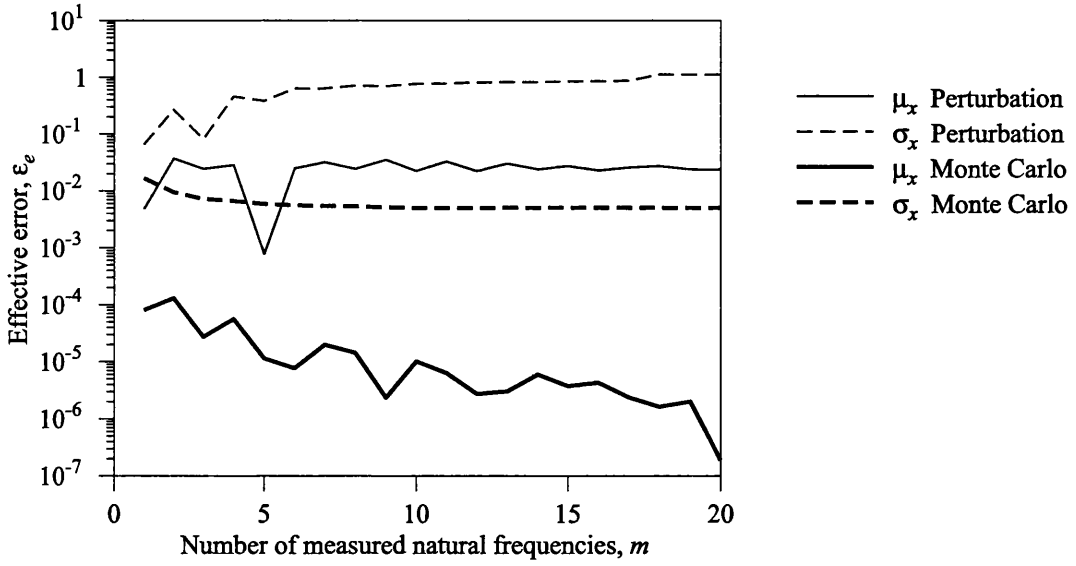

Figure 4.12: Application 1 – effect of using higher natural frequencies in the estimation.

In this particular example there is a single parameter, and therefore measuring a single natural frequency (for example the first) would suffice for estimating the parameter. Figure 4.12 shows the effect of using more than one natural frequency to estimate the discrete mass position. The extra information available using more natural frequencies should allow more averaging of the measured data and therefore more accurate estimates. However, this example highlights an undesirable property of the perturbation approach, where adding more redundant information (in the sense of adding new natural frequencies rather than more samples) can make the estimates worse. The problem is caused by the loss in accuracy of the linearised solution for the higher natural frequencies, and figure 4.7 has already demonstrated that the higher natural frequencies vary more with mass position than the lower frequencies.

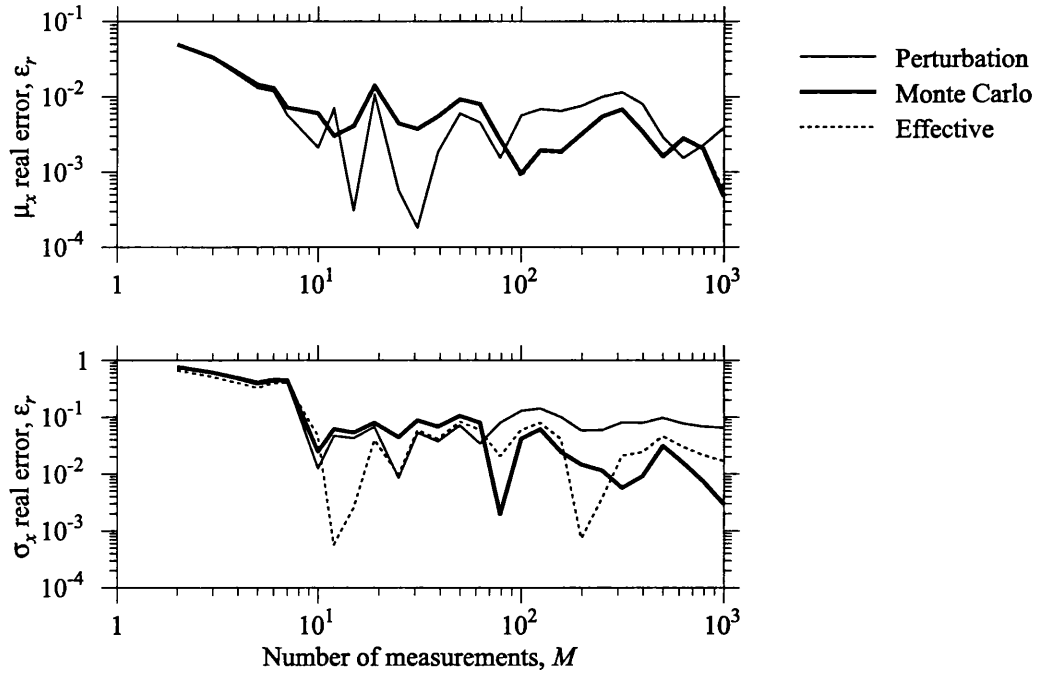

Figure 4.13: Application 1 – influence of the number of measurements on the real estimation error.

As more measurements are taken the estimates obtained by both approaches generally improve, as shown in figure 4.13. The convergence of perturbation approach is limited by the response nonlinearities as mentioned earlier.

4.3.2 Cantilever beam – experiment

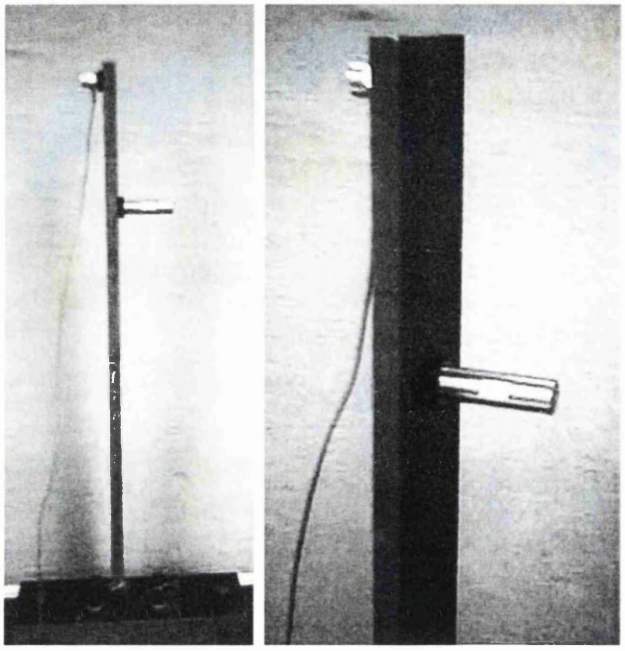

Figure 4.14: Application 2 – experimental setup of the cantilever beam with a lumped mass at an uncertain position.

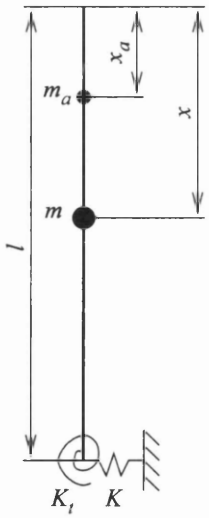

Figure 4.15: Application 2 – model of the experimental cantilever beam system.

For experimental validation a similar system to the one analysed in section 4.3.1

was created, and is shown in figure 4.14. The model was modified to account for the accelerometer (with mass $m_a = 34.1\,\mathrm{g}$ positioned at $x_a = 20\,\mathrm{mm}$ from the beam free end) and to allow for some translational and rotational clamping flexibility (K and K_t), as illustrated in figure 4.15. The beam has length $l = 60\,\mathrm{cm}$, a rectangular section of $70 \times 12\,\mathrm{mm}^2$ and is made of steel with Young's modulus $E = 210$ GPa and density $\rho = 7800\,\mathrm{kg/m^3}$. The discrete mass is $m = 93.6\,\mathrm{g}$ and its position x follows a normal distribution $X \sim \mathrm{N}(\mu = 15\,\mathrm{cm}, \sigma = 5\,\mathrm{cm})$.

Table 4.1: Application 2 – model updating of the clamping stiffnesses of the beam without the discrete mass

Mode	Measured (Hz)	Updated (Hz)	Δ (Hz)
1	25.9049	25.8906	-0.0143
2	162.9649	163.1180	+0.1532
3	456.7434	456.5961	-0.1473
4	890.0572	889.5894	-0.4678

The clamping stiffnesses were determined by model updating of the beam without the mass, by minimising the relative error in the first three natural frequencies. The estimated stiffnesses were $K = 91.466 \times 10^6\,\mathrm{N/m}$ and $K_t = 109.825 \times 10^3\,\mathrm{N/rad}$, and the first four measured and updated natural frequencies are given in table 4.1. The resulting model is clearly excellent, although with two unknown parameters and three natural frequencies some residual error will exist, as shown in table 4.1.

Fifty samples of x were generated and rounded to the nearest mm. The discrete mass was positioned accordingly and the measurements of the first natural frequency taken. Figure 4.16 shows these measurements and compares them with the response of the model.

For each test the mass centre was aligned with the respective position along the beam. The beam was excited by an impact hammer at the accelerometer location but on the opposite side of the beam, and the average of three runs was taken at each location. The data acquisition and analysis was performed using the SigLab system with a bandwidth of 128 Hz and 1024 frequency lines. The first natural frequency was estimated from the transfer function using circle-fitting.

Even after model updating there is a small bias Δ between the measured natural frequencies and the ones derived by the model, given in table 4.1. To reduce these modelling errors (which would otherwise yield an offset in the mean estimate) a bias

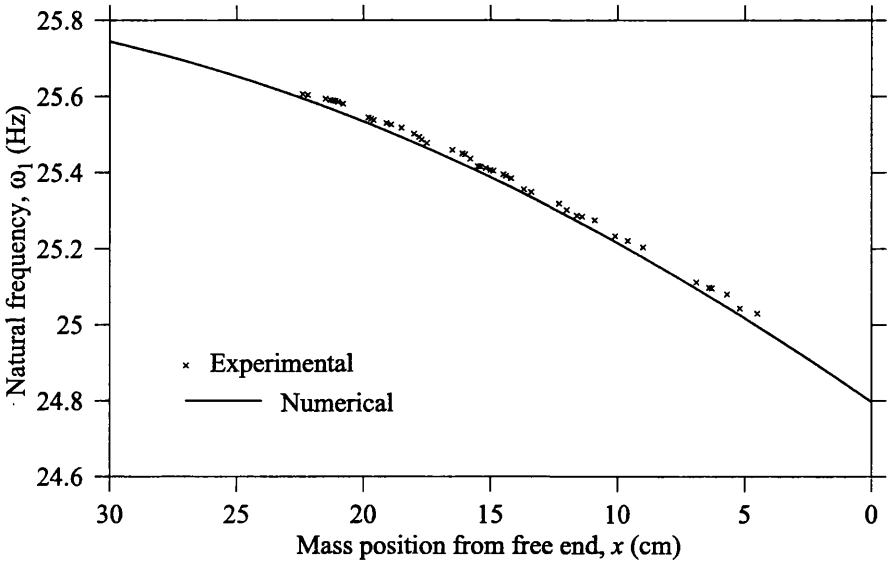

Figure 4.16: Application 2 – Natural frequency response (experimental vs. model).

is introduced in equation (2.1) as

$$\mathbf{y} = \mathbf{f}(\mathbf{x}) + \Delta \tag{4.17}$$

Table 4.2: Application 2 – Estimated mean and variance for the experimental example.

	μ_x (cm)	σ_x (cm)
Real	15.00	5.00
Effective	15.15	4.95
Perturbation estimate	14.95	5.04
Monte Carlo estimate	15.34	4.85

Table 4.2 shows the estimates of μ_x and σ_x compared with their real and effective counterparts. The estimates obtained by the Monte Carlo method are only slightly closer to the effective values than those obtained by the perturbation method. In this application the perturbation method performs well, and this is because variation of the first natural frequency is almost linear.

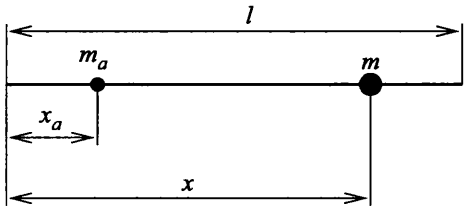

Figure 4.17: Application 3 – The model of the free beam experiment.

4.3.3 Free beam

A rectangular beam of length 1 m, width 40 mm, height 5 mm, and made from bright mild steel ($E = 210\,\text{GPa}$ and $\rho = 7.8 \times 10^3\,\text{kg/m}^3$) was suspended using flexible supports to simulate free-free conditions. A small 47 g mass (magnet) was attached to the beam and its position was varied using a normal distribution with mean $\mu = 800\,\text{mm}$ and standard deviation $\sigma = 30\,\text{mm}$. 50 mass positions were sampled from this distribution. The experimental setup is illustrated schematically in figure 4.17. The accelerometer mass is 6 g and it was positioned 20 mm from the end.

The test procedure is documented in [26] and the experimental data is available on the web[1].

For comparison a numerical model was created using 50 elements. Figure 4.18 shows the first three natural frequencies as a function of the mass position, and the numerical results for comparison. The model is reasonably close and the offset in natural frequency is caused by small differences in the flexural rigidity, EI, that are likely to be within the measurement tolerance of the beam thickness. For the update exercise this difference in flexural rigidity will be represented by a factor, k, where EI becomes

$$EI = k\,(EI)_{\text{nominal}}. \tag{4.18}$$

Unlike the application in section 4.3.2, instead of deterministically updating the FE model for a particular point in parameter space (i.e., for a specific mass position) the EI factor k will be updated together with the distribution of the uncertain parameters, i.e., while identifying the mass position mean and variance.

Table 4.3 shows the uncertainty identification results for the perturbation and

[1] `http://www.aer.bris.ac.uk/research/uncertainty/`

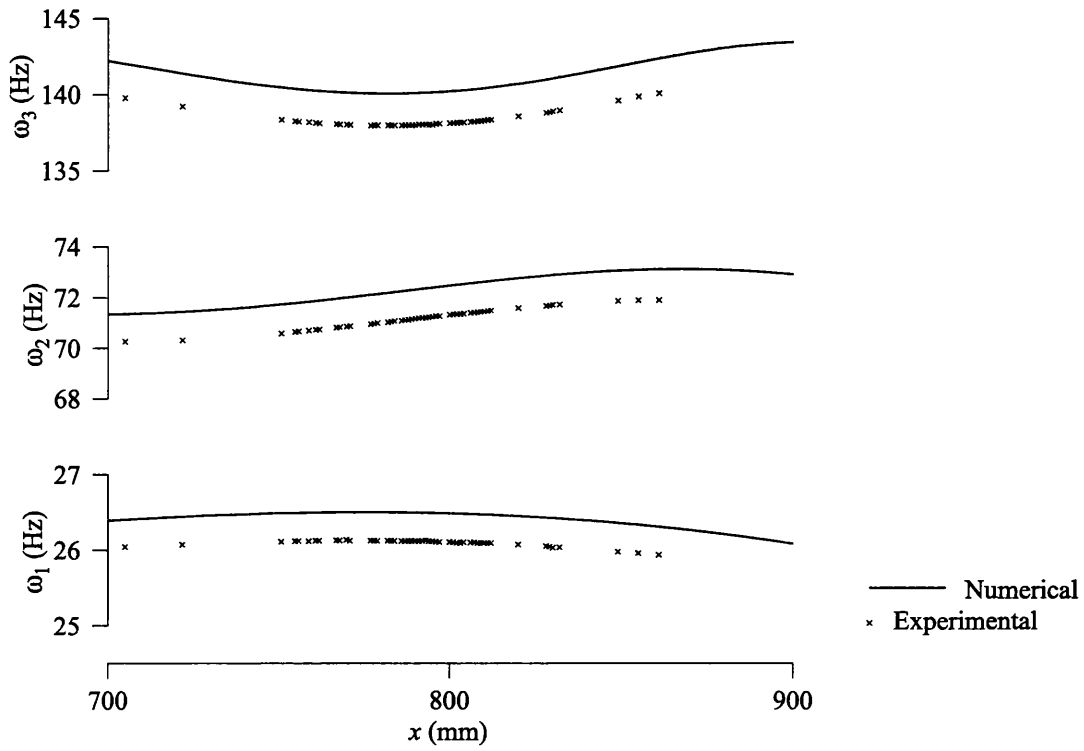

Figure 4.18: Application 3 – Variation of natural frequency with mass position for the free beam example.

Table 4.3: Application 3 – model updating results.

Description	**Method**	μ_x (mm)	ϵ_e (%)	σ_x (mm)	ϵ_e (%)	μ_k	σ_k
Real values		800.		30.		N/A	0
Effective values		792.1		29.93		N/A	0
Nominal EI	Perturbation	701.6	-11.42	23.36	-21.95	—	—
	Monte Carlo	940.4	18.72	0.03	-98.67	—	—
Unknown EI	Perturbation	871.7	10.04	23.36	-21.95	0.9487	—
	Monte Carlo	792.9	0.11	28.58	-4.52	1.0171	—
Variable EI	Perturbation	772.4	-2.48	34.69	15.88	0.9786	1.022E-02
	Monte Carlo	793.8	0.21	29.05	-2.93	0.9710	3.255E-04

Monte Carlo approach assuming a nominal EI ($k = 1$), an unknown but deterministic EI ($k = \mu_k$), or a random EI following the normal distribution ($k \sim \mathrm{N}(\mu_k, \sigma_k)$).

The standard deviation estimate by the perturbation approach is unaffected by a response offset between the model and measurements – in both instances σ_x is estimated to be 23.36 mm – only the mean estimate is affected. This feature may be useful for applications where variation is mainly sought – when determining the source of variability, for instance.

On the other hand, the Monte Carlo approach (which effectively models the nonlinear relationship between parameters and response) is sensitive to offset errors. The effective estimation error in the mass position mean and standard deviation drops from 19% and 99% to 0.11% and 4.5%, respectively, as EI is allowed to change. Once the model–experiment correlation is addressed, Monte Carlo gives excellent results for the mass position distribution.

The beam used throughout the experiment remained the same, therefore EI is unaccountable for any variability in the response. However, to determine how good the methods were in identifying unknown sources of variability (when prior knowledge on which parameters vary), k (hence EI) was taken as a random (Gaussian) variable. The Monte Carlo approach is successful in locating the uncertainty, as it estimates a negligible value for $\sigma_k = 3.255E-04$. The perturbation approach is less successful, attributing to EI a significant part of the variability.

4.4 Summary

As shown, the presented method does provide an efficient way to identify the parameter uncertainty from measurements. It can be used not only to identify aleatory uncertainty (parameter probability distributions), but also to identify epistemic uncertainty (deterministic parameters).

Although computationally efficient, the perturbation approach has problems when the linear approximation to the response is poor, and can lead to more information giving higher parameter estimation errors. Unless the response is known to be almost linear, it should only be used as an initial trial for a problem. Due to its lack of both accuracy and verifiability, any final conclusions should be deferred until applying the Monte Carlo approach.

The Monte Carlo approach produces accurate results, but care must be taken to ensure that the computational effort is realistic. For most practical applications a meta-model (which approximates the response surface on the parameter space region of interest) should be built, and then used for the Monte Carlo simulations.

Since the method copes with extraneous deterministic parameters, it can be applied to discover the main uncertainty contributors from a set of potential parameters – allowing the localisation of uncertainty sources.

Chapter 5

Robust design

5.1 Introduction

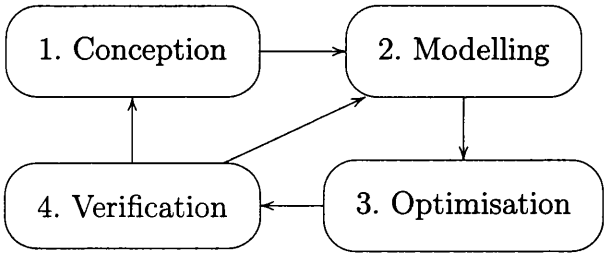

Figure 5.1: Phases of the design process

The design process Design is the process of producing something to meet specified functional and quality requirements.

The design process is usually achieved through the employment of optimisation methods. The objectives and restrictions are respectively modelled as functions and inequalities in terms of those variables which are under the designer control, referred as the *design variables.*

The design process can be applied directly to a system via experimentation, or to a model. The rest of this chapter assumes the latter, i.e., that a numerical model of the system is created as a reality surrogate, and that experimentation is only used for model validation and verification purposes.

Figure 5.1 shows the phases of the design process cycle.

Robustness in design The availability of well-established optimisation methods, together with increasingly computational power has allowed the modelling and design of large and complex structures, and providing answers with fine precision. However, these answers often prove to be poor when verified experimentally. This happens because there can be considerable uncertainty embedded in a model: parameters whose precise value is not known, uncontrollable external variables, and, if nothing else, there is always some uncertainty inherent in the act of modelling itself. Furthermore, the quality is desired to be high, and also consistent.

Robust design is the process of designing in face of uncertainty. It takes into account not only the nominal value of all input variables but also the uncertainty in those parameters whose value is imprecisely known or is intrinsically variable. From a mathematical point of view, robust design is the process of choosing the design variables while maximising the expected objectives and/or reducing its variance. That is, robust design aims to achieve designs which are less sensitive to uncertainty, and hence more robust.

5.1.1 Taguchi method

A successful methodology for robust design is the Taguchi method [68, 60] – an efficient and systematic methodology that applies statistical experimental design to improve product and manufacturing design.

Genich Taguchi realised that "in much industrial production, there is a need to produce an outcome on target, for example, to machine a hole to a specified diameter or to manufacture a cell to produce a given voltage", "that excessive variation lay at the root of poor manufactured quality and that reacting to individual items inside and outside specification was counter-productive" [79].

Quality and cost Poor quality results in losses to the manufacturer at the time of production. These losses are due to discarding items that fall outside the specification. Taguchi defended the wider view that it should also be considered the loss to the customer and society as a whole from the time a product is shipped. These losses are due to rework, waste of resources during manufacturing, warranty costs, customer complaints and dissatisfaction, time and money spent by customers on

failing products, and the eventual loss of market share [73].

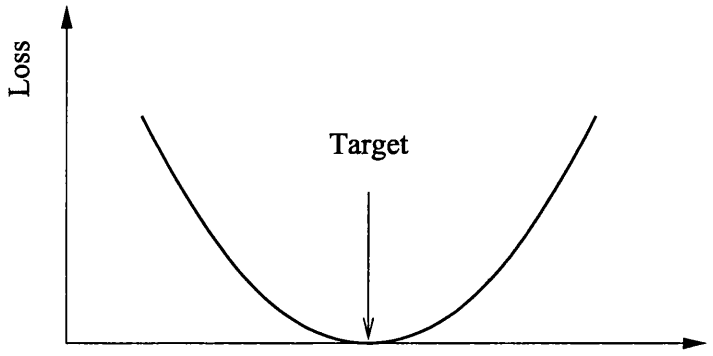

Figure 5.2: Quadratic loss function

These losses are naturally small when an item is near to the nominal product. To represent the losses Taguchi identified three situations: larger the better (for example, agricultural yield); smaller the better (for example, carbon dioxide emissions); and on-target, minimum-variation (for example, the mating of parts in an assembly). The first two situations are represented by simple monotonic loss functions, and the third situation by a squared-error loss function. Taguchi's quadratic loss function relates the quality cost to product variability (figure 5.2), allowing engineers to calculate the optimum design based on cost analysis and experimentation with the design.

Quality by design To achieve quality through variability reduction, Taguchi's proposed a strategy divided into three stages: system design, parameter design, and tolerance design.

System design System design is the development of a functional system under an initial set of nominal conditions. System design is the design at the conceptual level, involving creativity and innovation.

Parameter design Once the concept is established, during the parameter design stage, nominal values of the various dimensions and design parameters are set to levels that make the system less sensitive to variation in manufacture, environment and cumulative damage, thereby enhancing the system's robustness.

Table 5.1: L_9 (3^4) orthogonal array

	A	B	C	D
1	1	1	1	1
2	1	2	2	2
3	1	3	3	3
4	2	1	2	3
5	2	2	3	1
6	2	3	1	2
7	3	1	3	2
8	3	2	1	3
9	3	3	2	1

In order to determine the best combination of design parameters with a practical number of experimental evaluations, Taguchi resorted to orthogonal arrays from the design of experiments theory. Orthogonal refers to columns being mutually orthogonal, i.e., for any pair of columns, all combinations of factor levels occur and an equal number of times. Table 5.1 shows the orthogonal array for testing four parameters A, B, C, and D, at three levels each, called the L_9 orthogonal array, where the 9 designates the number of rows or configurations to be experimented. The orthogonal array experiment setup requires a fraction of the number of experiments when compared to all possible combinations. A full factorial combination for the same number of parameters and levels would require 81 (3^4) experimental evaluations instead of 9. There are greater savings in testing for larger arrays. For example, using an L_{27} array, 13 parameters can be studied at three levels by running only 27 experiments instead of $1,594,323$ (3^{13}) [73].

Factors are divided in two types: control factors and noise factors. Control factors are easily controllable by the experimenter. Noise factors are either difficult or expensive to control during manufacturing or operation. The experiments are setup as a cross array, where the control factors are varied according to an orthogonal array and for each combination of the control factors, the noise factors are varied systematically to another orthogonal array. The noise array provides "replications" for each control setting which are used to calculate statistics such as the mean response and the signal-to-noise (S/N) ratio. Figure 5.3 illustrates such experience setup.

Noise factors

j	1	2	3	4
X	1	1	2	2
Y	1	2	1	2
Z	1	2	2	1

Control factors

i	A	B	C	D
1	1	1	1	1
2	1	2	2	2
3	1	3	3	3
4	2	1	2	3
5	2	2	3	1
6	2	3	1	2
7	3	1	3	2
8	3	2	1	3
9	3	3	2	1

Data

$y_{i,j}$			

Figure 5.3: Example of Taguchi's cross array experimental setup

The purpose of the S/N ratio is to estimate the influence of noise factors on the response and help to minimise that influence [3]. The control factors are then divided into two groups: the adjustment and non-adjustment factors. The adjustment factors affect the mean response but do not significantly affect the S/N ratio. The non-adjustment factors affect the S/N. All other factors which do not influence either the mean or the S/N ratio can be used to reduce the cost, but are of no relevance in the parameter design problem itself.

Tolerance design After a successfully completed parameter design, and an understanding of the impact that each parameter has on performance has been attained, resources can be focused on reducing and controlling the variation in the few critical dimensions, loosening tolerances where possible and tightening where necessary.

Critics to Taguchi's approach The greatest achievement with Taguchi's robust parameter design approach was to provide a systematic and effective methodology for quality engineering. His techniques had worldwide influence. The main reason

for the popularity of his approach is that it is simple, easy to understand and follow, and does not require a strong background in statistics and mathematics.

However, Taguchi's work was carried out in isolation from the mainstream of Western statistics, and the solutions are often not optimal from that point of view. His approach suffers from some potential problems, as the loss model approach and product array experimental format may lead to suboptimal solutions, information loss, efficiency loss, and less flexible and unnecessarily expensive experiments [72].

5.1.2 Reliability-based design optimisation

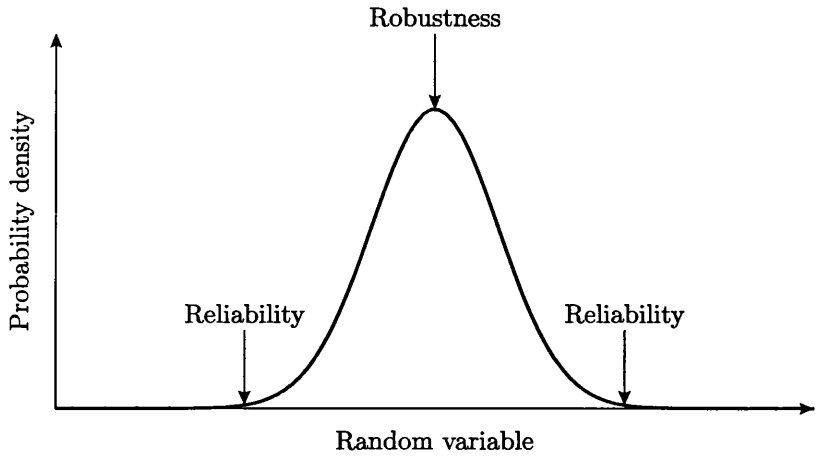

Figure 5.4: Reliability versus robustness in terms of the probability density function (adapted from [82]).

The reliability-based design problem is another class of uncertainty-based design problems that is complementary to the robust design problem. In a typical robust design problem a design with a performance measure that is relatively insensitive to uncertainty is sought, but in a typical reliability-based design problem a design with an acceptable (low) probability of failure is sought. Robust design is concerned with the event distribution near the mean of the probability density function, whereas reliability-based design is concerned with the event distribution in the tails [82], as illustrated in figure 5.4.

The domains of applicability of robust design and reliability-based design are different, but the same abstract mathematical formulation can be used to describe

both.

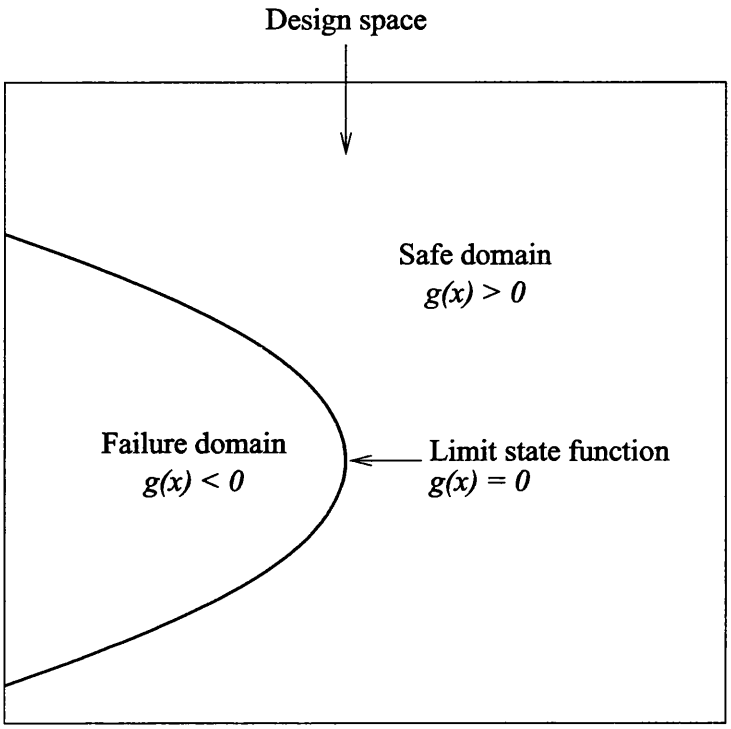

Figure 5.5: Limit state function

Reliability analysis Reliability analysis relies on the concept of the limit state function $g(\mathbf{x})$ – a nonlinear relationship between the design parameters where $g(\mathbf{x}) \leq 0$ defines the system failure condition (figure 5.5).

The probability of failure is then given by

$$P(g(\mathbf{x}) \leq 0) = \int_{g(\mathbf{x})\leq 0} f_{\mathbf{X}}(\mathbf{x})\,\mathrm{d}x \tag{5.1}$$

The integral in the right-hand side of equation (5.1) is difficult to evaluate directly, because of the high dimensionality of the design space and the complexity of the domain boundaries [82].

The First-Order Reliability Methods (FORM) and the Second-Order Reliability Methods (SORM) approximate the failure probability by transforming the design space into standard normal space and replacing the limit state function with

first-order and second-order Taylor series approximations, respectively, at the most probable point (MPP) of the limit state function.

Design optimisation The reliability index given by equation (5.1) can be used to achieve more robust designs. Hou et al. [32] devised a robust based design optimisation procedure by deriving the reliability sensitivities.

Limitations The FORM and SORM methods are efficient and give satisfying approximations to the failure probabilities in many cases. However, there are known counter-examples where these methods fail, such as when the normal transformation can distort the limit state function considerably, when there are multiple important failure regions, or when the first-order and second-order approximations are insufficient [58]. Thacker et al. [71] suggested using Monte Carlo sampling to find the multiple MPPs and then to compute the system failure probability by applying FORM and SORM at each MPP.

5.2 Conventional design optimisation

This section describes the standard formulation of design optimisation, which will serve as a starting point for a probabilistic robust design formulation in section 5.3.1.

Design optimisation is the process of determining the combination of design parameters which better meets the design objectives. Design objectives are specified as target functions and a set of restrictions.

5.2.1 Problem formulation

This subsection describes the problem formulation, which concerns the modelling stage of figure 5.1.

Design parameters The design parameters are those parameters which are controllable from the designer point of view. For instance, the length of a structural member or the thickness of a plate. Conventional design focus mostly on the nominal values of the design parameters.

The vector of design parameters will be denoted as

$$\mathbf{x} = [x_1 \; x_2 \; \ldots]^{\mathrm{T}} \tag{5.2}$$

System parameters The system parameters are those parameters which the designer either cannot or does not want to control. They are intrinsic to the system, and because of that are often omitted from design considerations.

Common system parameters are modelling parameters such as damping factors, external loads to the structure such as wind or ground motion, or noise factors in the manufacturing process.

The vector of system parameters will be denoted as

$$\mathbf{p} = [p_1 \; p_2 \; \ldots]^{\mathrm{T}} \tag{5.3}$$

When system parameter values are not precisely known then their estimates must be used instead, usually taken from worst-case scenarios.

Objectives An objective is a variable that is to be maximised or minimised. For example, a designer may wish to minimise production cost, maximise performance, minimise weight, minimise FRF peaks, minimise static displacement, etc.

Objectives will be denoted by

$$\mathbf{J}(\mathbf{x}, \mathbf{p}) = [J_1(\mathbf{x}, \mathbf{p}) \; J_2(\mathbf{x}, \mathbf{p}) \; \ldots]^{\mathrm{T}} \tag{5.4}$$

When there is more than one objective, they can either be weighted to form a single objective or considered simultaneously.

Constraints A constraint is a formal condition which any candidate solution must observe, regardless how fit it is with respect to the objectives.

Common design constraints are structural limits such as yield stress, geometric limits such as the maximum allowable deflection or maximum overall dimensions, economic limits such as a fixed budget, etc.

Constraints can be formulated as a set of inequalities

$$\mathbf{g}(\mathbf{x}, \mathbf{p}) \leq 0 \tag{5.5}$$

where $\mathbf{g}$ is the vector of constraints. Constraint inequalities can be reversed by multiplying by -1. Equality constraints can be replaced by two inequality constraints.

Constraints can either be used explicitly by the optimisation algorithm, or incorporated into the objective function [77].

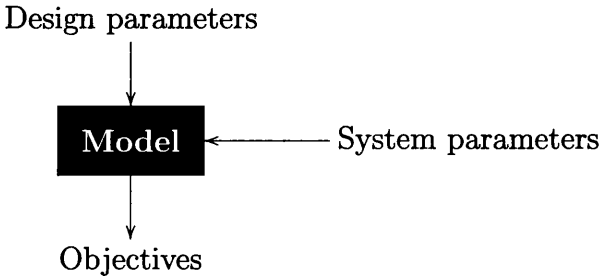

Figure 5.6: Design model

Model The model relates the constraints and the objectives to the design parameters and system parameters (figure 5.6), and may be regarded as a black-box.

5.2.2 Problem solution

This subsection describes the problem solution, which concerns the optimisation stage of figure 5.1.

Single objective problems If there is a single objective, then the optimum solution is given by

$$\mathbf{x}_{\text{opt}} = \arg\max_{\mathbf{x}} \mathbf{J}(\mathbf{x}, \mathbf{p}) \tag{5.6}$$

for the set of $\mathbf{x}$ which satisfies equation (5.5). This problem can be solved using appropriate optimisation techniques, such as gradient-based algorithms or the simplex method.

Multiple objectives problems If there is more than one objective then there is no unique optimum solution.

The multiple objective problem can be transformed into a series of single-objective problems [38], of the form

$$\arg\max_{\mathbf{x}} \sum_i \frac{\lambda_i}{sf_i} \mathbf{J}_i(\mathbf{x}, \mathbf{p}) \tag{5.7}$$

where sf_i is the scale factor and λ_i is the weight of the i-th objective, respectively. Weights are typically chosen such that $\sum_i \lambda_i = 1$ and $\lambda_i \geq 0$ resulting in a convex combination of the objectives.

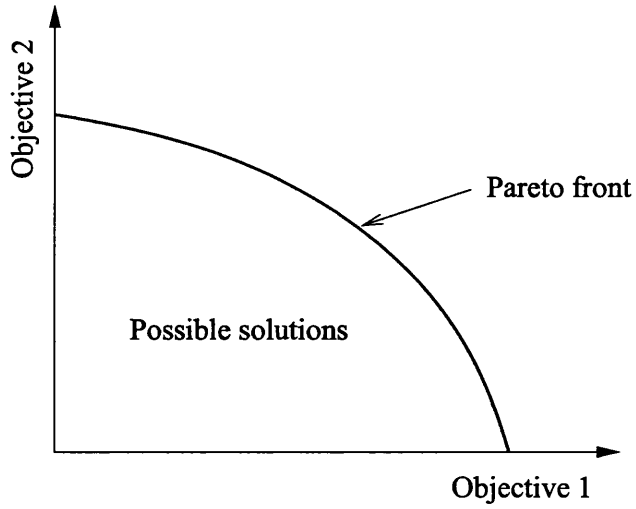

Figure 5.7: Typical Pareto front for a two objective problem

The set of solutions of equation (5.7) forms the so called *Pareto front* – a set of solutions such that no objective can be improved further without worsening another at the same time. Figure 5.7 illustrates the Pareto front for a two objective problem.

The final choice of design variables is left to the decision maker, who weights the objectives according to the trade-offs, thereby implicitly providing an aggregated objective function.

5.2.3 Limitations

The main limitation of the conventional design methodology described above is that the uncertainty, both in the design and system parameters, is unaccounted for in the optimisation.

Conventional design also does not provide an integrated process to design tolerances along with the nominal values. This is usually done by a posterior analysis, based on the parameter sensitivities.

Resorting to worst-case values or high safety factors on system parameters to compensate for the uncertainty/variability leads to over-dimensioned designs.

All of the these limitations usually lead to more iterations of the design cycle (figure 5.1). More experiments are required to fine tune the system parameter values and to adjust the tolerances of the design parameters to reach an acceptable design.

5.3 Probabilistic design optimisation

Robust design tries overcome the limitations of conventional design by taking into account the variability of the manufacturing process and the uncertainty in the modelling. This section describes a probabilistic approach to robust design, taking as base the formulation of conventional design in section 5.2.

5.3.1 Problem formulation

Design parameters In robust design, the designer can not only control the nominal values of the design parameters, but also their tolerances. Other design variables within the manufacturing process can also affect the variability in the design parameters. Generally, the designer can shape the probability density function of the design parameters.

The design parameter vector $\mathbf{x}$ will now be a realisation of the design parameter random vector $\mathbf{X}$. This vector is assumed to follow a probability distribution belonging to a family of probability distributions, such as

$$\mathbf{X} \sim \mathrm{D}_x(\tilde{\mathbf{x}}) \tag{5.8}$$

where $\mathbf{X}$ is the design parameter random vector, D_x is the probability distribution family, and $\tilde{\mathbf{x}}$ are the distribution parameters.

For example, when designing the length of a structural beam, the distribution family D_x could be a uniform distribution and the design variables $\tilde{\mathbf{x}}$ would be the nominal value and tolerance. When designing the thickness of a plate, the distribution family could be an AR(1) random field, and the design variables would be the mean thickness, the thickness standard deviation, and the surface smoothness (the random field correlation length).

The design variables $\tilde{\mathbf{x}}$ are distinct from the design parameters $\mathbf{x}$. The design variables are controlled by the designer, but the design parameters are fed to the model. The former shapes the latter, but does not completely determine it – the gap between them is filled by the uncertainty due to the manufacturing process.

System parameters Like the design parameters, system parameters will be reformulated as probability distributions in order to account for their uncertainty. The system parameter vector $\mathbf{p}$ will be the realisation of the system parameter random vector $\mathbf{P}$ which follows a given distribution $\mathbf{D}_p$

$$\mathbf{P} \sim \mathrm{D}_p \tag{5.9}$$

Uncertainty in the system parameters can stem from lack of knowledge. For example, damping factors are difficult to model precisely. Such system parameters have reducible uncertainty. Bayesian probability theory can be used to update the parameter probability distribution D_p from experimental measurements. The nature of other parameters is truly random, such as the loading caused by wind. The uncertainty of these parameters is irreducible.

Constraints In robust design, constraints can no longer be satisfied in a Boolean true or false sense. In general, for every combination of the design variables there is a nonzero probability that either the constraint is observed or not.

So, enforcing a zero probability of the constraint not being satisfied could narrow the set of admissible designs to the empty set. However, it is usually acceptable that the constraint is unsatisfied with a probability lower than a small residual probability

α:

$$P(\mathbf{g}(\mathbf{x},\mathbf{p}) > 0|\tilde{\mathbf{x}}) \leq \alpha \tag{5.10}$$

The complement probability, $1-\alpha$, is referred as the confidence level or reliability.

The value of α depends on the gravity of the violation of the constraint. The probability of structural failure should be low, but the probability of structural collapse should obviously be even lower.

According to equation (5.10), the constraints of equation (5.5) are reformulated as

$$\tilde{\mathbf{g}}(\tilde{\mathbf{x}}) = P(\mathbf{g}(\mathbf{x},\mathbf{p}) > 0|\tilde{\mathbf{x}}) - \alpha \leq 0 \tag{5.11}$$

The probability in equation (5.10) is given by the integral

$$P(\mathbf{g}(\mathbf{x},\mathbf{p}) > 0|\tilde{\mathbf{x}}) = \iint_{\mathbf{g}(\mathbf{x},\mathbf{p})>0} f_{\mathbf{X}}(\mathbf{x}|\tilde{\mathbf{x}})\, f_{\mathbf{P}}(\mathbf{p})\, \mathrm{d}\mathbf{p}\, \mathrm{d}\mathbf{x} \tag{5.12}$$

or alternatively

$$P(\mathbf{g}(\mathbf{x},\mathbf{p}) > 0|\tilde{\mathbf{x}}) = \iint f_{\mathbf{X}}(\mathbf{x}|\tilde{\mathbf{x}})\, f_{\mathbf{P}}(\mathbf{p})\, \delta(\mathbf{g}(\mathbf{x},\mathbf{p}))\, \mathrm{d}\mathbf{p}\, \mathrm{d}\mathbf{x} \tag{5.13}$$

where

$$\delta(\mathbf{x}) = \begin{cases} 1 & \text{if } x_i > 0 \text{ for all } i \\ 0 & \text{otherwise} \end{cases} \tag{5.14}$$

Equality constraints cannot be handled in a similar fashion to the inequality constraints, as the probability of an equality constraint being satisfied is always zero. Instead, equality constraints should be seen as a decrement in number of degrees of freedom of the model. Effectively, the presence of equality constraints implies that, for every equality constraint, the value of a parameter can be determined from all remaining parameters. Therefore, equality constraints can be hidden inside the model and the respective dependent parameter eliminated, as viewed from outside of the model.

Objectives Like constraints, objectives can only be meet in a statistical sense. Robust design objectives should be restated as maximising the original objectives

in a mean sense

$$\tilde{\mathbf{J}}(\tilde{\mathbf{x}}) = \mathrm{E}(\mathbf{J}(\mathbf{x}, \mathbf{p})|\tilde{\mathbf{x}}) \tag{5.15}$$

which is given by the integral

$$\tilde{\mathbf{J}}(\tilde{\mathbf{x}}) = \iint f_{\mathbf{X}}(\mathbf{x}|\tilde{\mathbf{x}})\, f_{\mathbf{P}}(\mathbf{p})\, \mathbf{J}(\mathbf{x}, \mathbf{p})\, \mathrm{d}\mathbf{p}\, \mathrm{d}\mathbf{x} \tag{5.16}$$

Utilities Maximising the mean implies that favourable or unfavourable scenarios are respectively desirable or undesirable in an equal manner. However, the designer may wish either to maximise the windfall likelihood or to minimise the risk instead. This can be accomplished by attributing a utility to each possible response, via the composition of a monotonic utility function $\mathbf{u}(\cdot)$ to the objectives.

The reason this is unusually relevant for conventional design is because the position of the maximum response is unaffected by the composition with a monotonic utility function. In other words, for conventional design, the best outcome is always the best, regardless how better it is compared with all the others. But for robust design, owing to the multitude of possible outcomes considered simultaneously, the relative importance of each outcome does matter.

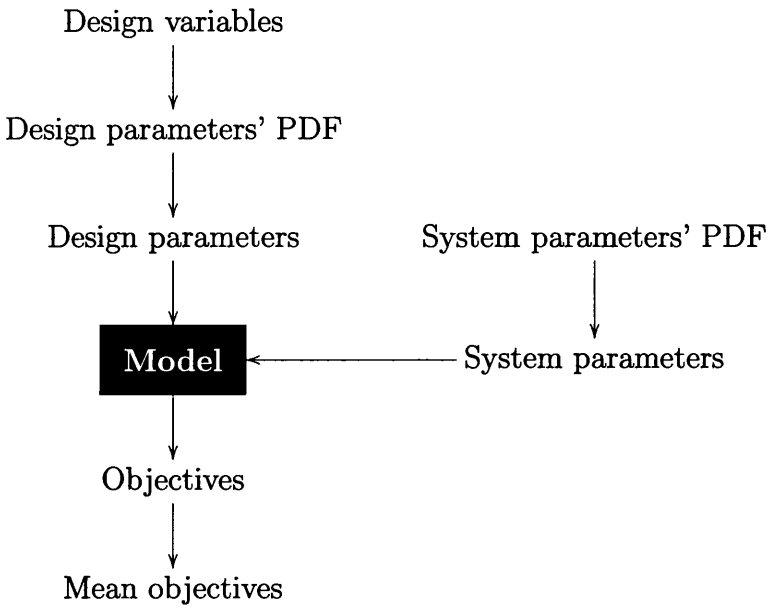

Figure 5.8: Robust design model

Model Robust design takes only a different perspective of the same reality from conventional design. Therefore the model, which describes the underlying reality, remains basically unaltered in robust design. The difference is in the kind of inputs fed to the model and in the outputs produced by it. The model parameters (inputs) are now joint probability density functions, and so is the expected response (output). The shift from deterministic (conventional) design optimisation to probabilistic (robust) design is more a change in substance than in form (figure 5.8).

Therefore, a good model for conventional design should also be good enough for robust design. When moving to robust design the remaining modelling effort is in choosing the appropriate probability distributions for the design and system parameters.

Nevertheless, robust design may require more detailed parameters. Specifically, whenever a nominal design parameter occurs more than once in the model a different parameter should be used for each instance. Imagine for example, the diameter of a set of spot welds. Although all of the spot welds have the same nominal diameter, the actual diameter of each spot weld differs from the others because of the variability in the welding process. So, although they can be modelled as a single diameter parameter in the deterministic model, in the nondeterministic model there should be a separate diameter parameter for each individual spot weld. This is necessary to faithfully model the statistical independence between parameters.

5.3.2 Problem solution

Since the robust design problem formulation results in a problem equivalent to conventional design, the solution procedures for conventional design described in section 5.2.2 also apply to robust design.

The main difficulty is calculating the integrals of equations (5.13) and (5.16), which can be reduced to the form

$$\iint f_{\mathbf{X}}(\mathbf{x}|\tilde{\mathbf{x}})\, f_{\mathbf{P}}(\mathbf{p})\, h(\mathbf{x},\mathbf{p})\, \mathrm{d}\mathbf{p}\, \mathrm{d}\mathbf{x} \tag{5.17}$$

Section 5.4 describes the traditional perturbation approach (similar to the techniques used for reliability analysis in section 5.1.2) which is efficient, if the necessary

conditions for its application (smooth response surface and small variations) are met.

Section 5.5 describes a novel and general approach based on the Monte-Carlo simulation method to evaluate these integrals.

As in chapter 4, the main idea behind both approaches is to factorise out of equation (5.17) as much computation as possible, allowing those factors to be pre-calculated before entering the iterative loop of the optimisation.

5.4 Perturbation approach

The application of the perturbation uncertainty propagation method provides a fast and often sufficiently accurate approximation to the integral of equation (5.17).

This is accomplished first by changing the domain of integration from the parameter space into the response space

$$\iint f_{\mathbf{X}}(\mathbf{x}|\tilde{\mathbf{x}})\, f_{\mathbf{P}}(\mathbf{p})\, h(\mathbf{x},\mathbf{p})\, \mathrm{d}\mathbf{p}\, \mathrm{d}\mathbf{x} = \int f_{\mathbf{y}}(y|\tilde{\mathbf{x}})\, \mathrm{d}y \tag{5.18}$$

where $y = h(\mathbf{x},\mathbf{p})$ is the response variable. The response y is then approximated by a first order Taylor series in h

$$y \approx h(\mathbf{x}^0,\mathbf{p}^0) + \left[\frac{\partial h}{\partial \mathbf{x}}(\mathbf{x}^0,\mathbf{p}^0)\right] \cdot (\mathbf{x}-\mathbf{x}^0) + \left[\frac{\partial h}{\partial \mathbf{p}}(\mathbf{x}^0,\mathbf{p}^0)\right] \cdot (\mathbf{p}-\mathbf{p}^0) \tag{5.19}$$

around point $(\mathbf{x}^0,\mathbf{p}^0)$. If the parameters $\mathbf{x}$ and $\mathbf{p}$ follow multivariate normal distributions

$$X \sim \mathrm{N}(\boldsymbol{\mu}_x, \boldsymbol{\Sigma}_x), \quad P \sim \mathrm{N}(\boldsymbol{\mu}_p, \boldsymbol{\Sigma}_p) \tag{5.20}$$

with mean vectors $\boldsymbol{\mu}_x$ and $\boldsymbol{\mu}_p$, and covariance matrices $\boldsymbol{\Sigma}_x$ and $\boldsymbol{\Sigma}_p$, respectively, then the response y will follow a normal distribution

$$Y \sim \mathrm{N}(\mu_y, \sigma_y) \tag{5.21}$$

where the mean response is

$$\mu_y = h(\mathbf{x}^0, \mathbf{p}^0) + \left[\frac{\partial h}{\partial \mathbf{x}}(\mathbf{x}^0, \mathbf{p}^0)\right] \cdot (\boldsymbol{\mu}_x - \mathbf{x}^0) + \left[\frac{\partial h}{\partial \mathbf{p}}(\mathbf{x}^0, \mathbf{p}^0)\right] \cdot (\boldsymbol{\mu}_p - \mathbf{p}^0) \tag{5.22}$$

and the response variance is

$$\sigma_y^2 = \left[\frac{\partial h}{\partial \mathbf{x}}(\mathbf{x}^0, \mathbf{p}^0)\right] \boldsymbol{\Sigma}_x \left[\frac{\partial h}{\partial \mathbf{x}}(\mathbf{x}^0, \mathbf{p}^0)\right]^{\mathrm{T}} + \left[\frac{\partial h}{\partial \mathbf{p}}(\mathbf{x}^0, \mathbf{p}^0)\right] \boldsymbol{\Sigma}_p \left[\frac{\partial h}{\partial \mathbf{p}}(\mathbf{x}^0, \mathbf{p}^0)\right]^{\mathrm{T}} \tag{5.23}$$

In particular, equation (5.16) becomes

$$\tilde{\mathbf{J}}_i(\boldsymbol{\mu}_x, \boldsymbol{\Sigma}_x) = \mu_y, \quad y = \mathbf{J}_i(\mathbf{x}, \mathbf{p}) \tag{5.24}$$

for every i-th objective, and equation (5.12) becomes

$$P(\mathbf{g}_j(\mathbf{x}, \mathbf{p}) > 0 | \boldsymbol{\mu}_x, \boldsymbol{\Sigma}_x) = 1 - F_y(0), \quad y = \mathbf{g}_j(\mathbf{x}, \mathbf{p}) \tag{5.25}$$

for every j-th constraint, where F_y is the response (Gaussian) probability distribution function.

Even if the parameter distributions are not multivariate normal, they can be transformed to be so, as described in section 2.2.5.

For the best approximation, the linearisation point $(\mathbf{x}^0, \mathbf{p}^0)$ should be as close as possible to the point $(\boldsymbol{\mu}_x, \boldsymbol{\mu}_p)$. However, the final optimum value $\boldsymbol{\mu}_x$ is unknown beforehand since it is the final result of the optimisation. Therefore an estimate of $\boldsymbol{\mu}_x$ must be used initially for $\mathbf{x}^0$, and if these two points differ too much then a further linearisation and optimisation pass must be performed using the new estimate.

The perturbation method suffers from the usual limitations, already outlined in previous chapters. The Monte Carlo simulation method, on the other hand, although more computationally demanding, is generally appliable and is therefore the main focus of this work.

5.5 Monte Carlo simulation approach

The Monte Carlo simulation method approximates the integral of equation (5.17) by sampling N values of $\mathbf{x}_i$ and $\mathbf{p}_i$ from the $\mathrm{D}_x(\tilde{\mathbf{x}})$ and D_p distributions respectively, reducing the integral to a sum

$$\int\int\int\int f_{\mathbf{X}}(\mathbf{x}|\tilde{\mathbf{x}})\, f_{\mathbf{P}}(\mathbf{p})\, h(\mathbf{x},\mathbf{p})\, \mathrm{d}\mathbf{p}\, \mathrm{d}\mathbf{x} \approx \frac{1}{N}\sum_{i=1}^{N} h(\mathbf{x}_i,\mathbf{p}_i) \tag{5.26}$$

Every new test value of the design variables $\tilde{\mathbf{x}}$ corresponds to a different probability distribution being taken from the probability distribution family, $\mathrm{D}_x(\tilde{\mathbf{x}})$. This, in turn, implies that a new set of N samples of $\mathbf{x}_i$ must be generated for every new value of $\tilde{\mathbf{x}}$, and the respective points $h(\mathbf{x}_i,\mathbf{p}_i)$ reevaluated. Resampling can be very time consuming, even if a meta-model is used as surrogate for the h function, since the number of samples needed for good accuracy in the Monte Carlo method is usually high.

The estimates given by equation (5.26) are nondeterministic, i.e., two evaluations using the same values of $\tilde{\mathbf{x}}$ will not necessarily give the same value, as the set of random samples generated differs. Furthermore, near the border, the constraints of equation (5.11) may sometimes be satisfied, but other times not. This phenomena is a serious obstacle to the employment of most optimisation algorithms.

The use of a pseudo-random number sequence generator with constant seed may reduce the problem, but that still does not guarantee the desirable smoothness of the objective and constraint surfaces.

To completely overcome this limitation, a higher number of samples N must be generated in order to reduce the randomness in the objective and constraint functions to below the sought precision in the design variables $\tilde{\mathbf{x}}$.

A better approach is to resort to the same reweighting technique developed for the uncertainty quantification in section 4.2.2.

Reweighting Instead of resampling for every trial of $\tilde{\mathbf{x}}$, a single set of samples is reweighted according to the desired distribution, as illustrated in figure 5.9.

The samples $\mathbf{x}_i$ are generated according to a different probability distribution

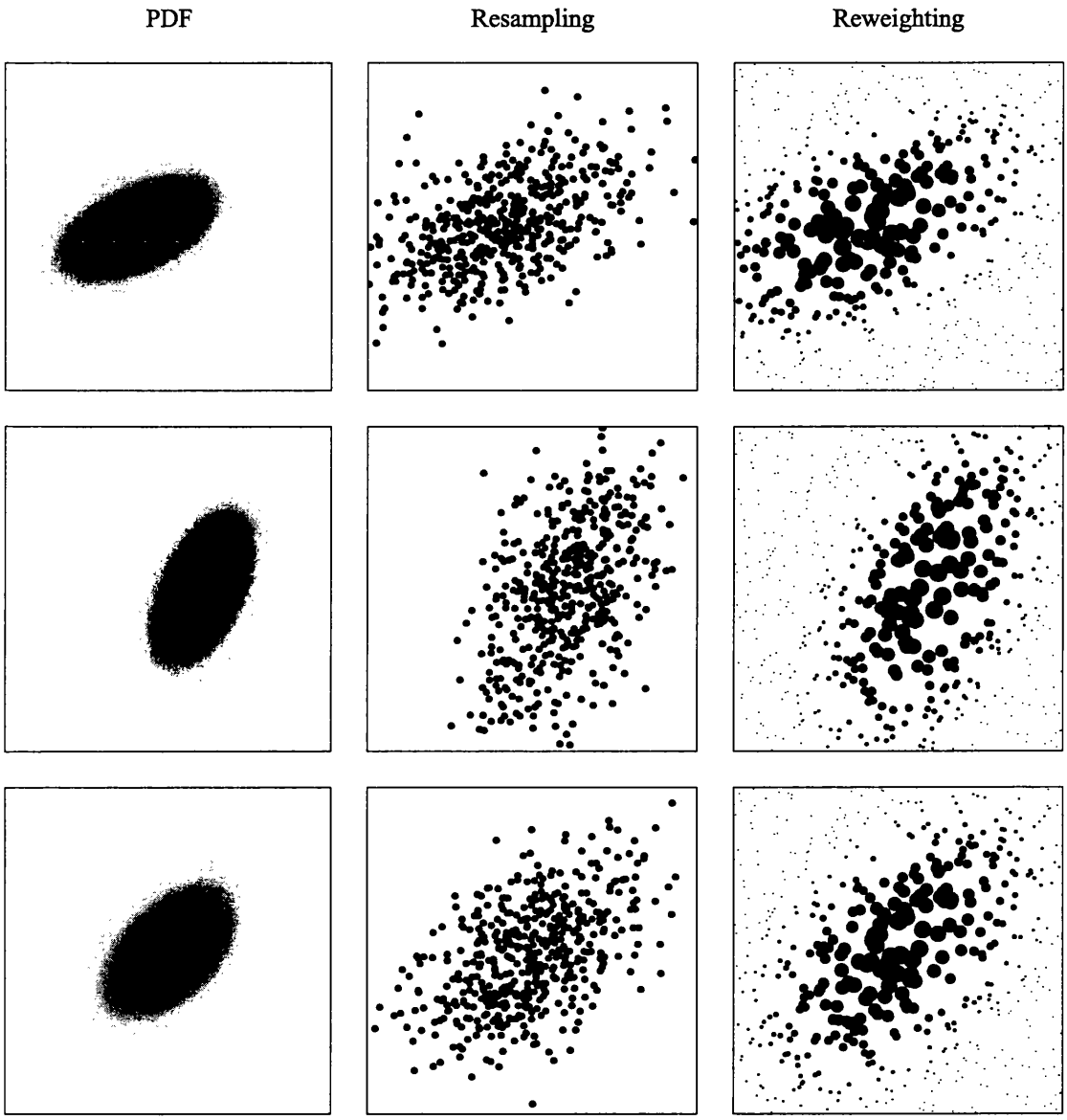

Figure 5.9: Reweighting versus resampling – there is a different distribution for each row; the left column shows the PDF, where the density is indicated by the shade of grey; the middle column shows samples taken according to each PDF, represented by blobs; and the right column shows a fixed set of samples, reweighted according to each PDF, where the sample weight is indicated by the blob size.

$g_{\mathbf{X}}(\mathbf{x})$, and equation (5.26) is rewritten as

$$\iint f_{\mathbf{X}}(\mathbf{x}|\tilde{\mathbf{x}})\, f_{\mathbf{P}}(\mathbf{p})\, h(\mathbf{x},\mathbf{p})\, \mathrm{d}\mathbf{p}\, \mathrm{d}\mathbf{x} \approx \frac{1}{N}\sum_{i=1}^{N} w_i(\tilde{\mathbf{x}})\, h(\mathbf{x}_i,\mathbf{p}_i) \tag{5.27}$$

where

$$w_i(\tilde{\mathbf{x}}) = \frac{f_{\mathbf{X}}(\mathbf{x}_i|\tilde{\mathbf{x}})}{g_{\mathbf{X}}(\mathbf{x}_i)} \tag{5.28}$$

Therefore only the weights w_i depend on $\tilde{\mathbf{x}}$, eliminating the need to resample $\mathbf{x}_i$ or reevaluate h.

Choosing the sample distribution The probability distribution $g_{\mathbf{X}}$ should be as close as possible to the probability distribution $f_{\mathbf{X}}$ that we want to test. If they are too different then some weights will drop to zero, because of the positiveness and unit integral properties of the probability density functions. The more different the distributions are, the more weights will be close to zero; the effective number of samples used drops to a small fraction of N; and the accuracy of the integral approximation will suffer.

The employment of an appropriate $g_{\mathbf{X}}$ can be determined by applying a simple statistical test. Lets assume that the integrand is the unit function, $h(\cdot) = 1$. Replacing this in equation (5.17) yields

$$\iint f_{\mathbf{X}}(\mathbf{x}|\tilde{\mathbf{x}}) f_{\mathbf{P}}(\mathbf{p})\, \mathrm{d}\mathbf{p}\, \mathrm{d}\mathbf{x} = \int f_{\mathbf{X}}(\mathbf{x}|\tilde{\mathbf{x}})\, \mathrm{d}\mathbf{x} \cdot \int f_{\mathbf{P}}(\mathbf{p})\, \mathrm{d}\mathbf{p} = 1 \tag{5.29}$$

since both $f_{\mathbf{X}}$ are $f_{\mathbf{P}}$ are probability density functions. Since equation (5.27) is an approximation to that integral, then

$$\frac{1}{N}\sum_{i=1}^{N} w_i(\tilde{\mathbf{x}}) \approx 1 \tag{5.30}$$

which is equivalent to saying that the mean weight $\overline{w} \approx 1$. If a large number of samples N is taken (true for virtually all applications) then, owing to the central limit theorem, the mean weight $\overline{w}$ will approximately follow a normal distribution

with $\mathrm{N}(\mu = \overline{w}, \sigma^2 = s_w/N)$, where s_w is the variance of w, given by

$$s_w = \frac{1}{N-1}\sum_{i=1}^{N}(w_i - \overline{w})^2. \tag{5.31}$$

That can be verified by the following statistical test for the mean of w [30]

$$\frac{\overline{w} - 1}{\sqrt{s_w/N}} \in [-z(\alpha), z(\alpha)] \tag{5.32}$$

where α is the desired level of confidence, and $z(\alpha)$ the inverse of the normal tail probability. This simple test can determine whether the given weights are effectively consistent with the $\overline{w} = 1$ statement and, therefore, if an adequate $g_{\mathbf{X}}$ was chosen.

Normalising the weights From equation (5.30) it follows that the mean weight $\overline{w}$ does not generally match unity – a consequence of the number of samples being less than infinity and the samples not covering all the parameter space. This can yield strange results when estimating probabilities, such as probabilities outside the $[0, 1]$ interval. To prevent this, it is advisable to normalise the weights in such circumstances, such as with equation (5.13), by using

$$\iint f_{\mathbf{X}}(\mathbf{x}|\tilde{\mathbf{x}})\, f_{\mathbf{P}}(\mathbf{p})\, h(\mathbf{x}, \mathbf{p})\, \mathrm{d}\mathbf{p}\, \mathrm{d}\mathbf{x} \approx \frac{1}{N}\sum_{i=1}^{N}\frac{w_i}{\overline{w}} h(\mathbf{x}_i, \mathbf{p}_i) \tag{5.33}$$

instead of equation (5.27).

5.6 Application

The approach described earlier will now be demonstrated using a numerical application.

5.6.1 Description

Model The application is a two dimensional beam truss structure with rigid joints and circular cross section beams (figure 5.10). Each beam is modelled with four

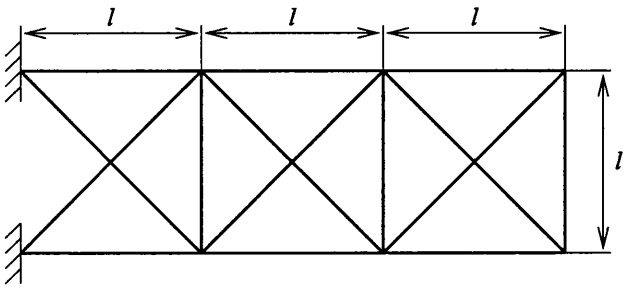

$l = 0.6\,\mathrm{m}$

Figure 5.10: Application – beam truss

Euler-Bernoulli beam elements vibrating in the plane. Every node has three degree of freedoms – displacement in x and y directions and a rotation in the out-of-plane direction. The outer-left nodes are clamped.

The beams are made of steel, with a Young's modulus of $E = 210\,\mathrm{GPa}$ and a density of $\rho = 7800\,\mathrm{kg}\,/\,\mathrm{m}^3$.

Figure 5.11 shows the lower natural frequencies and respective mode shapes for a nominal value of the diameter.

Design variables The design parameter is the beam diameter d.

$$\mathbf{x} = [d] \tag{5.34}$$

The hypothetical metalworking lathe that will be used to cut the circular beams produces circular shapes with a deviation which follows a normal distribution with $3\sigma = 1\,\mathrm{mm}$. Beams with a desired tolerance Δ_d are produced by scraping those whose dimensions are outside the specification. Therefore the diameter follows a truncated normal distribution (figure 5.12).

The robust design variables are the beam mean diameter μ_d, and its tolerance Δ_d.

$$\tilde{\mathbf{x}} = [\mu_d \; \Delta_d]^{\mathrm{T}} \tag{5.35}$$

Objective The main objective is to minimise production cost, where only the material costs will be considered.

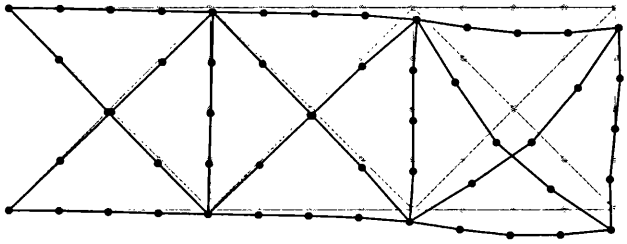

5.11.1: $\omega_1 = 112.81\,\text{Hz}$

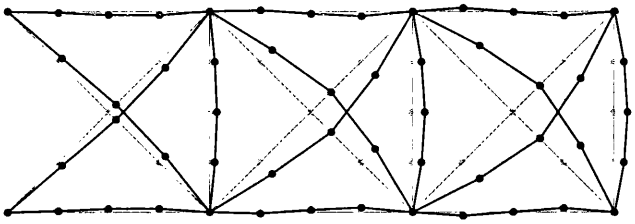

5.11.2: $\omega_2 = 136.73\,\text{Hz}$

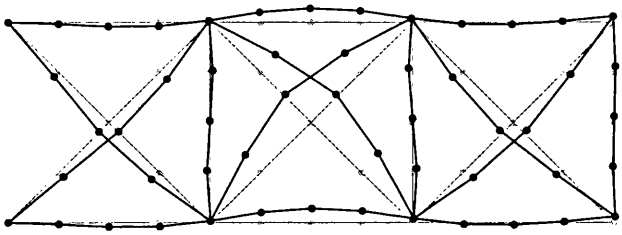

5.11.3: $\omega_3 = 137.33\,\text{Hz}$

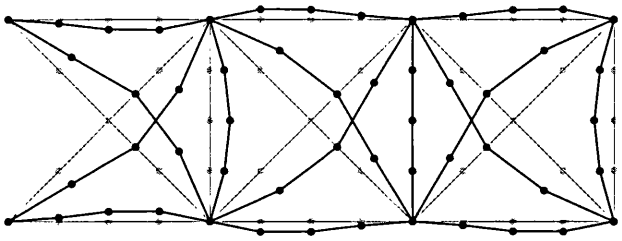

5.11.4: $\omega_4 = 148.42\,\text{Hz}$

Figure 5.11: Application – mode shapes for a nominal diameter ($d = 20\,\text{mm}$)

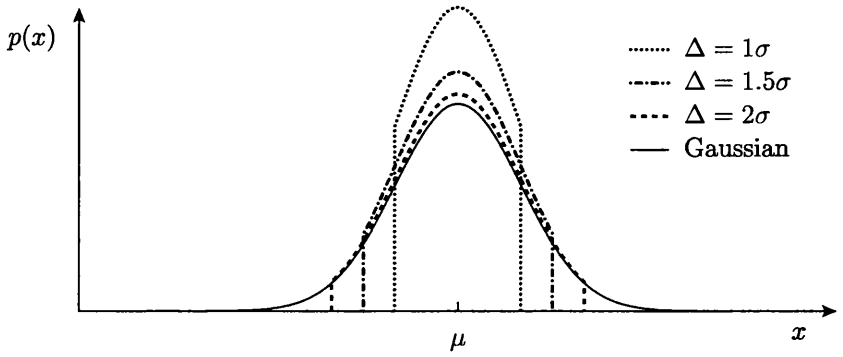

Figure 5.12: Truncated normal distribution probability density functions

The mass of a single beam of length l is

$$M(d) = l\frac{\pi d^2}{4}\rho \tag{5.36}$$

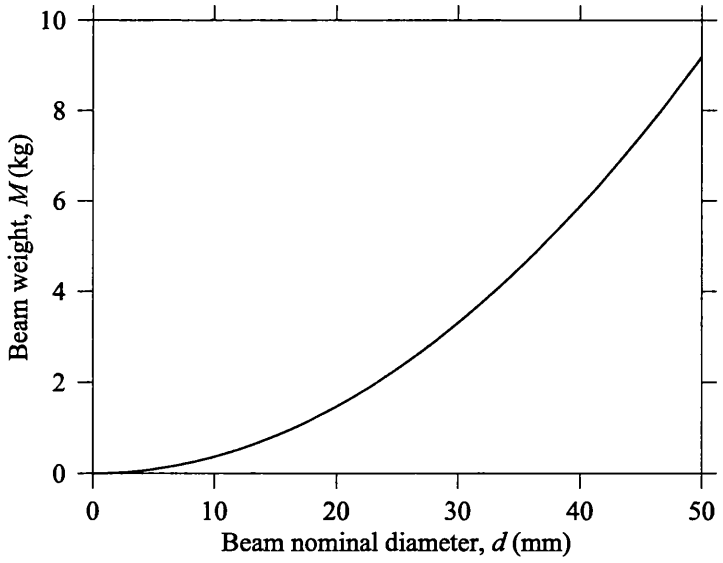

Figure 5.13: Application – the mass of a horizontal or vertical beam.

Figure 5.13 shows the mass associated with a horizontal or vertical beam. The design objective is then

$$\mathbf{J}(\mathbf{x}) = [M(d)] \tag{5.37}$$

For robust design purposes, the cost will include the mass of the structure, but also the mass of the scrapped metal

$$C \propto M \times N \tag{5.38}$$

where N is the expected number of beams which have to be produced in order to find one within specification.

Let p be the probability that a beam diameter is on specification. Then the probability that the first beam will have a diameter on spec is p, for the second is $(1-p)\times p$, the third is $(1-p)\times(1-p)\times p$, and so on. Therefore the average number of beams which have to be produced in order to find a beam on specification is

$$N = \sum_{i=1}^{\infty} i \times (1-p)^{i-1} \times p = \frac{1}{p} \tag{5.39}$$

The probability p is given by

$$p = F_z(\Delta_d/\sigma) - F_z(-\Delta_d/\sigma) \tag{5.40}$$

where F_z is the zero mean unit standard deviation Gaussian probability distribution function.

Figure 5.14 shows the predicted impact of the tolerance on the structure production cost given by equations (5.39) and (5.40). Tolerances lower than the tolerance normally given by the machine imply that a larger number of items will be scrapped. Tolerances higher than the intrinsic machine tolerance have almost no impact in the cost. Equations (5.39) and (5.36) show that the direction for lower costs is associated with lower diameters and higher tolerances.

The objective function is then

$$\tilde{\mathbf{J}}(\tilde{\mathbf{x}}) = [M(\mu_d) \times N(\Delta_d)] \tag{5.41}$$

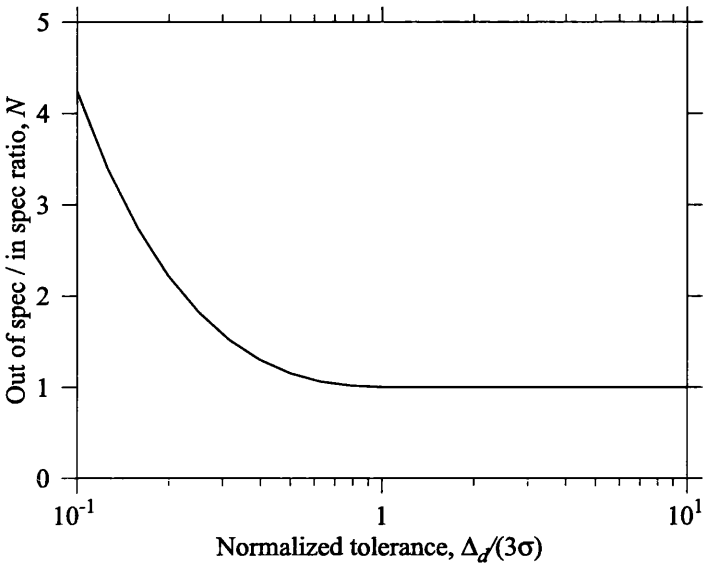

Figure 5.14: Application – cost associated with tolerance. The vertical axis has the expected number of beams which have to be produced in order to find a beam on specification. The horizontal axis has the specified tolerance normalised by the three times the lathe's standard deviation.

Constraints The only constraint will be that the fundamental natural frequency of the whole structure must lie above 100 Hz.

$$\mathbf{g}(\mathbf{x}) = [100 - \omega_1(\mathbf{x})] \leq 0 \tag{5.42}$$

$$\tilde{\mathbf{g}}(\tilde{\mathbf{x}}) = [P(\omega_1(\mathbf{x}) < 100) - \alpha] \leq 0 \tag{5.43}$$

for $\alpha = 10\%$.

5.6.2 Deterministic design

It is important to perform an initial deterministic analysis and design on the model. This gives insight into the model response surface and its peculiarities. Furthermore, the results from the deterministic design can be reused as initial estimates for the robust design. This is even more important since the quality of the initial guesses have a decisive impact on the results of the described methods.

Figure 5.15 shows the evolution of the first natural frequency of the truss, ω_1,

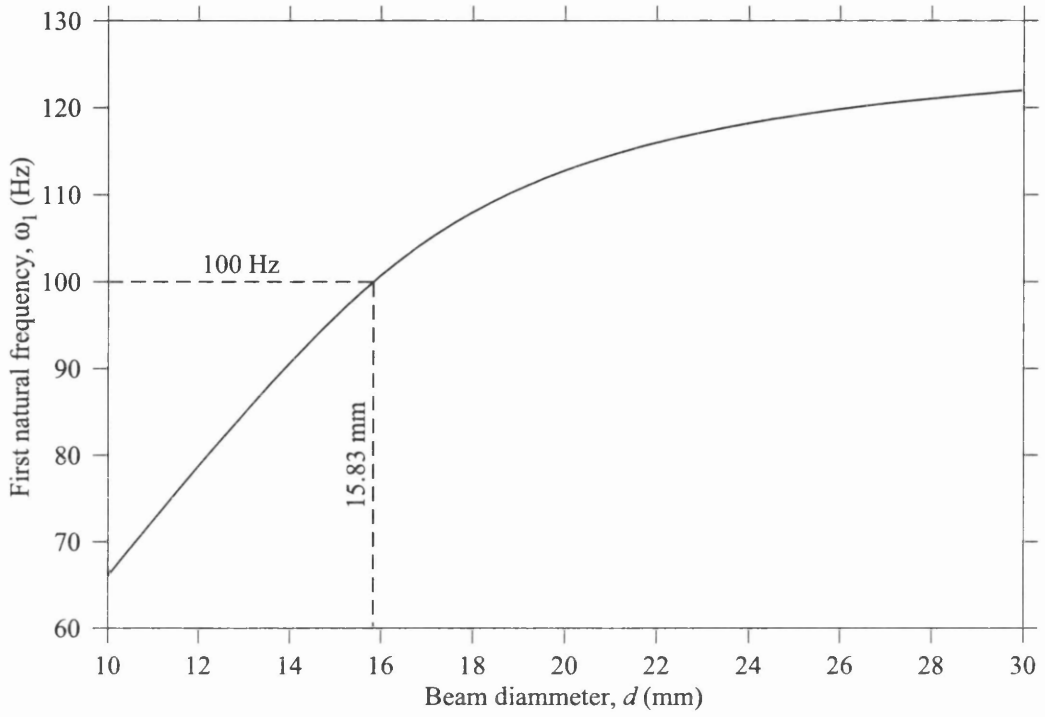

Figure 5.15: Application – deterministic response

with respect to the beam diameter, d.

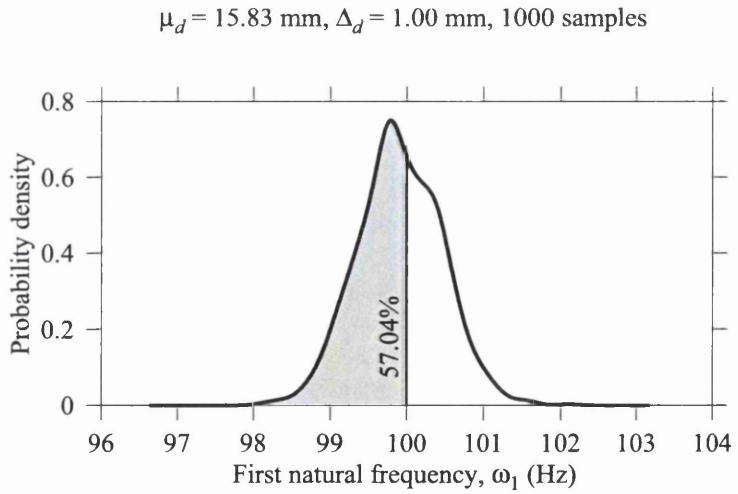

Figure 5.16: Application – response probability density function for the deterministic design optimum solution

From equations (5.37) and (5.42) it follows that a beam diameter of $d = 15.83\,\text{mm}$ would theoretically make the first natural frequency lie exactly at $\omega_1 = 100\,\text{Hz}$. But this value leaves no margin for variations. Figure 5.16 shows the resulting probability density function obtained by running the forward Monte Carlo simulation method, estimated from the samples using KDE. Clearly the structure does not observe the design constraints even approximately, as more than half of the samples violate the natural frequency constraint. Considering the need for a nonzero tolerance and the monotonic nature of the response curve, this diameter value is necessarily a lower bound for the final design value.

The curvature of the response curve is negative, which means that for higher values of the diameter d the first natural frequency ω_1 becomes less sensitive to variations.

5.6.3 Robust design – first stage

For robust design equations (5.41) and (5.43) will be used.

In this initial stage, the beam diameters will be considered to be identical.

Taking in account the considerations from the preliminary deterministic analysis in the previous section, the samples of the response curve will be taken uniformly around and above the deterministic optimum.

Figure 5.17 shows the objectives and the estimated failure probability over the area of interest of the parameter space, as well as the optimum design found. As expected, the probability that the constraint is unobserved drops as μ_d increases, and this drop is steeper for lower tolerances than for higher tolerances.

Considering all of the beam diameters to be equal is unrealistic. It is expected that the fluctuation of fifteen independent parameters would sometimes cancel out, resulting in less total variance due to averaging. Figure 5.18 shows the resulting response probability density function by running the forward Monte Carlo simulation method with the optimum design found, and it corroborates this statement as the failure probability is well below admissible 10%. So, for the real optimum design to be found, the beam diameters have to be considered individually.

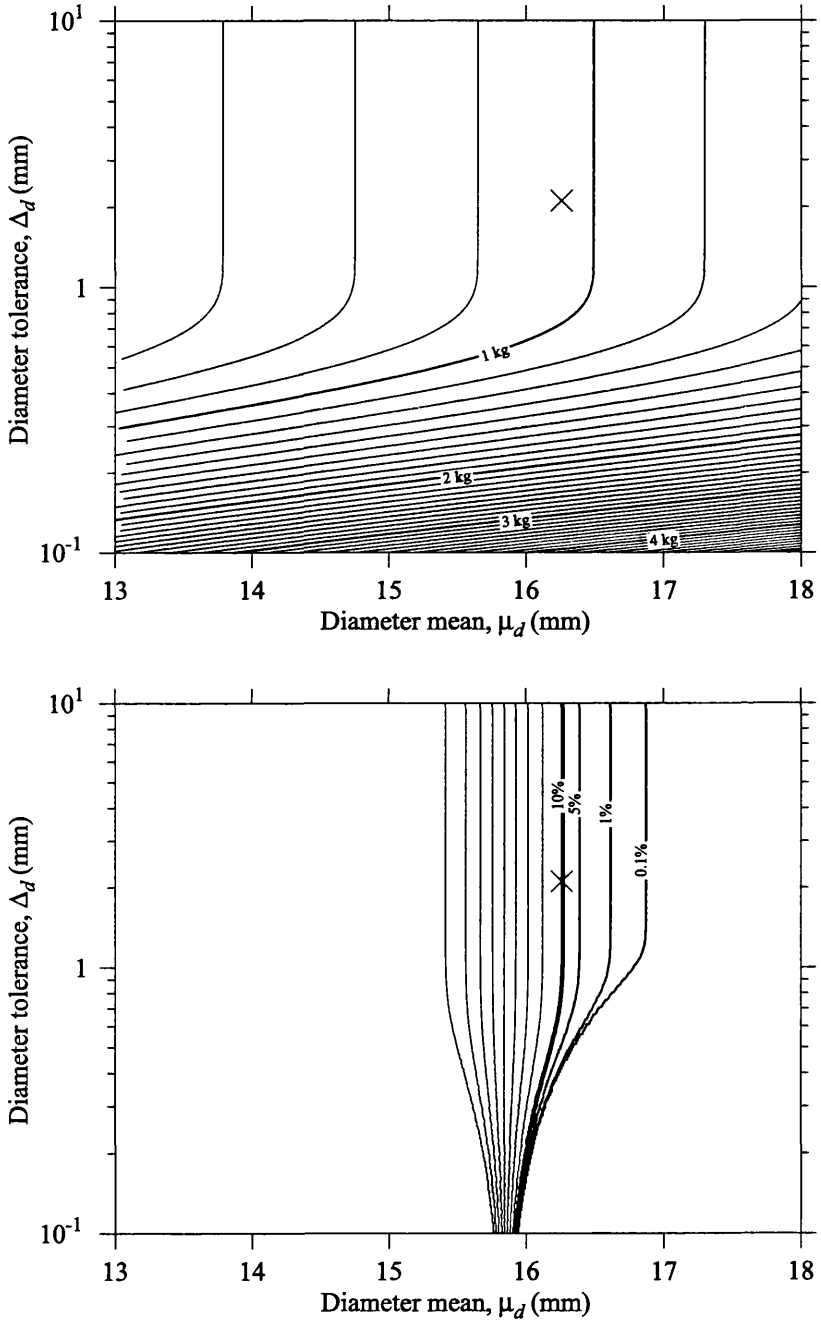

Figure 5.17: Application – objectives (above) and failure probability (below). The optimum design is marked with $\times$

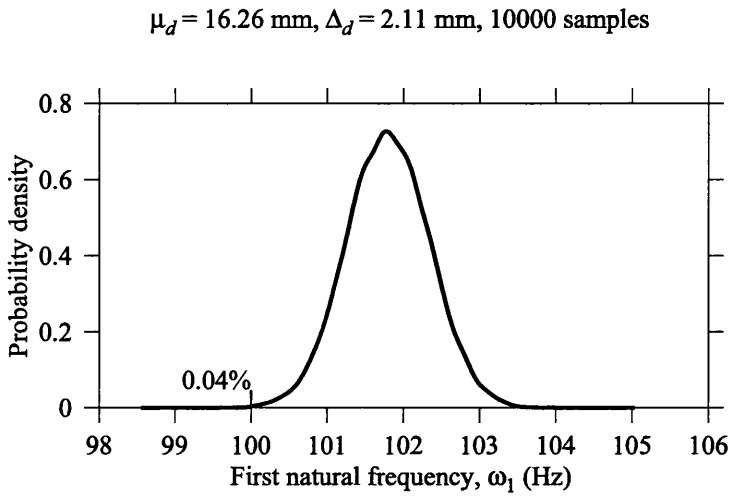

Figure 5.18: Application – response probability density function for robust design optimum stage 1 solution

5.6.4 Robust design – second stage

In this second stage of robust design, the diameters of the individual beams which make up the truss will be considered independent of each other. Equation (5.34) will be replaced by

$$\mathbf{x} = [d_1 \; d_2 \; \ldots \; d_{15}]^{\mathrm{T}} \tag{5.44}$$

The main difficulty of this stage is the dimensionality of the parameter space, as fifteen different parameters are considered instead of just one.

The first approach used to sample the parameter space was uniform sampling. But this attempt produced no results, as virtually all of the weights (with the exception of one or two) in equation (5.28) dropped down to almost zero. Zero weights occur when the distribution used for sampling does not produce enough points on the likely subspace of the distribution being tested. It is easy to understand why this happens with this application: although all of the diameters are independent, they all follow the same distribution. Thus the true distribution of the parameters will always be centred along the $d_1 = d_2 = \cdots = d_{15}$ line. Points sampled from a multivariate uniform distribution will be spread over a 15-dimensional volume, instead of being concentrated on the identity line manifold. This is illustrated by figure 5.19 for a two-dimensional parameter space.

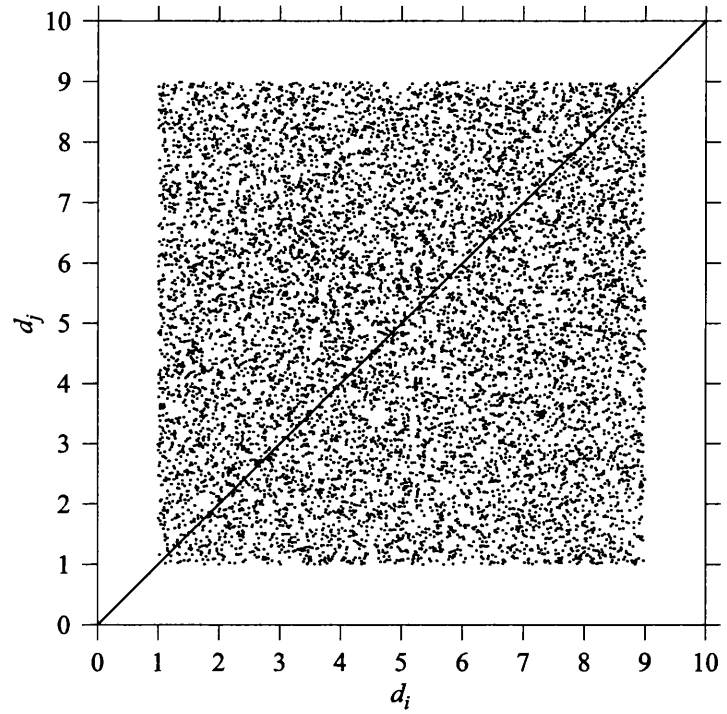

Figure 5.19: Application – uniform sampling of the parameter space

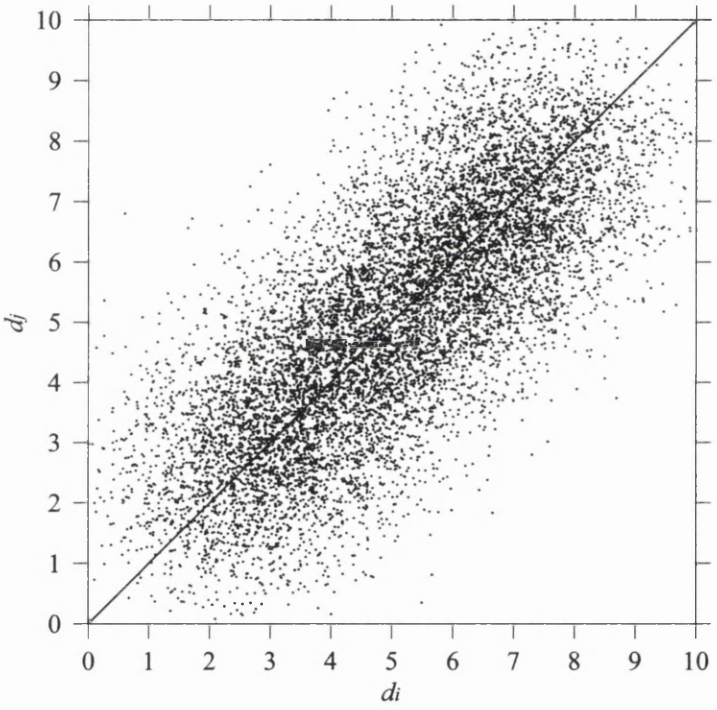

Figure 5.20: Application – efficient sampling of the parameter space – samples

A more efficient approach in this kind of application is to sample from the sum of a univariate distribution plus a zero centred distribution, such as a zero mean normal distribution:

$$\mathrm{U}(a, b) + \mathrm{N}(0, \sigma) \tag{5.45}$$

where $[a, b]$ specifies the range of interest to sample and σ specifies the spread of the samples around the identity line, as illustrated by figure 5.20.

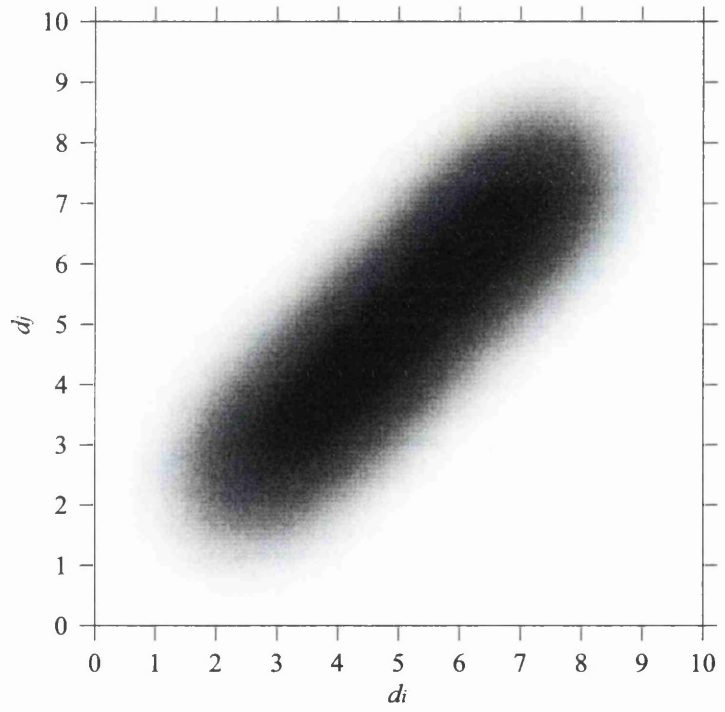

Figure 5.21: Application – efficient sampling of the parameter space – PDF

This distribution probability density function is given by

$$f(x) = \int_a^b \frac{1}{b-a} f_N(x - z)\,\mathrm{d}z \tag{5.46}$$

Equation (5.46) can be computed without much effort using numerical integration along z. Figure 5.21 shows the joint probability density function obtained for the same configuration as figure 5.20.

With this new distribution there were enough samples with nonzero weights. The optimisation converged to a new optimum result, with a lower nominal diameter and

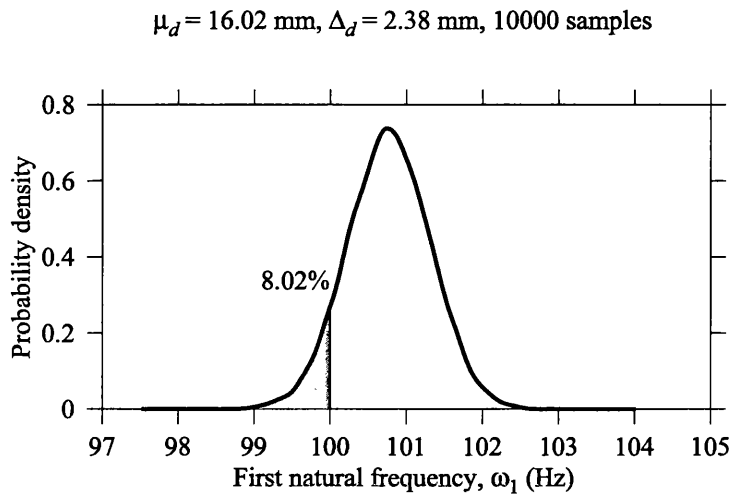

Figure 5.22: Application – response probability density function for robust design optimum stage 2 solution

higher tolerance, closer to the allowed 10%, as shown by figure 5.22.

These results could not be achieved if this stage was taken before the previous. There would be insufficient information to sample the parameter space effectively, rendering most sample points useless; and the presented method would give no advantage over the conventional Monte Carlo simulation method.

5.7 Summary

In this chapter the concept of design and robust design was introduced. The merits and criticisms of the Taguchi robust design approach were highlighted. A novel probabilist robust design methodology was presented, which allows the specification of design parameters and objectives in an intuitive manner, coping with uncertainty in both the control and noise parameters.

Numerically, the method is based on reusing the same set of samples by reweighting. Doing so is more efficient than the constant resampling performed with a straightforward application of the Monte Carlo method. Another advantage is that the resulting objective function becomes smooth and deterministic, facilitating the performance of optimisation algorithms.

The method was demonstrated on an application which, albeit purely academic,

included realistic features of cost and requirements. A staged approach to robust design was illustrated, starting with the deterministic design problem and ending with the fully-fledged robust model. This staged approach allows the accumulation of knowledge of the problem, ensures a successful design optimisation, and prevents the waste of computational resources.

The main disadvantage of the presented method is the requirement to know beforehand a reasonable estimate of the optimum design in order to efficiently sample the parameter space. Therefore this method is more appropriate for rapid convergence in the neighbourhood of the optimum design solution. If no prior estimate of the optimum design is available then a globally more convergent approach, such as resorting to simplified models or the regular Monte Carlo simulation method, should be employed in order to get a reliable initial estimate.

Chapter 6

Conclusions

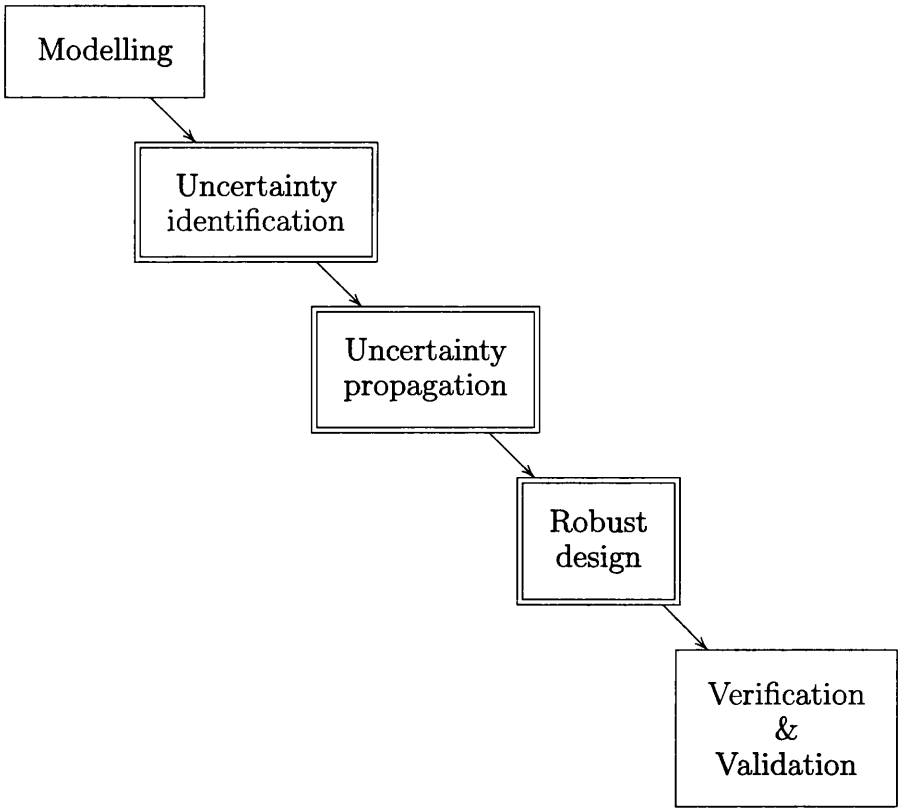

Figure 6.1: Uncertainty cascade

Figure 6.1 illustrates the stages of a typical uncertainty based analysis cascade. The first stage is modelling (deterministically) the system under analysis. The

last stage is the experimental verification and validation. The work presented here covered the inner stages: uncertainty identification, uncertainty propagation, and robust design.

Central to all uncertainty-based methods are the uncertainty propagation methods. The three most common uncertainty propagation methods – Monte Carlo simulation method, perturbation method, and fuzzy method – were compared in chapter 3. Owing to its generality and simplicity, Monte Carlo simulation remains the workhorse method of uncertainty methods. Because of its computational time-saving, the perturbation method can be useful to quickly obtain first estimates and eventually discard irrelevant parameters. However, considering today's available computing power and the Monte Carlo algorithm's parallel nature there is little reason to base design decisions on the unreliable predictions of other uncertainty propagation methods.

After a deterministic model is created, the uncertainty sources must be identified and characterised. Since direct measurement is often prohibitively costly or even impossible, a novel method to characterise uncertainty sources from indirect measurements was developed and presented in chapter 4. This method can accurately estimate the probability distribution of parameters of the uncertain model by maximising the likelihood of the indirect measurements. The measurement likelihood is estimated using highly efficient variations of the Monte Carlo simulation and perturbation methods. The developed method effectively acts as an uncertainty back-propagation method. The approach was verified experimentally in several applications with promising results.

The ultimate purpose of using uncertainty-based methods is almost always to perform robust design, i.e., achieving designs that are less sensitive to the unavoidable uncertainty and, therefore, with more consistent quality. In chapter 5 a probabilistic procedure for robust design was proposed. It is based on reweighting of the Monte Carlo samples to avoid the numerical inefficiencies of resampling for every design candidate. Although not globally convergent, the proposed method is able to quickly estimate with high accuracy the optimum design.

The main focus of this work was on structural dynamics, but care was taken to make the novel uncertainty identification and robust design methods general enough to allow other kinds of structural and non-structural analyses.

6.1 Directions for future work

Uncertainty representation This work was centred around the probabilistic uncertainty representation. Probability theory has received many critics, mostly because it relies upon the characterisation of probability density functions which are too often difficult to define precisely. Admittedly, if the probability distributions are imprecisely defined then the uncertainty quantification is compromised. Despite the shortcomings of probability theory, it is the author's strong belief that the probabilistic representation of uncertainty is not only a huge step forward from the deterministic-based design, but is also the most sure step. Probability theory provides a sound framework for quantifying uncertainty.

Other representations, such as intervals and fuzzy sets, have less demanding characterisation requirements. But they lead to non-optimum results when compared with the probability theory, since they convey often incomplete information.

If there really is little information to characterise a source of uncertainty in a model, then little reliable information should be expected from it. As the saying goes "garbage-in, garbage-out". Therefore this situation cannot be significantly altered by simply choosing a different uncertainty representation. Effort should be spent further characterising the uncertainty instead. That is, the "garbage-in" should be replaced by real information to prevent the "garbage-out".

In the future, higher order theories, such as imprecise probability theories, may proliferate in the uncertainty quantification field. Such theories provide the benefits of both worlds, at the expense of added complexity. They have the potential to address that middle ground where some probability information is indeed available, but it is incomplete or inaccurate.

Uncertainty propagation There is no such thing as an exhaustive comparison. No matter how extensive a comparison is, some things are always left out. The review in chapter 3 is not an exception.

There are many other variations of these three basic methods studied with more or less popularity that could enrich the comparison. A valuable addition would be to consider the Monte Carlo simulation plus meta-modelling, which has the potential to be a one-size-fits-all approach, rather than just pure straightforward Monte Carlo.

Even if just considering linear vibrations alone, there is a big gap between the most complex structure compared and those of real world applications, leaving unclosed the question of how far the conclusions drawn from these simple applications can be applied to real world applications.

Only Gaussian distributions and random fields were used to model parameter uncertainty on the studied applications. Although many physical phenomena follow the Gaussian distribution, many do not. The reason for choosing Gaussian distributions in this work was mainly convenience, because of its well known statistics and availability in software. But the suitability of the Gaussian to model some real world parameters is questionable, owing to its non-positiveness and symmetry.

Uncertainty identification Future work on the uncertainty identification method presented in chapter 4 could include determining the impact in the estimation results of choosing the wrong parameter distribution family. Or how the method copes with an arbitrary distribution family, such as polynomial chaos.

Robust design A substantial improvement for the method presented in chapter 5 would be to include adaptive sampling. Allowing the incorporation of more samples in the middle of the optimisation process, as better estimates of the optimum solution are available, would permit consideration of a wider range within the design space. The knowledge of a close initial estimate would then be less important, making the method more globally convergent.

Substructuring Uncertainty-based methods demand large computing resources. Substructuring analysis methods, such as component mode synthesis, provide efficient means to manage the complexity of built-up structures. So there is a potential time-saving benefit from integrating these methods into the proposed approach. The synergy potential is even greater when the different subsystems are statistically independent.

Appendix A

Implementation details

The integration of the uncertainty-based methods into finite element modelling poses a programming challenge. Virtually anything in a finite element model can be subject to uncertainty, and may therefore be parameterised. Node coordinates, material properties, element properties, and external excitations may all depend on parameters. Uncertainty propagation methods other than the Monte Carlo simulation method require non-trivial modifications to the finite element code for an efficient implementation. Uncertainty identification and robust design techniques introduce another higher class of parameters (parameterisations of the probability distributions themselves), distinct from uncertain parameters. So, uncertainty-based methods add a great deal of complexity to the finite element analysis.

This appendix describes how the finite element code, developed for the applications shown throughout this thesis, was implemented.

The code structure is described using *Unified Modelling Language* (UML) diagrams [52].

Programming language Finite element code, like most computer-intensive engineering codes, has traditionally been written in the FORTRAN language, due to its efficient translation of mathematical formula into machine code. However, for research purposes, the use of an interpreted, object oriented language provides many advantages. Object-oriented programming allows the mapping of the finite element concepts into an object hierarchy, thereby increasing code reuse and helping to manage complexity. Interpreted languages have quicker development cycles, owing to

the absence of the compilation stage and the use of dynamic typing. However, the interpretation causes a runtime overhead, which is non-negligible unless vectorial algebra is employed.

The first choice of language was MATLAB, also popular in engineering circles. MATLAB has powerful multidimensional array algebra abilities which reduces the interpretation overhead, provided the algorithms are rewritten in a vectorial fashion. Recent revisions of the MATLAB language also include object-oriented programming abilities. However, initial coding showed that its inefficient memory management prevented even the less complex uncertain finite element models to run in an acceptable time.

The final choice of language was Python[1], which is an interpreted, dynamically typed, object oriented language. The Numerical Python extension module[2] was also used, which adds MATLAB-like multidimensional-array abilities to the Python language.

Finite element modelling and analysis Figure A.1 describes the data structure of a finite element model. A model is composed of nodes, elements, element properties, and constraints. Every element is associated with multiple nodes and a single property.

Everything in a finite element model can potentially depend on parameters (either uncertain, or not). Also, every model constituent usually requires some initialisation and cleanup work to be done before and after a finite element analysis. So, in order to be treated uniformly by the code, every constituent in a finite element model implements the *Object* interface, which specifies pre- and post-processing hooks, and a model traverse hook.

The model traversing is accomplished with the aid of a visitor, which is called for every model constituent as the model is traversed. A visitor can be used to collect all uncertain parameters in the model, or design variables. This is illustrated in figure A.2 for the *Node* class (which checks if its coordinates are parameters, passing them to the visitor).

A property is either a field or a property sheet, i.e., a collection of properties

[1] `http://www.python.org/`
[2] `http://numeric.scipy.org/`

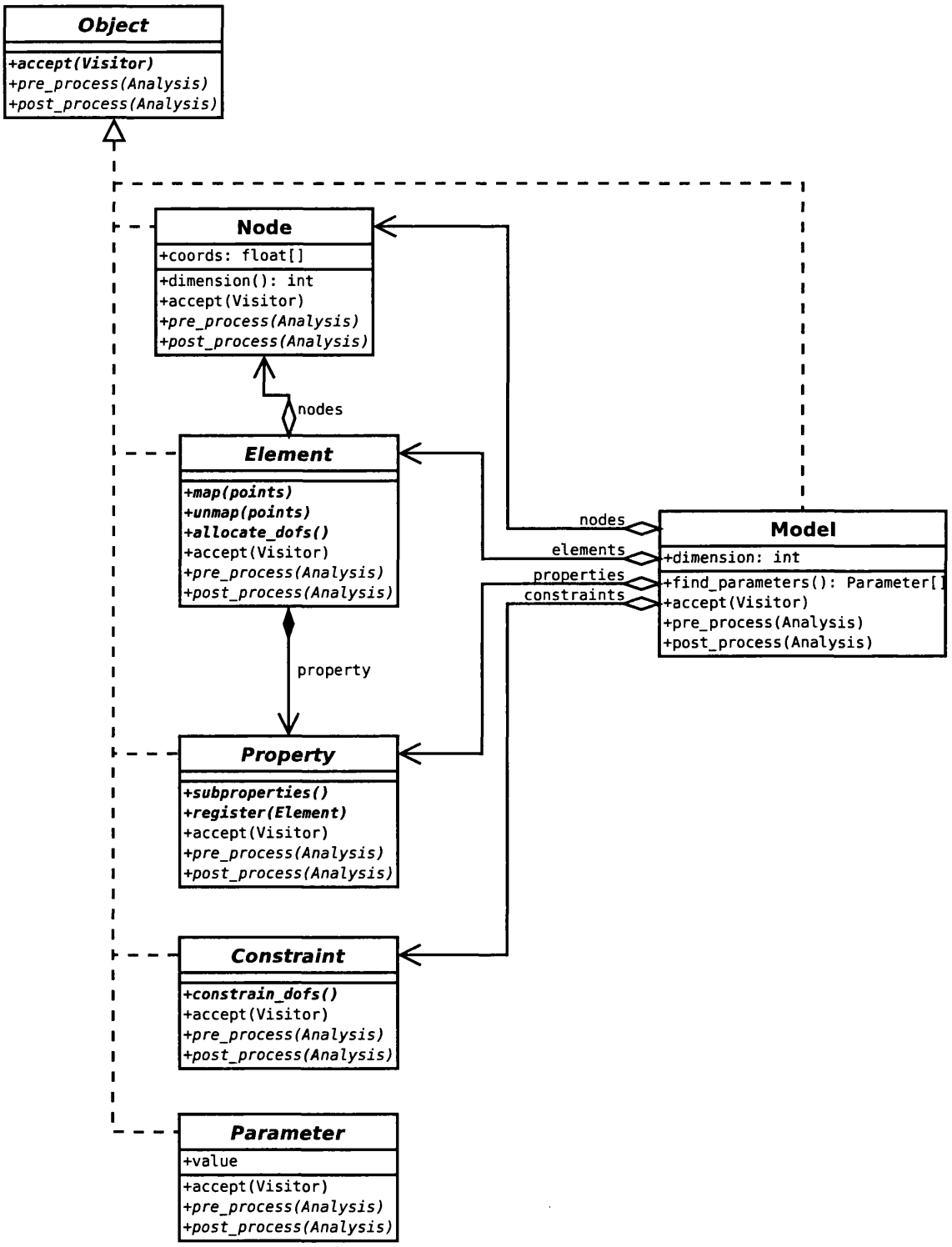

Figure A.1: Finite element model class diagram

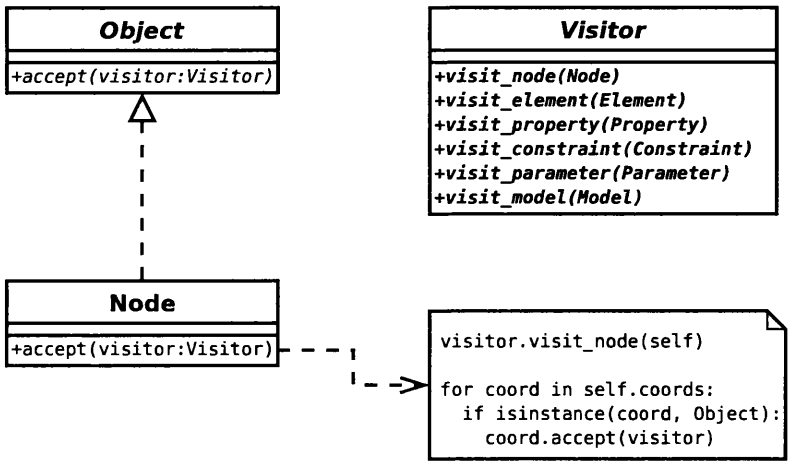

Figure A.2: Visitor class diagram

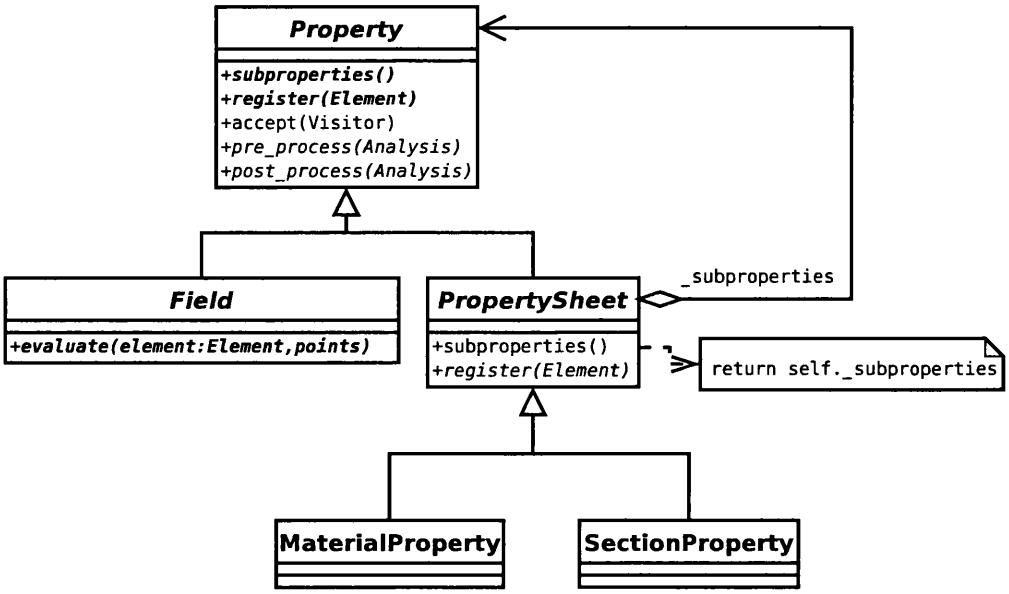

Figure A.3: Property class diagram

(figure A.3). Young's modulus, Poisson's ratio, the beam cross section, and the shell thickness are examples of fields. These are aggregated as materials properties, beam properties, and shell properties, which are examples of property sheets. This scheme allows the uniform treatment of individual fields, and collections of fields.

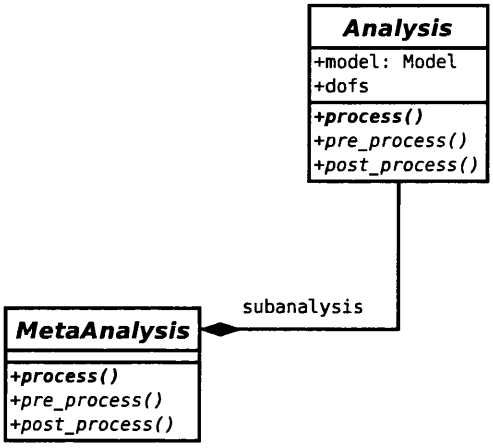

Figure A.4: Analysis class diagram

A basic analysis is associated with a model, and operates on a series of degrees-of-freedom (DoFs). There is another class of analysis, the *MetaAnalysis*, which operates on results of a sub-analysis instead (figure A.4).

Structural dynamics analysis Figure A.5 shows the class hierarchy for the structural elements. Every structural element must allocate DoFs (nodal displacements) during the pre-processing phase, and calculate its element stiffness and mass matrices during the processing phase. Much of this calculation code can be shared for classes elements. For the current implementation, these are the beam, shell, and solid element classes.

There are three variations of the beam element – *Beam1D*, *Beam2D*, and *Beam3D* – for one, two, and three dimensional spaces, respectively. *Beam1D* has in-plane bending only; *Beam2D* has in-plane bending and axial compression; and *Beam3D* has bending in two planes, axial compression, and axial torsion. The beam elements follow the Euler-Bernoulli theory for bending and the Saint-Venant theory for torsion.

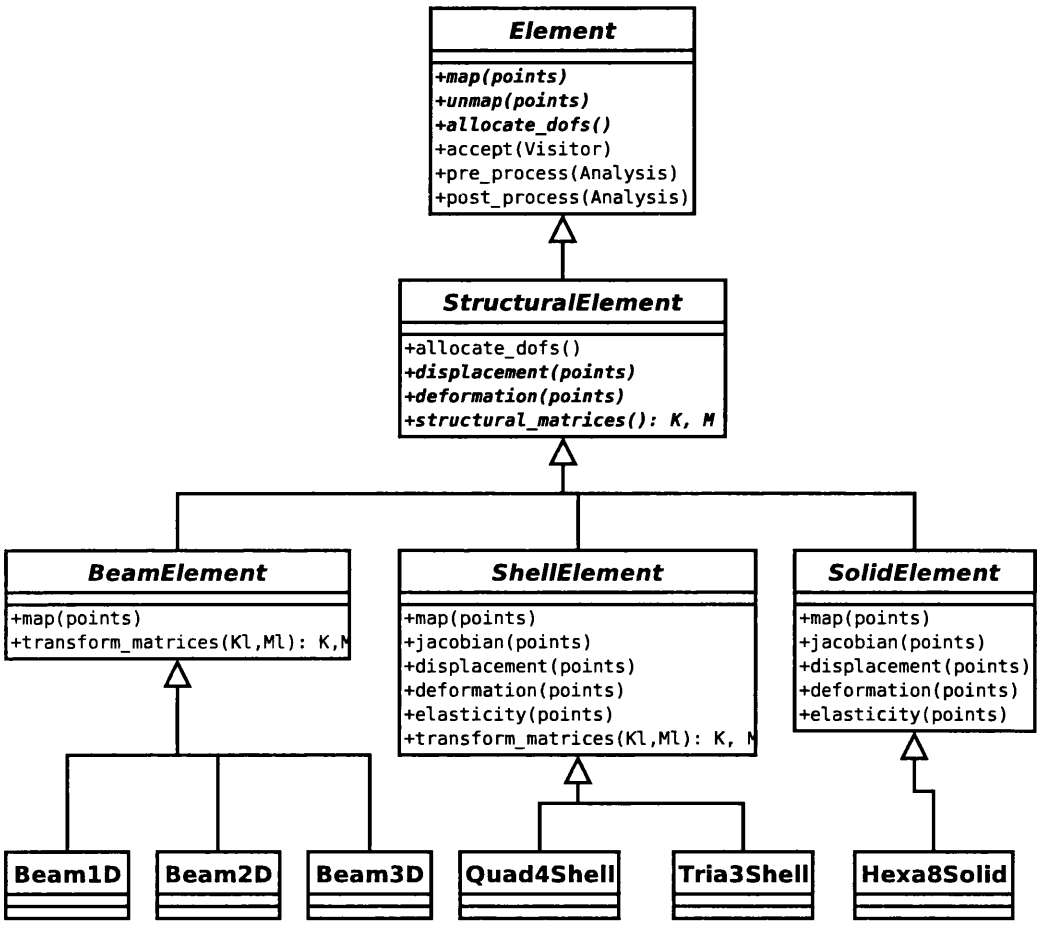

Figure A.5: Structural element class diagram

Shell elements follow the Reissner–Mindlin assumptions [83, cha. 8], with selective integration of the shear stresses.

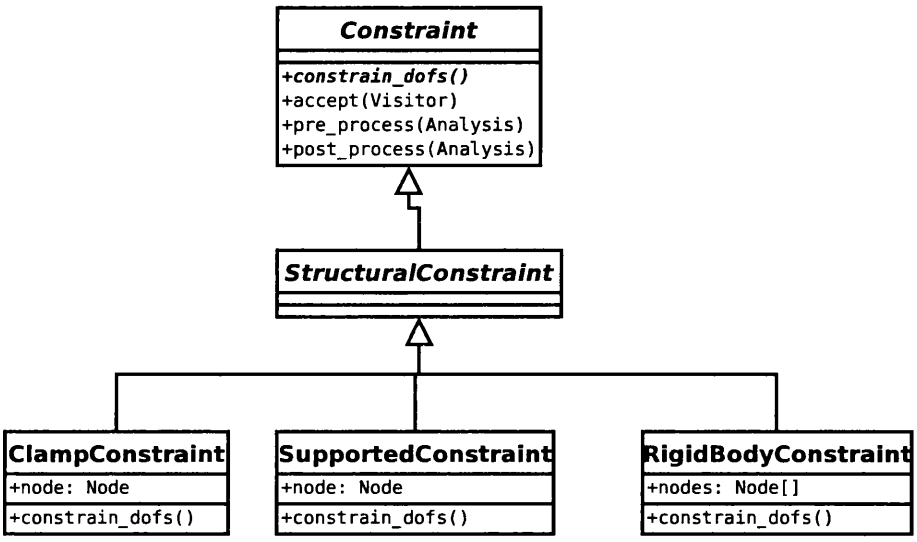

Figure A.6: Structural constraint class diagram

Figure A.6 shows the class hierarchy for the structural constraints. Every constraint must attach itself to DoFs (nodal displacements) during the pre-processing phase, and translate the constraint into a linear equation in term of DoFs during the processing phase.

Figure A.7 shows the class hierarchy for the structural analyses. The base structural analysis class assembles the global stiffness and mass matrices, which are used by derived class to calculate the modes, which in turn are used to calculate the FRFs.

Sparse matrices were used for the global stiffness and mass matrices. The ARPACK library[3] was used to determine the eigenvalues and eigenvectors of sparse matrices, and the UMFPACK library[4] was used to solve sparse linear systems.

Uncertainty representation and uncertainty propagation methods Uncertain parameters are a specialisation of the *Parameter* class, and can co-exist in the same model with other specialisations, such as design parameters (figure A.8).

[3] `http://www.caam.rice.edu/software/ARPACK/`
[4] `http://www.cise.ufl.edu/research/sparse/umfpack/`

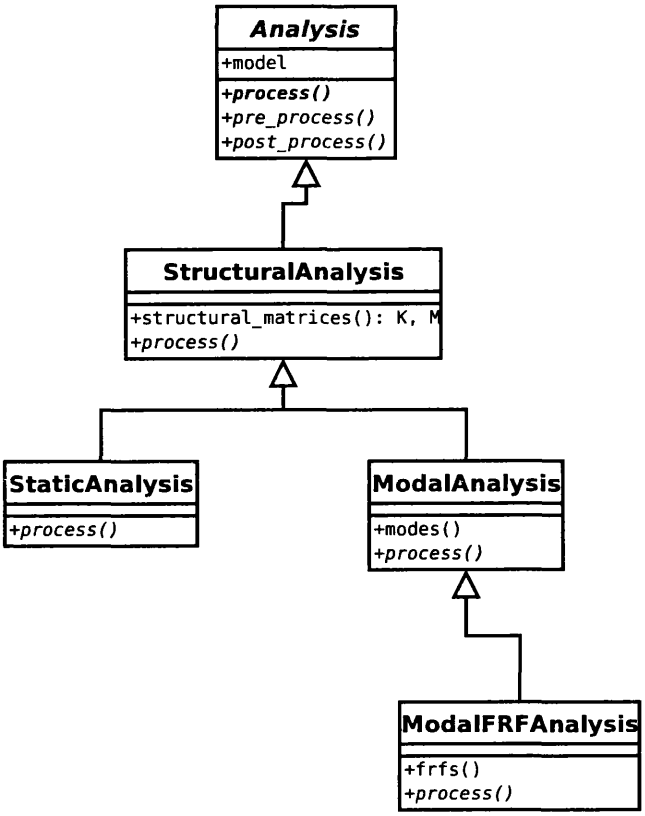

Figure A.7: Structural analysis class diagram

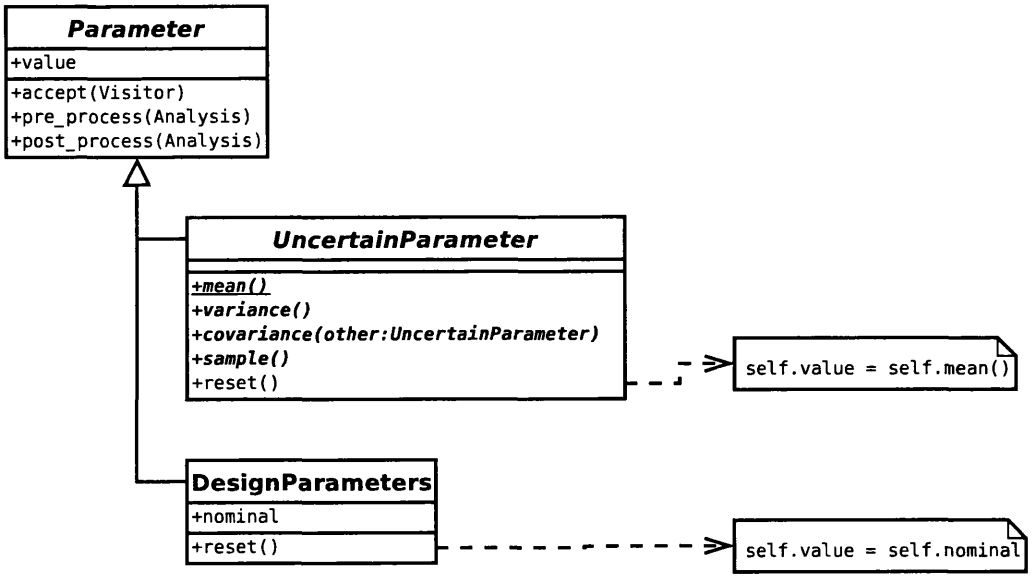

Figure A.8: Parameters class diagram

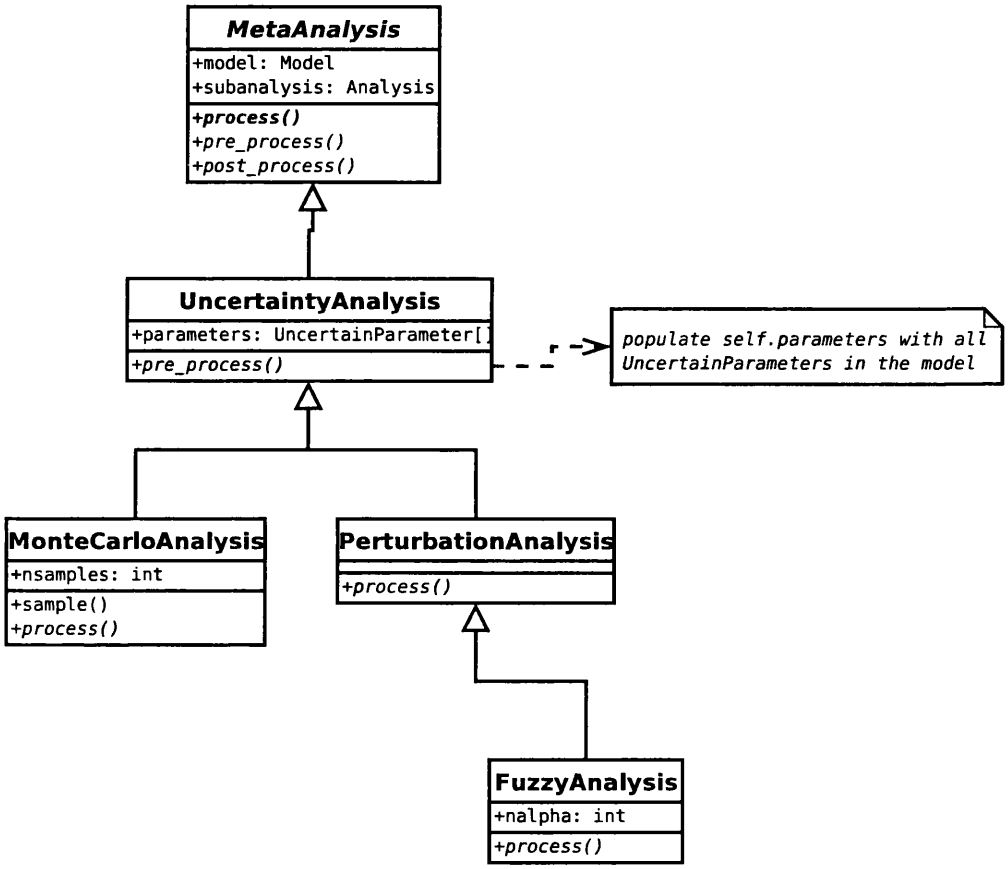

Figure A.9: Uncertainty analysis class diagram

Uncertainty analyses are specialisations of the *MetaAnalysis*. They must always be coupled with a sub-analysis, such as *ModalAnalysis* or *ModalFRFAnalysis* to propagate uncertainty through the model into the modes or FRFs, respectively.

Monte Carlo simulation method The Monte Carlo analysis simply samples the parameters; issues the sub-analysis to re-process itself; and computes the statistics of the sub-analysis results.

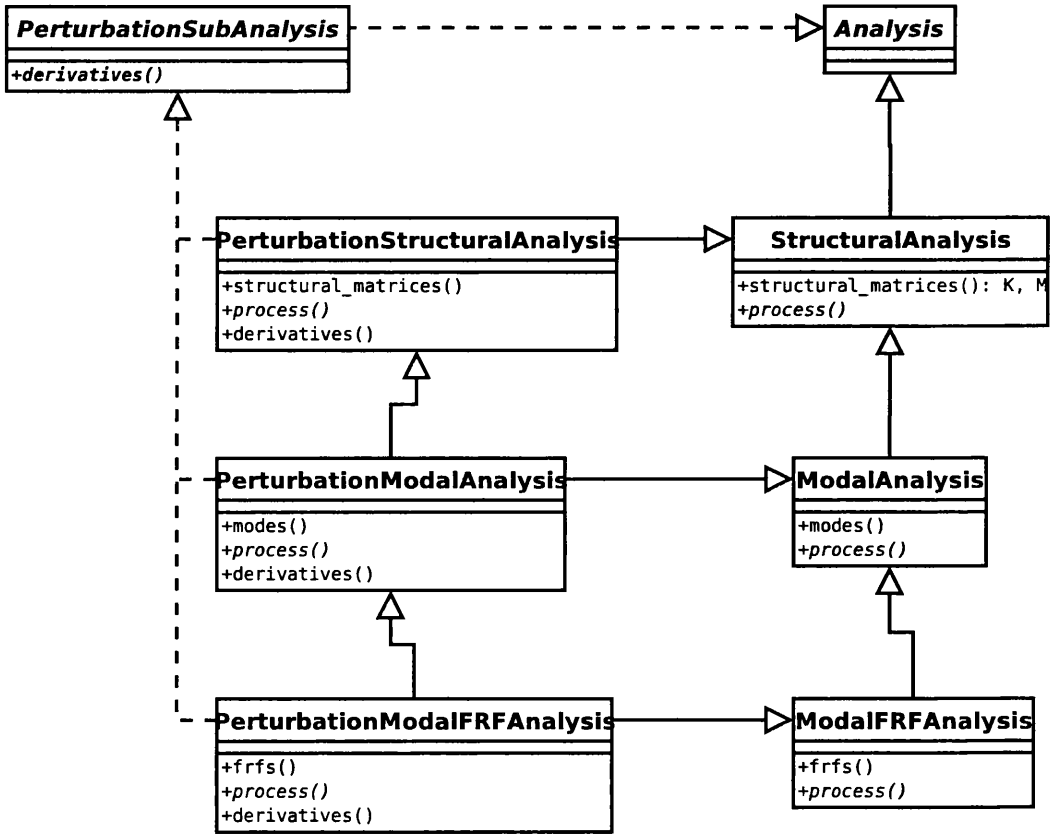

Figure A.10: Perturbation analysis class diagram

Perturbation method For an efficient implementation, the Perturbation analysis cannot be applied directly to any sub-analysis. It expects that the analysis results include not only the response evaluation, but also the evaluation of the response first order derivatives. Therefore, a parallel analysis class hierarchy was implemented, which also calculates stiffness matrices, mass matrices, modes, and

FRF derivatives (figure A.10). This added complexity allows for the derivatives to be calculated on a per-element basis. For each element, only the partial derivatives with respect to the parameters which affect that element are computed, and all of the other partial derivatives are zero. This yields an enormous computational time-saving compared to performing numerical derivatives of the global stiffness and mass matrices, whereby every element stiffness and mass matrices would have to be recomputed for each partial derivative. The modes, modal shapes, and FRF derivatives were calculated from the stiffness and mass matrices using the techniques referred to in section 2.3.2.

Fuzzy method In the current implementation, the fuzzy analysis is a specialisation of the perturbation analysis, as the sub-analysis result derivatives are used to reduce the parameter search space for each α-cut by assuming a monotonic response function.

Random fields Element and material properties are modelled as fields, defined over the mesh domain (figure A.11). Two kinds of fields are possible: constant and random fields. The *MidpointRandomField* class can discretise a homogeneous continuous random field model into a discrete set of random variable, creating the respective instances of the *UncertainParameter* class.

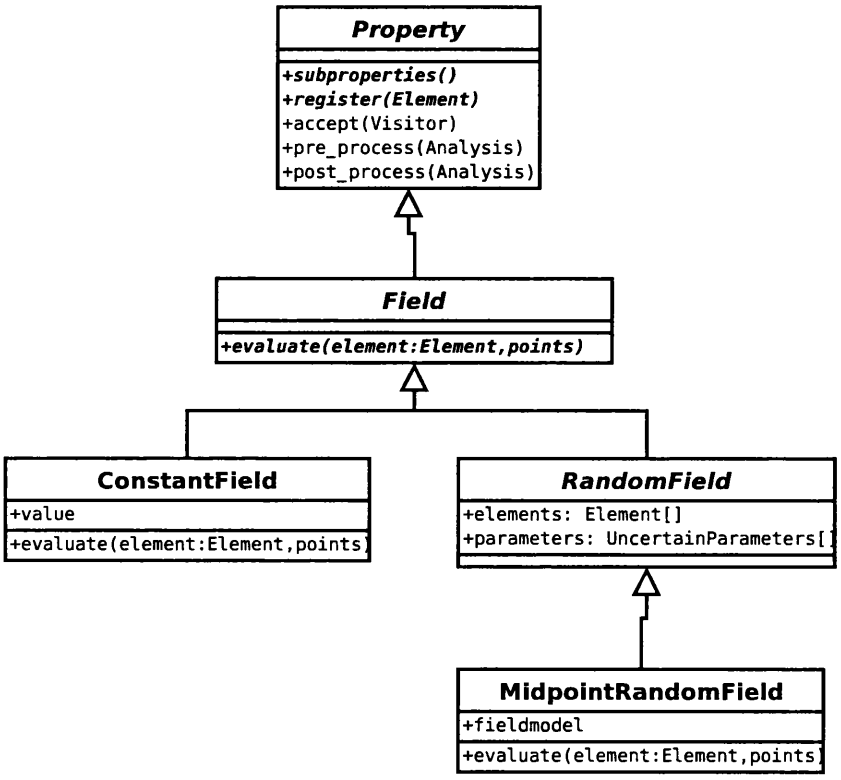

Figure A.11: Random field class diagram

Bibliography

[1] S. Adhikari and R. S. Langley. Distribution of eigenvalues of linear stochastic systems. In *Proceedings of the 9th International Conference on Applications of Statistics and Probability in Civil Engineering (ICASP 9)*, volume 1, pages 201–207. Millpress, July 2003.

[2] Jane M. Booker. A whirlwind tour of statistical methods in structural dynamics. In *Proceedings of the IMAC-XXIII*, Orlando, Florida, January 2005.

[3] J. Bérubé and C. F. J. Wu. Signal-to-noise ratio and related measures in parameter design optimization: an overview. *Sankhya*, 62:417–432, 2000.

[4] Li Chen and S. S. Rao. Fuzzy finite-element approach for the vibration analysis of imprecisely-defined systems. *Finite Elements in Analysis and Design*, 27:69–83, 1997.

[5] Jianye Ching and James L. Beck. New bayesian model updating algorithm applied to a structural health monitoring benchmark. *Structural Health Monitoring*, 3(4):313–332, 2004.

[6] J. D. Collins, G. C. Hart, T. K. Hasselman, and B. Kennedy. Statistical identification of structures. *AIAA Journal*, 12(2):185–190, 1974.

[7] N. Cottin and H. G. Natke. On the parameter identification of elastomechanical systems using weighted input and modal residuals. *Ingenieur- Archiv*, 56(2): 106–113, 1986.

[8] B. S. L. P. de Lima, E. C. Teixeira, and N. F. F. Ebecken. Probabilistic and possibilistic methods for the elastoplastic analysis of soils. *Advances in Engineering Software*, 32:569–585, 2001.

[9] Beatriz S. L. P. de Lima and Nelson F. F. Ebecken. A comparision of models for uncertainty analysis by the finite element method. *Finite Elements in Analysis and Design*, 34:211–232, 2000.

[10] B. Van den Nieuwenhof and J.-P. Coyette. Modal approaches for the time-harmonic analysis of random structures with the stochastic finite element method. In *Proceedings of the 2002 International Conference on Modal Analysis Noise and Vibration Engineering (ISMA2002)*, pages 1845–1851, 2002.

[11] G. Deodatis. Bounds on response variability of stochastic finite element systems. *Probabilistic Engineering Mechanics*, 116(3):565–585, March 1990.

[12] G. Deodatis. Bounds on response variability of stochastic finite element systems: effect of statistical dependence. *Journal of Engineering Mechanics, ASCE*, 5 (2):88–98, 1990.

[13] G. Deodatis. Weighted integral method. I: stochastic stiffness matrix. *Journal of Engineering Mechanics, ASCE*, 117(8):1851–1864, August 1991.

[14] G. Deodatis and M. Shinozuka. Weighted integral method. II: response variability and reliability. *Journal of Engineering Mechanics, ASCE*, 117(8):1865–1877, August 1991.

[15] I. Elishakoff, Y. J. Ren, and M. Shinozuka. Improved finite element method for stochastic problems. *Chaos, Solitons & Fractals*, 5(5):833–846, 1995.

[16] I. Elishakoff, Y. J. Ren, and M. Shinozuka. Some critical observations and attendant new results in the finite element method for stochastic problems. *Chaos, Solitons & Fractals*, 7(4):597–609, 1996.

[17] J. R. Fonseca, M. I. Friswell, J. E. Mottershead, and A. W. Lees. Uncertainty identification by the maximum likelihood method. *Journal of Sound and Vibration*, 288(3), December 2005.

[18] José Fonseca, Cris Mares, Mike Friswell, and John Mottershead. Review of parameter uncertainty propagation methods in structural dynamic analysis. In *Proceedings of the 2002 International Conference on Modal Analysis Noise and Vibration Engineering (ISMA2002)*, volume 4, pages 1853–1860, 2002.

[19] José Fonseca, Cris Mares, Mike Friswell, and John Mottershead. The propagation of parameter uncertainty through structural dynamics models. In *Proceedings of the IMAC-XXI*, 2003.

[20] José Fonseca, Mike Friswell, Arthur Lees, and John Mottershead. Uncertainty identification and robust design. In *Proceedings of the 2004 International Conference on Modal Analysis Noise and Vibration Engineering (ISMA2004)*, pages 3267–3272, 2004.

[21] José R. Fonseca, Mike I. Friswell, and Arthur W. Lees. Uncertainty quantification using measured vibration data. In *Proceedings of the 9th ASCE Specialty Conference on Probabilistic Mechanics and Structural Reliability (PMC2004)*, 2004.

[22] R. L. Fox and M. P. Kapoor. Rates of change of eigenvalues and eigenvectors. *AIAA Journal*, 6(12):2426–2429, 1968.

[23] M. I. Friswell. The adjustment of structural parameters using a minimum variance estimator. *Mechanical Systems and Signal Processing*, 3(2):143–155, 1989.

[24] M. I. Friswell and J. E. Mottershead. *Finite Element Model Updating in Structural Dynamics.* Kluwer Academic Press, 1995.

[25] M. I. Friswell, J. E. Mottershead, and H. Ahmadian. Finite element model updating using experimental test data: Parameterisation and regularisation. *Transactions of the Royal Society of London, Series A: Mathematical, Physical and Engineering Sciences*, 359:169–186, 2001.

[26] M. I. Friswell, J. E. Coote, M. J. Terrell, S. Adhikari, J. R. Fonseca, and N. A. J. Lieven. Experimental data for uncertainty quantification. In *Proceedings of the IMAC-XXIII*, 2005.

[27] R. Ghanem and P. Spanos. *Stochastic Finite Elements: A Spectral Approach.* Springer, 1991.

[28] R. G. Ghanem and P. D. Spanos. Spectral stochastic finite-element formulation for reliability analysis. *Journal of Engineering Mechanics*, 117(10):2351–2372, October 1991.

[29] L. Graham and G. Deodatis. Variability response functions for stochastic plate bending problems. *Structural Safety*, 20(2):167–188, 1998.

[30] Rui Campos Guimarães and José A. Sarsfield Cabral. *Estatística*. McGraw-Hill, Lisbon, 1997.

[31] Michael Hanss and Kai Willner. A fuzzy arithmetical approach to the solution of finite element problems with uncertain parameters. *Mechanics Research Communications*, 27(3):257–272, 2000.

[32] Gene J.-W. Hou, Clyde R. Gumbert, and Perry A. Newman. A most probable point-based method for reliability analysis, sensitivity analysis and design optimization. In *Proceedings of the 9th ASCE Specialty Conference on Probabilistic Mechanics and Structural Reliability (PMC2004)*, 2004.

[33] Alan Hájek. Interpretations of probability. In Edward N. Zalta, editor, *The Stanford Encyclopedia of Philosophy*. Summer 2003.

[34] Wolfgang Härdle, Marlene Müller, Stefan Sperlich, and Axel Wewatz. *Nonparametric and Semiparametric Models*. Springer Verlag, October 2003.

[35] Lambros S. Katafygiotis, Costas Papadimitriou, and Heung-Fai Lama. A probabilistic approach to structural model updating. *Soil Dynamics and Earthquake Engineering*, 17:495–507, 1998.

[36] R. B. Kearfott. Interval computations: Introduction, uses, and resources. *Euromath Bulletin*, 2(1):95–112, 1996.

[37] R. Baker Kearfott. *Rigorous Global Search: Continuous Problems*. Kluwer Academic Publishers, Dordrecht, Netherlands, 1996. ISBN 0-7923-4238-0.

[38] I. Y. Kim and O. L. de Weck. Adaptive weighted-sum method for bi-objective optimization: Pareto front generation. *Structural and Multidisciplinary Optimization*, 2(29):149–158, February 2005.

[39] W. Knabe, J. Przewlócki, and G. Różyński. Spatial averages for linear elements for two-parameter random field. *Probabilistic Engineering Mechanics*, 13(3): 147–167, 1998.

[40] B. Lallement, A. Cherki, T. Tison, and A. Level. Fuzzy modal finite element analsysis of structures with imprecise material properties. *Journal of Sound and Vibration*, 220(3):353–364, 2000.

[41] C. Li and A. Der Kiureghian. Optimal discretization of random fields. *Journal of Engineering Mechanics*, 119(6), June 1993.

[42] G. Manson. Sharper eigenproblem estimates for uncertain multi degree of freedom system. In *Proceedings of the IMAC-XXI*, 2003.

[43] G. Manson. Fuzzy finite element analysis using the transformation. In *Proceedings of the IMAC-XXIII*, Orlando, Florida, January 2005.

[44] C. Mares, J. E. Mottershead, and M. I. Friswell. Stochastic model updating: part 1 – theory and simulated examples. *Mechanical Systems and Signal Processing.* In press, available online 1 September 2005, doi:10.1016/j.ymssp.2005.06.006.

[45] R. E. Melchers. *Structural Reliability Analysis and Prediction.* John Wiley and Sons Ltd., 1999.

[46] R. C. Micaletti. Direct generation of non-gausssian weighted integrals. *Journal of Engineering Mechanics*, 126(1):66–75, January 2000.

[47] J. E. Mottershead, C. Mares, S. James, and M. I. Friswell. Stochastic model updating: part 2 – application to a set of physical structures. *Mechanical Systems and Signal Processing.* In press, available online 16 September 2005, doi:10.1016/j.ymssp.2005.06.007.

[48] R. B. Nelson. Simplified calculation of eigenvector derivatives. *AIAA Journal*, 14(9):1201–1205, 1976.

[49] Jeremy Oakley and Anthony O'Hagan. Bayesian inference for the uncertainty distribution of computer model outputs. *Biometrika*, 89(4):769–784, 2002.

[50] W. L. Oberkampf, J. C. Helton, C. A. Joslyn, S. F. Wojtkiewicz, and S. Ferson. Challenge problems: Uncertainty in system response given uncertain parameters. `http://www.sandia.gov/epistemic/prob.statement.12-01.pdf`, November 2001. Draft.

[51] William L. Oberkampf, Timothy Trucano, and Charles Hirsch. Verification, validation, and predictive capability in computational engineering and physics. In *Foundations for Verification and Validation in the 21st Century Workshop*, Laurel, Maryland, October 2002. Johns Hopkins University/Applied Physic Laboratory.

[52] *Unified Modeling Language Specification.* Object Management Group, Inc., Version 1.5 edition, March 2003. Available online from `http://www.uml.org/`.

[53] D. H. Oh and L. Librescu. Free vibration and reliability of composite cantilevers featuring uncertain properties. *Reliability Engineering and System Safety*, 56: 265–272, 1997.

[54] C. Papadimitriou, J. L. Beck, and L. S. Katafygiotis. Updating robust reliability using structural test data. *Probabilistic Engineering Mechanics*, 16:103–113, 2001.

[55] W. H. Press, S. A. Teukolsky, W. T. Vetterling, and B. P. Flannery. *Numerical Recipes in C.* Cambridge University Press, Cambridge, 1995.

[56] Zhiping Qiu, Suhuan Chen, and Isaac Elishakoff. Non-probabilistic eigenvalue problem for structures with uncertain parameters via interval analysis. *Chaos, Solitons & Fractals*, 7(3):303–308, 1996.

[57] Zu-Qing Qu. Accurate methods for frequency responses and their sensitivities of proportionally damped systems. *Computers and Structures*, 79:87–96, 2001.

[58] Rudiger Rackwitz. Reliability analysis – a review and some perspectives. *Structural Safety*, 23:365–395, 2001.

[59] Ramesh Rebba and Sankaran Mahadevan. Validation of structural dynamics models under uncertainty. In *Proceedings of the IMAC-XXIII*, 2005.

[60] Philip J. Ross. *Taguchi techniques for quality engineering.* McGraw-Hill, New York, 2nd ed. edition, 1996.

[61] C. S. Rudisill and Y. Y. Chu. Numerical methods for evaluating the derivatives of eigenvalues and eigenvectors. *AIAA Journal*, 13(6):834–837, 1975.

[62] Jerome Sacks, William J. Welch, Toby J. Mitchell, and Henry P. Wynn. Design and analysis of computer experiments. *Statistical Science*, 4(4):409–435, 1989.

[63] Cedric J. SALLABERRY and Jon C. HELTON. A method for extending the size of latin hypercube sample. In *Proceedings of the IMAC-XXIII*, 2005.

[64] Marco Savoia. Structural reliability analysis through fuzzy number approach, with application to stability. *Computers and Structures*, 80:1087–1102, 2002.

[65] G. I. Schüeller. A state-of-the-art report on computational stochastic mechanics. *Probabilistic Engineering Mechanics*, 12(4):197–321, October 1997.

[66] B. W. Silverman. Density estimation for statistics and data analaysis. In *Monographs on Statistics and Applied Probability*, volume 26. Chapman & Hall, London, 1986.

[67] P. D. Spanos and R. G. Ghanem. Stochastic finite element expansion for random media. *Journal of Engineering Mechanics*, 115(5):1035–1053, May 1989.

[68] Genichi Taguchi. *Introduction to quality engineering: Designing Quality into products and processes.* Asian Producitivity Organization, Tokyo, 1986.

[69] T. Takada. Weighted integral method in stochastic finite element analysis. *Probabilistic Engineering Mechanics*, 5(3):146–156, 1990.

[70] T. Takada. Weighted integral method in multi-dimensional stochastic finite element analysis. *Probabilistic Engineering Mechanics*, 5(4):158–166, 1990.

[71] Ben H. Thacker, David S. Riha, Harry R. Millwater, and Michael P. Enright. Errors and uncertainties in probabilistic engineering analysis. In *Proceedings of the 42nd AIAA/ASME/ASCE/AHS/ASC Structures, Structural Dynamics, and Materials Conference*, AIAA 2001-1239, Seattle, WA, April 2001.

[72] Kwok-Leung Tsui. A critical look at Taguchi' s modelling approach for robust design. *Journal of Applied Statistics*, 23(1):81 – 95, 1996.

[73] Resit Unal and Edwin B. Dean. Taguchi approach to design optimization for quality and cost: An overview. In *Proceedings of the International Society of Parametric Analysts 13th Annual Conference*, New Orleans LA, May 21-24 1991.

[74] E. VanMarcke. *Random Fields: Analysis and Synthesis.* MIT Press, Cambridge MA, 1983.

[75] E. VanMarcke. *Random Fields: Analysis and Synthesis.* Princeton University, Princeton NJ, web edition by Rare Book Services edition, 1998. URL `http://www.princeton.edu/~evm/randomfields.html`. This is the web edition of the book by VanMarcke [74].

[76] E. VanMarcke and M. Grigoriu. Stochastic finite element analysis of simple beams. *Journal of Engineering Mechanics*, 109(5):1203–1214, October 1983.

[77] T. Wang and B. Wah. Handling inequality constraints in continuous nonlinear global optimization. In *Proceedings of the 2nd World Conference on Integrated Design and Process Technology*, volume 1, pages 267–274, Austin, Texas, December 1996.

[78] Wikipedia. Bayesian probability — wikipedia, the free encyclopedia, 2005. URL `http://en.wikipedia.org/wiki/Bayesian_probability`. [Online; accessed 02-May-2005].

[79] Wikipedia. Taguchi methods — wikipedia, the free encyclopedia, 2005. URL `http://en.wikipedia.org/wiki/Taguchi_methods`. [Online; accessed 05-Jul-2005].

[80] K. Worden, G. Manson, T. M. Lord, and M. I. Friswell. Some observations on uncertainty propagation through a simple nonlinear system. *Journal of Sound and Vibration*, 288(3), December 2005.

[81] C. Zang, M. I. Friswell, and J. E. Mottershead. Robust design for structural optimization problems due to parameter uncertainties. In *Proceedings of the IMAC-XXI*, 2003.

[82] Thomas A. Zang, Michael J. Hemsch, Mark W. Hilburger, Sean P. Kenny, James M. Luckring, Peiman Maghami, Sharon L. Padula, and W. Jefferson Stroud. Needs and opportunities for uncertainty-based multidisciplinary design methods for aerospace vehicles. Technical Memorandum NASA/TM-2002-211462, NASA, Langley Research Center, Hampton, Virginia, July 2002. An electronic version can be found at `http://techreports.larc.nasa.gov/ltrs/` or `http://techreports.larc.nasa.gov/cgi-bin/NTRS`.

[83] O. C. Zienkiewicz and R. L. Taylor. *The Finite Element Method*, volume 2: Solid Mechanics. Butterworth-Heinemann, 5th edition, 2000.